

DESIGN, SIMULATION, AND PERFORMANCE ANALYSIS OF
MULTIFUNCTIONAL SOLAR-ASSISTED HEAT PUMP SYSTEMS FOR RESIDENTIAL
BUILDINGS

by

Amirahmad Zare

A dissertation submitted to the faculty of
The University of North Carolina at Charlotte
in partial fulfillment of the requirements
for the degree of Doctor of Philosophy in
Mechanical Engineering

Charlotte

2021

Approved by:

Dr. Weimin Wang

Dr. Nenad Sarunac

Dr. Russell Keanini

Dr. Mona Azarbayjani

©2021
Amirahmad Zare
ALL RIGHTS RESERVED

ABSTRACT

AMIRAHMAD ZARE. Design, Simulation, and Performance Analysis of Multifunctional Solar-Assisted Heat Pump Systems for Residential Buildings. (Under the directions of DR. WEIMIN WANG)

Residential buildings contribute about 22% of the national energy use in the U.S. Space heating, domestic hot water (DHW), and space cooling are the three major end uses, respectively accounting for 43%, 19%, and 8% of the residential sector's total primary energy consumption. Currently, fossil fuels are the predominant source of energy in the residential sector. To address the problems caused by the combustion of fossil fuels, alternative renewable, low-emission, and energy-efficient technologies for heating and cooling applications in residential buildings are highly needed. In this respect, solar-assisted heat pump (SAHP) systems are a promising solution by coupling solar collectors with heat pumps that can complement each other to achieve high solar utilization and high efficiency of the heat pump.

This research proposes and evaluates a hybrid multifunctional SAHP system that can provide space heating, space cooling, DHW, and onsite electricity generation. The indirect expansion SAHP system supports both parallel and series configurations. Major components of the SAHP system include unglazed PVT collectors, a liquid-to-liquid heat pump, a thermal storage tank, a DHW tank, auxiliary electric water heaters, and pumps. Photovoltaic-thermal (PVT) collectors are used to serve three functions, including electricity generation (daytime), heat collection (usually daytime), and radiative cooling (usually nighttime). The system design and controls support fourteen operational modes involving different components for space heating, space cooling, and DHW heating.

TRNSYS software is used to model and simulate the multifunctional SAHP system. The system performance is evaluated in two locations (i.e., Baltimore, MD and Las Vegas, NV) with different climates. Based on the performance analysis of the system simulation, three potential performance improvement strategies, including replacing the thermal storage tank with an outdoor swimming pool or a tank having phase change materials for latent thermal storage, and replacing the liquid-to-liquid heat pump with a dual-source heat pump are explored. The TRNSYS simulation results are also used to calculate the simple payback period of the incremental investment associated with the multifunctional SAHP system relative to a reference air-source heat pump system.

With a 2 m³ storage tank and 30 m² PVT collectors, the multifunctional SAHP system has a seasonal performance factor of 2.7 in Baltimore and 3.7 in Las Vegas. In comparison with the reference system, the SAHP system saves energy by 48% in Baltimore and 61% in Las Vegas. The seasonal performance factor of the SAHP system can be further improved by using a swimming pool to replace the storage tank in Las Vegas and using a dual-source heat pump in Baltimore.

Keywords: Photovoltaic-thermal (PVT) collectors, Heat Pump, TRNSYS, Building Simulation, Thermal Storage

ACKNOWLEDGMENTS

My Ph.D. was a long journey with many ups and downs along the way. This dissertation would not have been possible without the help and support of many amazing people around me. First and foremost, I would like to thank my advisor, Dr. Weimin Wang. Words cannot express my gratitude for him, who tirelessly supported me and encouraged me throughout the process. His technical knowledge, positive mindset, insight, and leadership have always amazed me and have set a high bar for me that I hope to reach one day. I would also like to thank my co-advisor, Dr. Nenad Sarunac, for his helpful suggestions, feedback, and assistance in moving my research forward. Additionally, I would like to thank the rest of my dissertation committee, Dr. Russell Keanini, and Dr. Mona Azarbayjani, for devoting their time to read my dissertation and providing invaluable comments. Lastly, I would like to thank my family for their love and encouragement during this challenging stage of my life. My deepest gratitude goes to my parents and my sister, Mahsa, who kept pushing me and never stopped believing in me, and especially to my loving wife, Tiffany, who patiently supported and encouraged me in all possible ways.

DEDICATION

I dedicate this dissertation to my daughter, Charlotte Pardis, who has brightened my life since she was born a year ago. Your smile means the world to me, and I love you so much.

TABLE OF CONTENTS

LIST OF TABLES	xi
LIST OF FIGURES	xiii
CHAPTER 1: INTRODUCTION	1
1.1 Background.....	1
1.2 Problem statement	2
1.3 Research objectives	4
1.4 Organization of dissertation.....	4
CHAPTER 2: LITERATURE REVIEW	6
2.1 Overview of photovoltaic-thermal (PVT) collectors.....	6
2.2 Overview of solar-assisted heat pump system configurations.....	15
2.3 Applications of solar-assisted heat pump systems	20
2.3.1 SAHP systems for domestic hot water heating	21
2.3.2 SAHP systems for space heating.....	22
2.3.3 SAHP systems for both DHW and space heating	24
2.3.4 Multifunctional SAHP Systems	27
2.4 Studies on using PVT collectors for radiative cooling	35
2.5 Summary of literature review	37
CHAPTER 3: SYSTEM DESIGN.....	39

3.1 Multifunctional solar-assisted heat pump system prototype design	39
3.2 Sequence of system operation	41
3.3 Reference system.....	47
3.4 Boundary considerations for the system design	48
3.4.1 Climate conditions.....	48
3.4.2 Building description	49
3.5 Component sizing.....	51
CHAPTER 4: SYSTEM SIMULATION.....	52
4.1 Type 560: PVT solar collectors	53
4.2 Type 927: Liquid-to-liquid heat pump	61
4.3 Types 156 & 158: Thermal storage	62
4.4 Type 114: Pump.....	64
4.5 Type 91: Plate heat exchanger.....	65
4.6 Type 138: Fluid heater.....	65
4.7 Type 119: Air-to-air heat pump.....	65
4.8 System simulation.....	66
CHAPTER 5: SYSTEM PERFORMANCE ANALYSIS	69
5.1 Verification of control implementation	69
5.1.1 System operation in the winter season	70

5.1.2 System operation in the summer season	72
5.1.3 System operation in the shoulder season.....	73
5.2 Statistical analysis of system operational modes.....	75
5.2.1 Run time analysis of modes related to space heating and cooling	75
5.2.2 Run time analysis of modes related to DHW heating	78
5.3 System performance evaluation and analysis	81
5.3.1 Solar utilization ratios	81
5.3.2 Solar fractions	85
5.3.3 Self-consumption	89
5.3.4 Area-specific cooling power of PVT collectors.....	91
5.3.5 Fractional energy savings relative to the reference system.....	92
5.3.6 Seasonal performance factors.....	97
5.4 Sensitivity analysis	100
5.4.1 Sensitivity analysis of collector area and storage tank volume.....	100
5.4.2 Impact of nighttime radiative cooling	102
5.4.3 Impact of thermal storage charging with the heat pump.....	103
5.5 Simplified control strategy	104
CHAPTER 6: INVESTIGATION OF SYSTEM PERFORMANCE IMPROVEMENT STRATEGIES.....	108
6.1 Strategy 1: Using an outdoor swimming pool for thermal storage.....	108

6.1.1 Swimming pool modeling	109
6.1.2 System simulation and results for Strategy 1	112
6.2 Strategy 2: Using a tank with integrated phase-change-material (PCM) modules for thermal storage.....	117
6.2.1 PCM storage tank modeling.....	117
6.2.2 System simulation and results for Strategy 2	120
6.3 Strategy 3: Dual-source heat pump	127
6.3.1 Dual-source heat pump modeling	128
6.3.2 System simulation results for Strategy 3.....	132
CHAPTER 7: SYSTEM ECONOMIC ANALYSIS	137
7.1 Capital cost estimation.....	137
7.2 Simple payback period	139
CHAPTER 8: SUMMARY, CONTRIBUTIONS, AND FUTURE WORK.....	143
8.1 Summary.....	143
8.2 Contributions	145
8.3 Future work.....	146
REFERENCES	149
Appendix A: Reviewed studies of SAHP systems	161
Appendix B: Normalized data files of heat pumps.....	166

LIST OF TABLES

Table 2-1: Comparison of direct and indirect expansion SAHP systems	18
Table 2-2: Operational modes and corresponding refrigerant circulations in the SAHP system presented by Wang et al. (2011)	30
Table 3-1: The schedule of pumps and valves of the multifunctional SAHP system.....	46
Table 3-2: Thermal performance of exterior building envelope.....	51
Table 4-1: Parameters of unglazed PVT collectors	60
Table 4-2: Parameters of the liquid-to-liquid heat pump.....	61
Table 4-3: Parameters of the thermal storage and DHW tanks	63
Table 4-4: parameters of the air-to-air heat pump	66
Table 4-5: Control parameters of the proposed and reference systems	68
Table 5-1: Seasons defined in the two locations.....	75
Table 5-2: Annual SPF of the system before and after the simplification.....	107
Table 6-1: PCM tank major parameters.....	119
Table 6-2: Air-to-liquid heat pump parameters	129
Table 6-3: Comparison of the system running time in different modes and with different sources for space heating	135
Table 6-4: Comparison of the system running time in different modes and with different sources for space cooling.....	135
Table 7-1: Estimated equipment costs of the proposed SAHP system.....	138
Table 7-2: Estimated equipment costs of reference conventional air-source heat pump system	139

Table 7-3: Annual electricity consumption and production of the single-family house simulated in this work in Baltimore and Las Vegas	141
Table 7-4: Simple payback periods of the solar-assisted multifunctional heat pump system against the conventional air-source heat pump system	142
Table A-1: Reviewed studies of SAHP systems for domestic hot water heating	161
Table A-2: Reviewed studies of SAHP systems for space heating	162
Table A-3: Reviewed studies of SAHP systems for both DHW and space heating	164
Table B-1: Normalized heating data file of the WaterFurnace (model NSW040) liquid-to-liquid heat pump.....	166
Table B-2: Normalized cooling data file of the WaterFurnace (model NSW040) liquid-to-liquid heat pump.....	171
Table B-3: Normalized heating data file of the Carrier (Model 30AWH012-3Ph) air-to-water heat pump	177
Table B-4: Normalized cooling data file of the Carrier (Model 30AWH012-3Ph) air-to-water heat pump	178

LIST OF FIGURES

Figure 2-1: PVT collector energy outputs	7
Figure 2-2: Utilization of solar spectrum of a PVT collector (Lämmle et al. 2020)	7
Figure 2-3: Covered PVT collectors manufactured by Endef (2020).....	9
Figure 2-4: Uncovered PVT collectors	10
Figure 2-5: Concentrating PVT collectors manufactured by Sunoyster (n.d.)	11
Figure 2-6: PVT collector technologies and applications based on the operating temperature (Lämmle et al. 2020).....	12
Figure 2-7: Energy balance of a radiative surface	14
Figure 2-8: Schematic of a direct SAHP system	17
Figure 2-9: Schematic of an indirect SAHP system	17
Figure 2-10: Schematic diagram of a Parallel SAHP system	19
Figure 2-11: Schematic diagram of a Series SAHP system.....	20
Figure 2-12: Schematic diagram of a Parallel/Series SAHP system	20
Figure 2-13: The schematic diagram of the SAHP system presented by Chu et al. (2014)	28
Figure 2-14: The schematic diagram of the SAHP system presented by Wang et al. (2011)	30
Figure 2-15: The schematic diagram of the SAHP system presented by Cai et al. (2016)	31
Figure 2-16: The schematic diagram of the SAHP system presented by Entchev et al. (2014)...	32
Figure 2-17: The schematic diagram of the SAHP system presented by Kang et al. (2016)	34
Figure 2-18: The schematic diagram of the SAHP system presented by Besagni et al. (2019)...	35
Figure 3-1: Schematic diagram of the proposed multifunctional SAHP system: the upper part for space conditioning and the lower part for DHW production.....	40

Figure 3-2: Flowchart diagram showing the system control sequence.....	42
Figure 3-3: Profiles of the monthly average outdoor dry-bulb temperature and the monthly average effective sky temperature.....	49
Figure 4-1: PVT schematic (Klein et al. 2018).....	53
Figure 4-2: Energy balance on fin element (Duffie and Beckman 2006).....	57
Figure 4-3: TRNSYS model of the multifunctional SAHP system	67
Figure 5-1: System operation on February 5	71
Figure 5-2: System operation on July 4	73
Figure 5-3: System operation on May 9	74
Figure 5-4: Monthly running time of operational modes related to space conditioning in Baltimore	77
Figure 5-5: Monthly running time of operational modes related to space conditioning in Las Vegas	78
Figure 5-6: Monthly running time of operational modes related to DHW production in Baltimore	80
Figure 5-7: Monthly running time of operational modes related to DHW production in Las Vegas	80
Figure 5-8: Solar yields and utilization ratios of the multifunctional SAHP system in Baltimore	84
Figure 5-9: Solar yields and utilization ratios of the multifunctional SAHP system in Las Vegas	84
Figure 5-10: Solar thermal fraction.....	86
Figure 5-11: System and site solar electrical fractions in Baltimore	88

Figure 5-12: System and site solar electrical fractions in Las Vegas	88
Figure 5-13: System and site self-consumption of onsite solar electricity generation in Baltimore	90
Figure 5-14: System and site self-consumption of onsite solar electricity generation in Las Vegas	90
Figure 5-15: Monthly and annual average of the area-specific cooling power of PVT collectors	92
Figure 5-16: Monthly fractional energy saving of the proposed system compared to the reference system for Baltimore.....	95
Figure 5-17: Monthly fractional energy saving of the proposed system compared to the reference system for Las Vegas	96
Figure 5-18: Annual energy consumption comparison between the proposed and reference systems and fractional energy saving of the proposed system compared to the reference system.	97
Figure 5-19: SPF comparison between the proposed and reference systems in Baltimore	99
Figure 5-20: SPF comparison between the proposed and reference systems in Las Vegas	99
Figure 5-21: Sensitivity analysis on PVT area and storage tank volume for Baltimore.....	101
Figure 5-22: Sensitivity analysis on PVT area and storage tank volume for Las Vegas.....	101
Figure 5-23: Impact of Mode 11 on the system energy consumption	102
Figure 5-24: Impact of Mode 6 on the system energy consumption	103
Figure 5-25: Flowchart diagram of the simplified control strategy for the proposed system.....	105
Figure 5-26: Schematic diagram of the SAHP system with simplified controls in Baltimore...	106
Figure 5-27: Schematic diagram of the SAHP system with simplified controls in Las Vegas ..	106
Figure 6-1: Schematic diagram of the SAHP system with a swimming pool	109

Figure 6-2: Energy balance of the swimming pool water.....	110
Figure 6-3: The modified section of the TRNSYS model for the pool case.....	113
Figure 6-4: The change of annual SPF with the pool temperature limit applied to Mode 6 in Baltimore.....	116
Figure 6-5: The change of annual SPF with the pool temperature limit applied to Mode 5 in Las Vegas.....	116
Figure 6-6: The modified section of the TRNSYS model for the PCM tank case	121
Figure 6-7: Comparison of the SPF for systems featured the use of PCM with different melting temperatures in Baltimore while keeping the PCM module at 50% of the tank volume.....	123
Figure 6-8: Comparison of the SPF for systems featured the use of PCM with different melting temperatures in Las Vegas while keeping the PCM module at 50% of the tank volume.....	124
Figure 6-9: Comparison of the SPF for systems with different percentages of the tank volume used by the PCM module having a melting temperature of 10°C (Baltimore)	126
Figure 6-10: Comparison of the SPF for systems with different percentages of the tank volume used by the PCM modules having a melting temperature of 10°C (Las Vegas)	126
Figure 6-11: Schematic diagram of the PVT-dual-source HP system	128
Figure 6-12: The modified section of the TRNSYS model for the dual-source heat pump case	130
Figure 6-13: The impact of temperature offset on annual SPF in Baltimore.....	133
Figure 6-14: The impact of temperature offset on annual SPF in Las Vegas.....	133
Figure 6-15: Baltimore monthly mode time activation.....	136
Figure 6-16: Las Vegas monthly mode time activation.....	136

CHAPTER 1: INTRODUCTION

1.1 Background

The building sector consumes the most energy in many countries of the world. In the U.S., buildings account for 40% of the total primary energy use, of which 22% is from residential buildings and 18% is from commercial buildings (EIA 2021). Residential buildings in the U.S. consume about 21 Quads BTU of primary energy per year, 88% of which is from fossil fuels (EIA 2021). Because fossil fuels are non-renewable resources and the combustion of fossil fuels emits greenhouse gases (GHGs), the cause of global climate change, efforts are needed to switch from fossil fuels to renewable energy to meet the demands of people.

Space heating, domestic hot water (DHW), and space cooling are three major energy end uses in residential buildings. The above three energy end uses respectively contribute to 43%, 19%, and 8% of the total energy consumed by the residential sector (EIA 2018). On average, the above three energy end uses make up 59% of the energy expenditure, which is an economic burden for nearly one-third of all households in the U.S. (EIA 2018). Therefore, it is critical to integrate renewable energy and energy-efficient technologies for the design and operation of high-performance residential buildings (Hadorn 2015).

Solar energy systems are the most commonly used renewable energy systems in residential buildings (Tsalikis 2015). Building-integrated solar energy systems have many advantages, including no need for additional land use, no waste emissions in the operation stage, silent operation, minimal maintenance requirement, and reduced energy transmission losses due to the short distance between the energy supply and the demand. In particular, the short distance between

energy generation and use is crucial for solar thermal systems as it is typically not practical to transport heat over long distances.

Building electrification represents an important opportunity to reduce GHG emissions. At the present, fossil fuels are the major fuel type for residential heating, with natural gas used in 53% of all households in the U.S. (EIA 2018). Replacing fossil fuel-based heating equipment with efficient heat pumps can significantly reduce energy consumption in residential buildings and address fossil fuel-associated environmental concerns. Geothermal heat pumps, ductless mini-split heat pumps, solar-assisted heat pumps, and heat pump water heaters are all promising technologies to be considered in the process of building electrification.

A solar-assisted heat pump (SAHP) combines solar collectors and a heat pump together to form an integrated system. In the system, the solar collectors perform the function of the heat pump's heat source, and this heat is used to boost the heat pump's evaporator temperature for heating. Thus, the heat pump has improved efficiency because of the boosted evaporator temperature. In addition, the solar collectors typically operate at a low temperature in SAHP systems, resulting in more solar collection, increased solar fraction, and reduced conventional source energy consumption (Banister and Collins 2015). To address the mismatch between solar energy generation and the building load, thermal energy storage can be used in SAHP systems. According to Hadorn (2015), SAHP systems are a promising solution for achieving high-performance or even net-zero energy residential buildings.

1.2 Problem statement

Many studies have been conducted on the development, design, testing, and techno-economic analysis of SAHP systems in residential buildings. However, previous studies have a

primary focus on space heating and DHW. The current practice is to have separate systems and equipment used for space heating, DHW heating, and space cooling. The standalone approach of separate system design and operation is simple but may limit the opportunity of energy cascading (i.e., the process of using the waste heat from one process as the energy source for another) and cause seasonal equipment use.

Most previous studies on SAHP systems use conventional solar collectors as the heating source. In recent years, using photovoltaic-thermal (PVT) collectors to convert solar radiation to electricity and heat simultaneously has attracted increasing attention in studying SAHP systems (IEA SHC Task 60). If PVT collectors are used in a SAHP system, the majority of existing studies rely on the use of PVT collectors for electricity generation and heating collection. Actually, PVT collectors can be used for cooling purposes through long-wave radiation heat losses from the PVT surface to the outer space over clear nights (Eicker and Dalibard 2011). However, the triple uses of PVT collectors in a SAHP system have rarely been explored.

Therefore, the research problems to be addressed with this research include the following:

- 1) How can a multifunctional SAHP system be designed to be capable of electricity generation, space heating, DHW heating, and space cooling?
- 2) How can the multifunctional SAHP system be controlled given the complexity of system operation?
- 3) How to evaluate the energy performance of the multifunction SAHP system using building simulation programs?
- 4) How is the performance, both energy and economics, of the multifunctional SAHP system when compared with the conventional reference system?
- 5) What is the impact of different component sizes and control options on the system performance?

1.3 Research objectives

The primary objective of this research is to develop a novel hybrid multifunctional PVT-HP system with a custom control capable of providing space heating, space cooling, DHW, and electricity in single-family houses. This research intends to achieve the following objectives:

- Proposing a novel multifunctional SAHP system based on PVT collectors with a detailed control strategy with many operational modes
- Applying the multifunctional SAHP system to a single-family residential building design and studying the impact of climate on system performance
- Investigating the impact of increasing the thermal storage capacity on system performance through utilizing the swimming pool and phase change materials (PCM) instead of thermal storage tank
- Exploring the benefits of using dual-source HP (using air-source and solar-source) instead of single-source HP (using solar-source) in the proposed SAHP system
- Performing economic analysis to evaluate the economic feasibility of the proposed SAHP system with and without incentives

1.4 Organization of dissertation

The dissertation is organized as follows:

- Chapter 2 presents the literature review about SAHP systems, focusing on the studies that used PVT collectors. In addition, the multifunctional SAHP systems are discussed in more detail in this chapter.

- Chapter 3 discusses the proposed SAHP system design and its control strategy. The hypothetical building and the baseline system used to facilitate the comparison with the proposed system are also introduced in this chapter.
- Chapter 4 describes the component models and the system simulation with the TRNSYS software.
- Chapter 5 gives the performance analysis of the TRNSYS simulation of the proposed and reference systems. In this chapter, the proposed system control implementation is verified through preliminary representative day analysis first. Later, statistical analysis of the proposed system operational modes is performed. Then, performance indicators are introduced, and energy calculations and comparisons for assessing system performance are presented. The sensitivity analysis to evaluate the impact of main system parameters is then followed. Lastly, the proposed system performance with a simplified control strategy is explored.
- Chapter 6 investigates three potential system performance improvement strategies on the basis of the SAHP system discussed in Chapter 3. The three strategies include using an outdoor swimming pool for thermal storage, using phase change materials to enhance the thermal storage capacity, and using a dual-source heat pump to replace the liquid-source-only heat pump.
- Chapter 7 presents a high-level economic analysis of the proposed system compared to the reference system. The simple payback period is calculated for the cases of with and without incentives.
- Chapter 8 ends this dissertation with a summary of major findings, contributions, and suggestions for future work.

CHAPTER 2: LITERATURE REVIEW

Solar-assisted heat pump (SAHP) systems are used to provide heating, cooling, and electricity in buildings. This chapter starts with an overview of photovoltaic-thermal collectors, the solar component used in the SAHP system in this work. Then, different configurations and applications of SAHP systems are reviewed. Lastly, the knowledge gaps identified from the literature review are presented to justify the need for this research.

2.1 Overview of photovoltaic-thermal (PVT) collectors

Conventionally, photovoltaic (PV) modules and solar thermal collectors (STC) are separate devices used to generate electricity and heating energy, respectively. Attaching an absorber plate to the back of a PV module leads to a hybrid PVT collector that can simultaneously convert solar energy into electricity and heat (Figure 2-1). The capability of using PVT collectors for heat generation lies in the low electrical efficiency of PV modules. As Figure 2-2 shows, PV modules made from crystalline Silicon can convert only 15%-20% of solar radiation to electricity, while approximately 65%-70% of the solar radiation is absorbed by the PV modules and converted to heat. The generated heat, if not dissipated from the PV modules timely, will cause the increase of PV cell temperature and lower the electrical efficiency. This problem can be addressed by using a heat transfer medium to take away the generated heat and reduce the PV cell temperature, which is the basic concept of PVT collectors. Therefore, compared to standalone PV modules, the PVT collectors usually have slightly higher electrical efficiency except for those collector designs targeted at high-temperature applications. Compared to standalone STC, the PVT collectors usually have lower thermal efficiency because some solar radiation is used for electricity

generation. In general, well-designed PVT collectors have higher overall efficiency (electrical plus thermal) than both standalone PV modules and solar thermal collectors (Zenhäusern 2017).

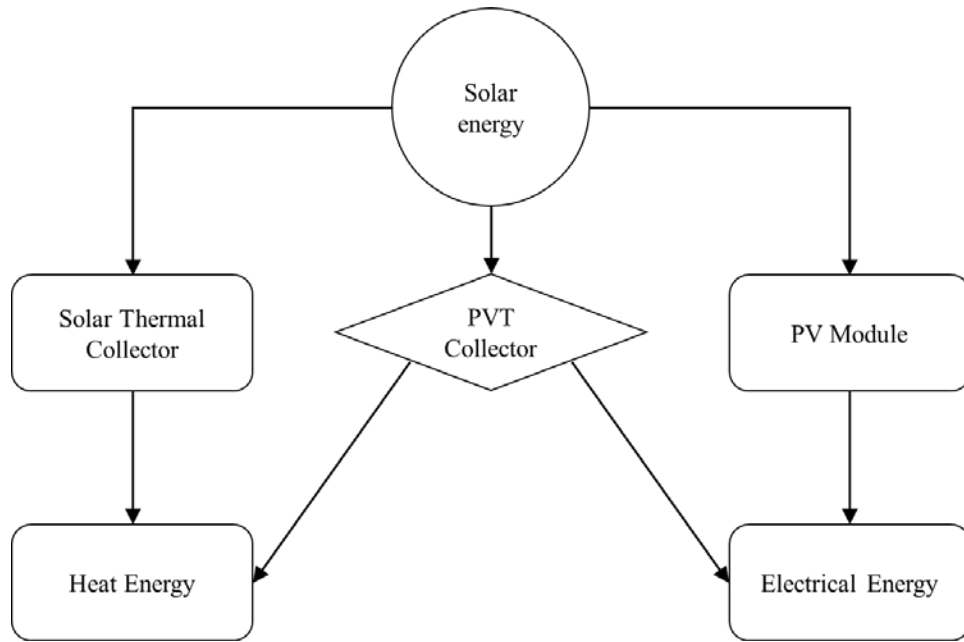


Figure 2-1: PVT collector energy outputs

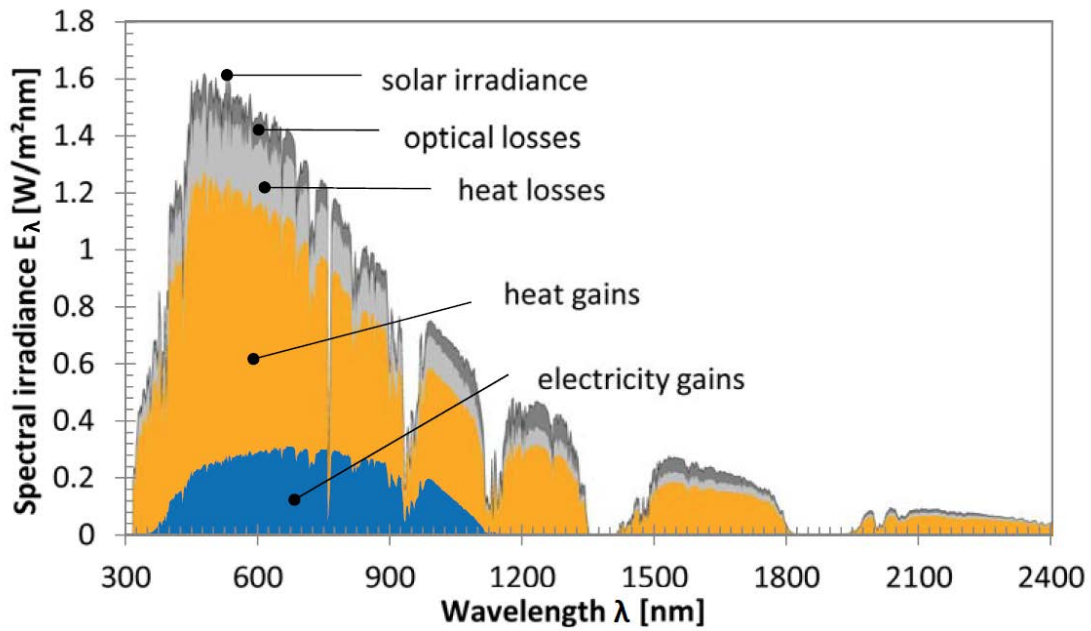


Figure 2-2: Utilization of solar spectrum of a PVT collector (Lämmle et al. 2020)

PVT collectors can be classified according to the heat transfer medium (water, air, and refrigerant), the design (uncovered or unglazed flat plate, covered or glazed flat plate, and concentrating), and the PV cell technology (thin film, monocrystalline silicon, and polycrystalline silicon). Different PVT collector designs are briefly described below.

- Covered flat-plate PVT collectors (Figure 2-3) are featured as having an air gap between the PV module and the transparent front cover, which reduces heat losses to the ambient. The insulating characteristics of the air gap are favorable for the thermal efficiency and allow for high operating temperatures. However, the high operating temperature and the optical losses due to the front cover may lower the electrical efficiency of the PV modules. Covered PVT collectors are used in medium operating temperature applications (e.g., DHW in large buildings, including hotels and resorts).
- Uncovered flat-plate PVT collectors (Figure 2-4) do not use the front cover, and the PV modules are exposed to the ambient directly. Due to the lack of the air gap above the PV modules to reduce heat losses, there is a high convective and long-wave radiative heat transfer coefficient between the PV modules and the ambient air, which is the reason why uncovered PVT collectors are called wind and infrared-sensitive collectors (WISC) in some European countries. Uncovered PVT collectors are beneficial for low-temperature (up to 50°C) applications (e.g., space heating and the source of heat pumps). In particular, when the operating temperature falls below the ambient temperature, the fluid flowing through uncovered PVT collectors can absorb heat from the surrounding air, which enables their use in periods with low or even no solar radiation.
- Concentrating PVT collectors (Figure 2-5) are constructed from concentrating PVs (e.g., parabolic trough and linear Fresnel reflector) and thermal absorbers. Because concentrating

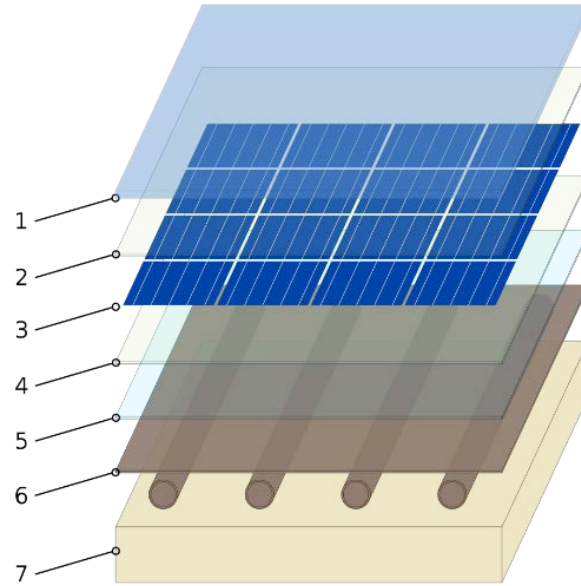
PVs greatly enhance the solar radiation gathering process, the specific area of PV cells per power generation can be significantly reduced from conventional flat-plate design. In addition, because of the high useful thermal energy generation, concentrating PVT collectors can be used in high operating temperature (above 80°C) applications such as thermal-driven cooling and industrial thermal processes.

According to Lämmle et al. (2020), uncovered PVT collectors are the dominant type, constituting 80% of the PVT market. They are mainly used for DHW production and space heating.



Figure 2-3: Covered PVT collectors manufactured by Endef (2020)

a)



b)



Figure 2-4: Uncovered PVT collectors

a) Schematics of an uncovered PVT collector 1 - Anti-reflective glass 2 - Encapsulant 3 - Solar PV cells
4 - Encapsulant 5 - Backsheet 6 - Heat exchanger 7 - Thermal insulation ((Lämmle et al. 2020) b)
Uncovered PVT collectors manufactured by Endef (2020)



Figure 2-5: Concentrating PVT collectors manufactured by Sunoyster (n.d.)

PVT collectors can be used for different applications, including the source of heat pumps, pool water heating, DHW and space heating for buildings (e.g., single-family and multi-family houses, hotels, and hospitals), and industrial and agricultural processes. Generally, which type of PVT collector design is suitable for a given application depends on multiple factors, such as the prioritization of heat or electricity generation, the desired temperature range, the area and location available for collector installation, and the economics. Figure 2-6 presents the PVT applications and corresponding suitable collector technology based on the operating temperature. IEA Task 60 reports that about two million square meters of PVT collectors were installed globally in the past five years with an anticipated annual growth rate of 10%. Over the past decades, a number of niche markets for PVT applications are observed: uncovered PVT collectors with air being the heat transfer medium for space heating (in France), DHW production in lodgings, and uncovered PVT

integration with heat pumps. In particular, with the advances of heat pump technology and the efforts on building electrification, there is an increasing attention to the coupled use of uncovered PVT collectors and the heat pump for DHW and space heating.

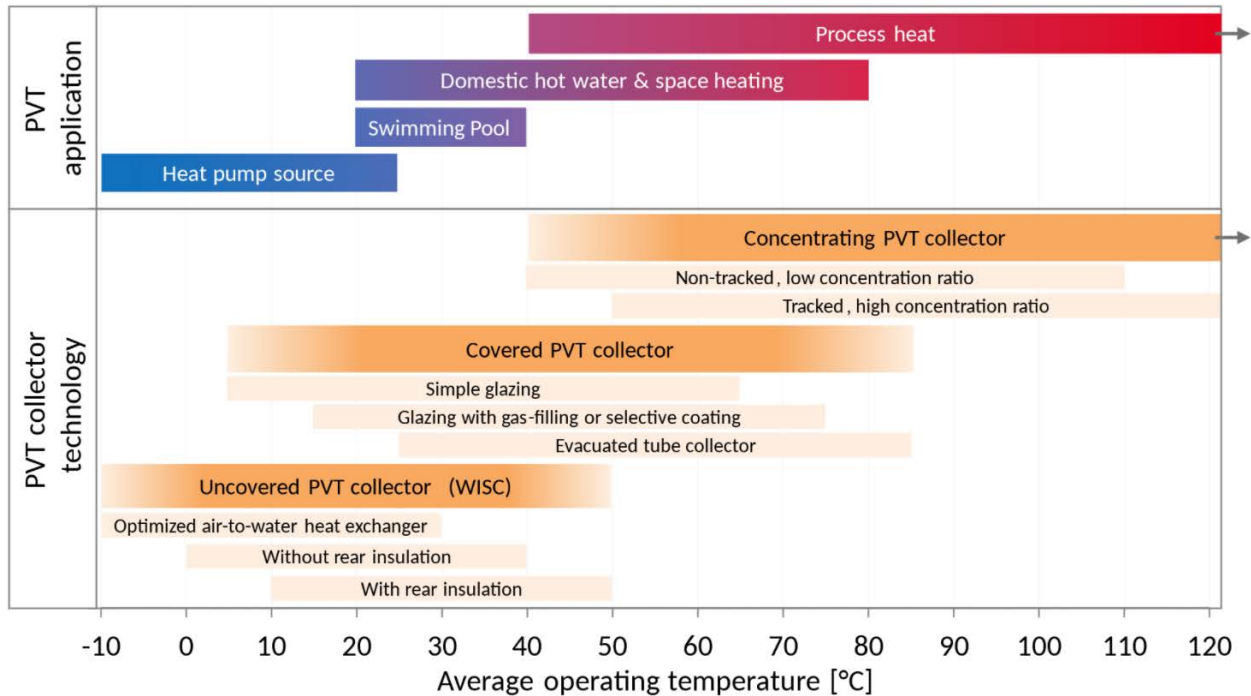


Figure 2-6: PVT collector technologies and applications based on the operating temperature (Lämmle et al. 2020)

Using PVT collectors as the source of solar-assisted heat pump systems has the following prominent advantages:

- The solar thermal energy produced by PVT collectors can boost the heat pump's evaporator operating temperature higher than the ambient air, which improves the heat pump's efficiency and heating capacity. Meanwhile, if uncovered PVT collectors are used, the PV cell's operating temperature is reduced, which increases the PV electrical efficiency.
- PVT collectors can generate both electricity and heat with one device and thus have a higher overall efficiency than the standalone PV modules and solar thermal collectors. This

makes the use of PVT collectors an attractive option when the roof area with favorable orientation for solar utilization is limited in a building.

- Relative to the side-by-side use of PV modules and solar thermal collectors, using PVT collectors is more appealing by providing aesthetic homogeneity to the roof.

Ever since the concept of inception, PVT collectors have been predominately used for the dual purposes of heating and electricity generation. However, it is more desirable to use PVT collectors to address the cooling needs because of the coincidence of high solar radiation and space cooling load. There are a couple of approaches to address the cooling demand via PVT collectors. One approach is to use thermal-driven technology for cooling (e.g., absorption and desiccant cooling). In this case, covered PVT collectors and concentrating PVT collectors are needed to generate medium-to-high temperature liquids. Another approach is based on the nighttime radiative cooling of uncovered PVT collectors. Hence, the PVT collector actually integrates the functions of PV modules (for electricity), solar thermal collectors (for heating), and radiative cooling panels (for cooling) together. Certainly, these functions do not play at the same time. Electricity and heating normally occur in the daytime with the presence of solar radiation, while cooling normally occurs at nighttime without solar radiation. Considering that nighttime radiative cooling is used in this research, but it is not well known, a brief description of radiative cooling is provided below.

Radiative cooling represents a process by which a body loses heat through long-wave thermal radiation (Vall and Castell 2017). Figure 2-7 illustrates the energy flow items involved in a radiator's cooling process, where P_{rad} denotes the thermal radiation to the sky, P_{atm} is the absorbed atmospheric radiation, P_{sun} is the absorbed solar radiation, P_{conv} is the convective heat

transfer rate between the surface and the ambient, and P_{cond} is the conductive heat transfer from the surface to the adjacent materials. The net radiative cooling power of the radiator can be expressed as:

$$P_{clg} = P_{rad} - P_{atm} - P_{sun} - P_{conv} - P_{cond} \quad (2-1)$$

The outer space is a perfect heat sink, with its temperature being close to absolute zero Kelvin. However, because the water vapor in the sky absorbs the infrared radiation emitted by the Earth, the sky temperature from the earth is much warmer than the outer space. The radiator surface emissivity and the temperature difference between the radiator surface and the sky determine the magnitude of radiative cooling power (P_{rad}). Since the cloud cover and ambient relative humidity affects the sky temperature, the radiative cooling power varies with weather conditions for a given radiator.

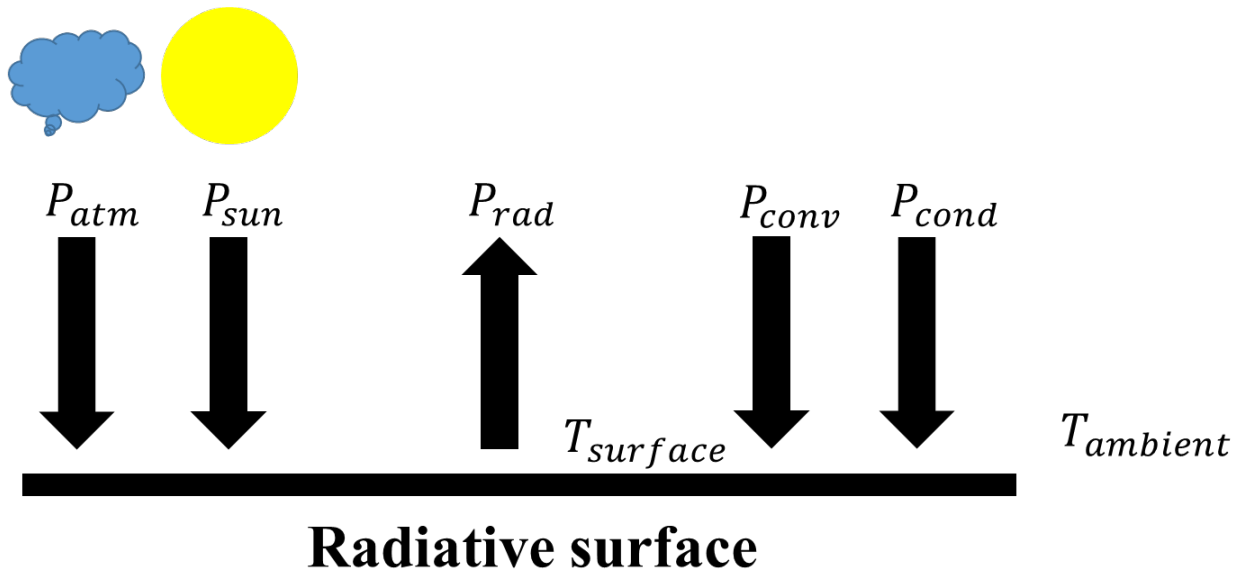


Figure 2-7: Energy balance of a radiative surface

Uncovered PVT collectors can function as nighttime radiative cooling panels because the glass material on the top of the PV module has an emissivity of around 0.9, and there is no air gap between that glass and the absorber plate. Similar to heat collection, different heat-carrying fluids, primarily air and water, can be cooled by PVT collectors via radiative cooling. The air-based design usually uses hollow channels formed between the PV laminate and the absorber plate for air distribution. In water-based design, PVT collectors normally have the PV laminate, the absorber plate, and the heat exchanger used to transfer heat between the absorber and the water flow bonded together. Water-based PVT collectors are commonly used for radiative cooling because water has a higher heat capacity than air and thus contributes to a higher overall efficiency of the system.

2.2 Overview of solar-assisted heat pump system configurations

Air-source heat pumps and solar collectors have been traditionally used separately to reduce the primary energy consumption in residential buildings, where the heat pump is used for space heating and cooling while the solar collectors are used for DHW heating. This common separate use often causes the following issues in winter when the air temperature is low. First, both the capacity and coefficient of performance (COP) of the heat pump decrease with the outdoor air temperature. The capacity may become insufficient to meet the heating load, which triggers the use of auxiliary electrical heating. In particular, many old-fashioned heat pumps have the cut-off ambient air temperature set at as high as -5°C , below which the heat pump no longer operates. Frosting on outdoor coils also deteriorates the problem of low capacity and efficiency of air-source heat pump operation in cold weather conditions. As for solar heating, the solar collectors cannot be used directly for DHW when the solar radiation is low. The heat losses to the ambient increases

when the outdoor air temperature is low. Coupling solar collectors with heat pumps can complement each other to achieve high COP of heat pumps and solar utilization. The solar collectors coupled with the heat pump can be conventional solar thermal collectors and hybrid PVT collectors (Mohanraj et al. 2018). In SAHP systems, the heat pump's COP is improved due to the boosted evaporator temperature. Meanwhile, when coupled to the heat pump, the solar collectors have a low operating temperature, leading to the increase of solar fraction (Bakker et al. 2005, Banister and Collins 2015). If PVT collectors are used, the low operating collector temperature is also beneficial to the PV module's electrical efficiency. With efforts on high performance and even net-zero energy buildings, SAHP systems have attracted increasing attention in recent years, as reflected by the two task forces (Task 44 and Task 60) of the International Energy Agency Solar Heating & Cooling Programme.

There are two major classifications of SAHP systems: direct expansion and indirect expansion systems (Vaishak & Bhale, 2019). In direct expansion SAHP systems (Figure 2-8), the refrigerant directly flows through the collector. The collector functions as an integral part of the heat pump (i.e., being the evaporator for heating and the condenser for cooling). In contrast, indirect expansion SAHP systems do not have the solar collector as an integral part of the heat pump. The collector and the heat pump are combined together via an intermediate heat exchanger for transferring solar energy. Thus, the collector working fluid is decoupled from the refrigerant loop in the heat pump (Figure 2-9). Table 2-1 compares the direct and indirect expansion SAHP systems with respect to their advantages and disadvantages (Kamel et al. 2015).

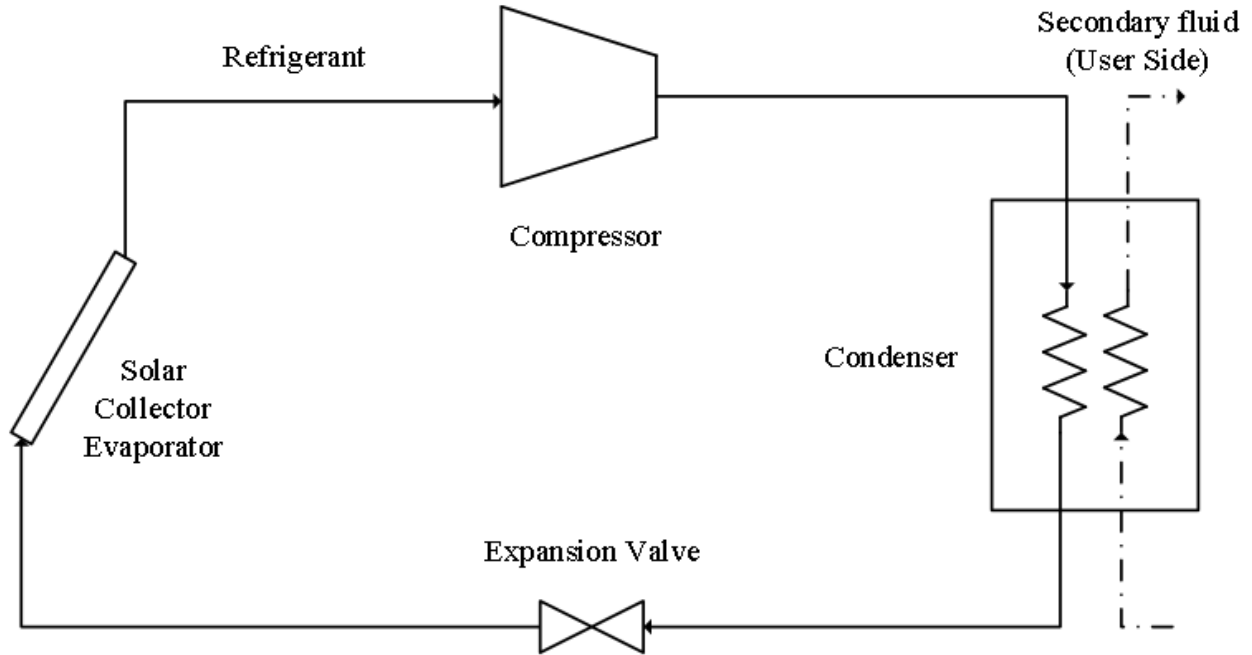


Figure 2-8: Schematic of a direct SAHP system

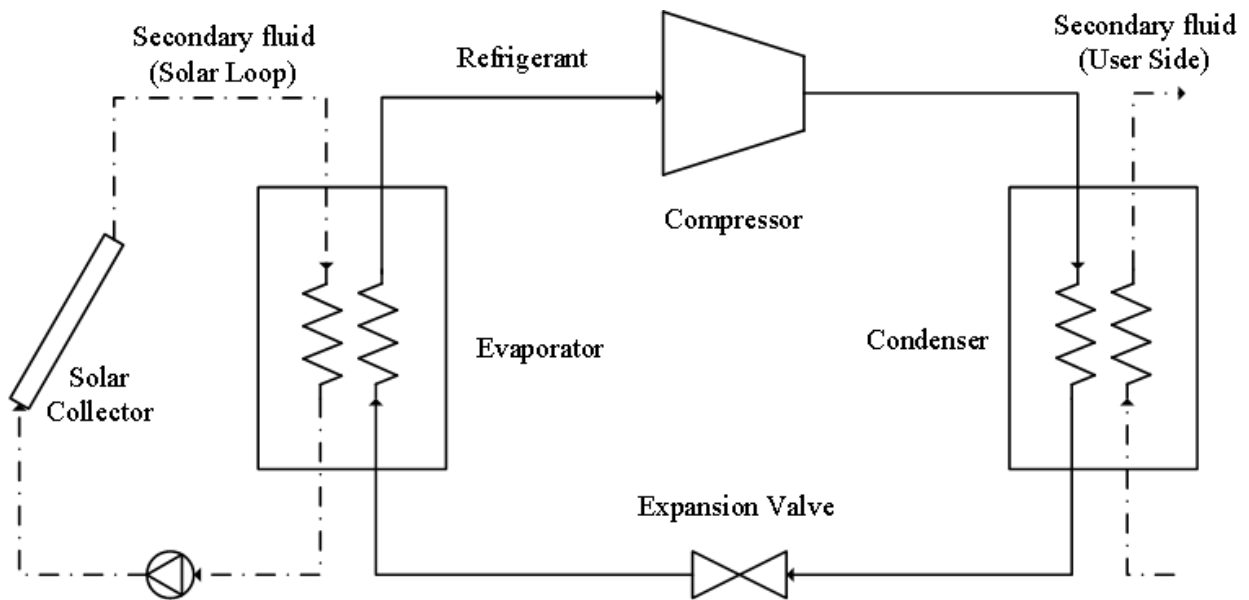


Figure 2-9: Schematic of an indirect SAHP system

Table 2-1: Comparison of direct and indirect expansion SAHP systems

SAHP System Integration Approach	Advantages	Disadvantages
Direct expansion	<ul style="list-style-type: none"> • Reduced number of units • High collector efficiency • Minimum corrosion to the collector • No freezing concern of working fluid 	<ul style="list-style-type: none"> • System performance is highly influenced by uncertain weather conditions • May require specially fabricated collectors
Indirect expansion	<ul style="list-style-type: none"> • Easy maintenance • Relatively well-developed technology • Commercial collectors are available • Flexible system configurations 	<ul style="list-style-type: none"> • Freezing issue needs to be addressed for liquid-based collectors • Possible impact on collector life due to water-based corrosion • Efficiency loss due to the use of intermediate heat exchanger

For indirect expansion SAHP systems, the collectors and the heat pump can be connected in parallel or series. In a parallel configuration, the collectors and the heat pump can independently supply useful energy for end uses. The useful energy is located on the load side of the heat pump, and it can be used instantly or stored for future use. Figure 2-10 is the schematic diagram representing typical parallel configurations. One major characteristic of parallel configuration is that the heat pump operates only if the collectors alone cannot meet the thermal load. In a series configuration, the collector is used as the source side of the heat pump either directly or through a thermal storage unit (Figure 2-11). The purpose of the series configuration is to increase the evaporator temperature of the heat pump for heating and therefore downsize or eliminate additional heat sources. Thermal storage is typically found on the source side of the heat pump in a series configuration to compensate for the fluctuating nature of solar thermal energy. In a parallel/series (P/S) configuration (Figure 2-12), the solar energy from collectors can be used on both sides of the heat pump (load side in parallel mode and source side in the series mode) depending on the

weather and system operating conditions. The solar thermal energy either replaces the heat pump heating (when used on the load side) or increases the temperature level of the source side of the heat pump (when used on the source side). Therefore, the system performance in the P/S configuration is potentially improved compared to series-only and parallel-only configurations (Hadorn 2015). According to the market analysis by Ruschenburg and Herkel (2013), 61% of installed SAHP systems are parallel, while 6% have series integration, and 34% represent a combination of different configurations.

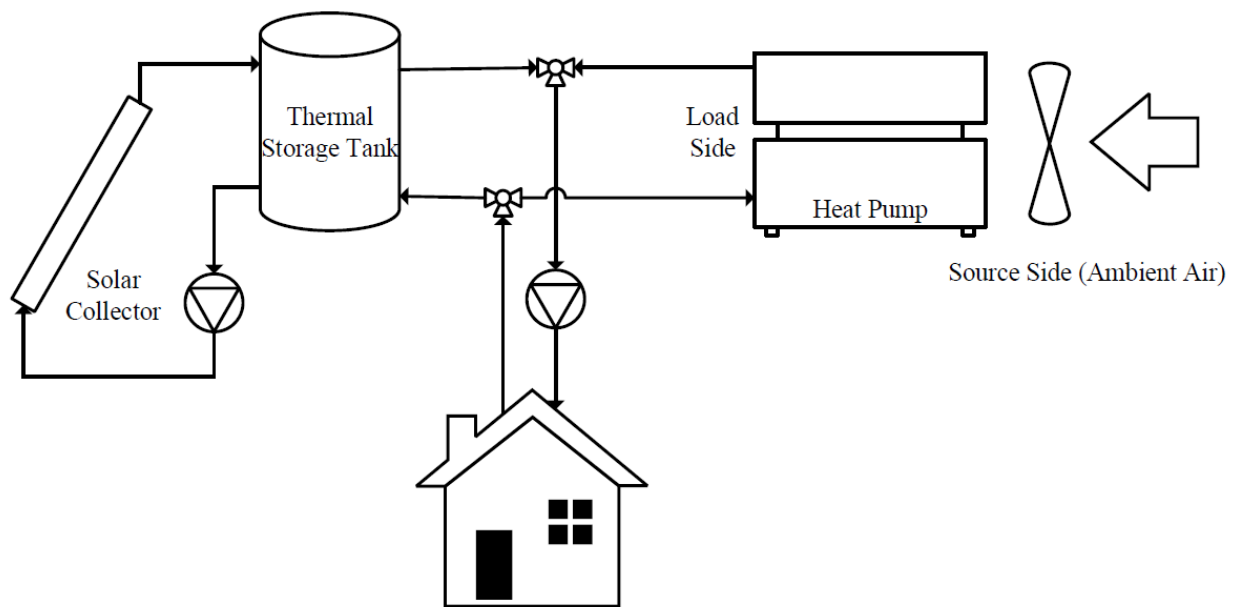


Figure 2-10: Schematic diagram of a Parallel SAHP system

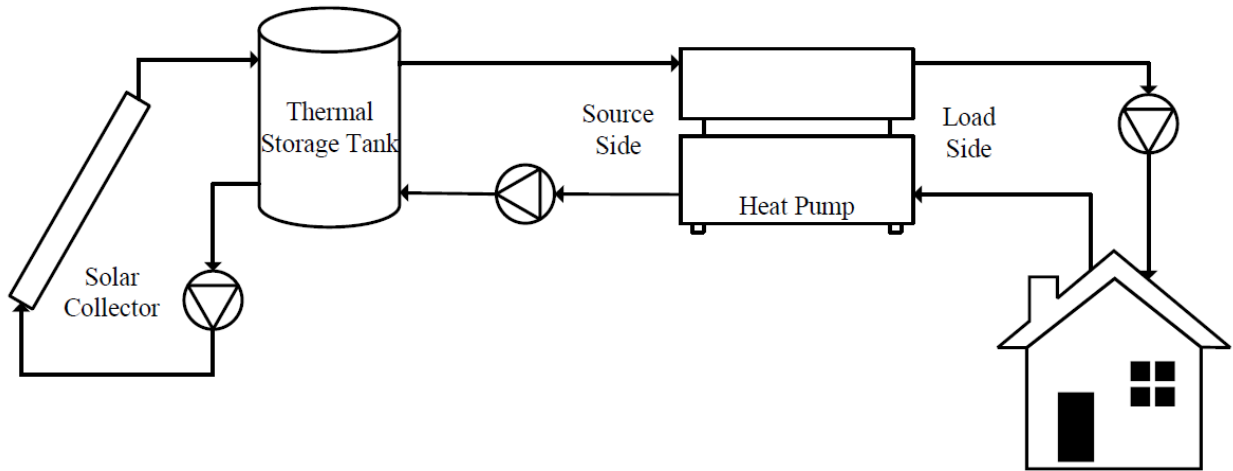


Figure 2-11: Schematic diagram of a Series SAHP system

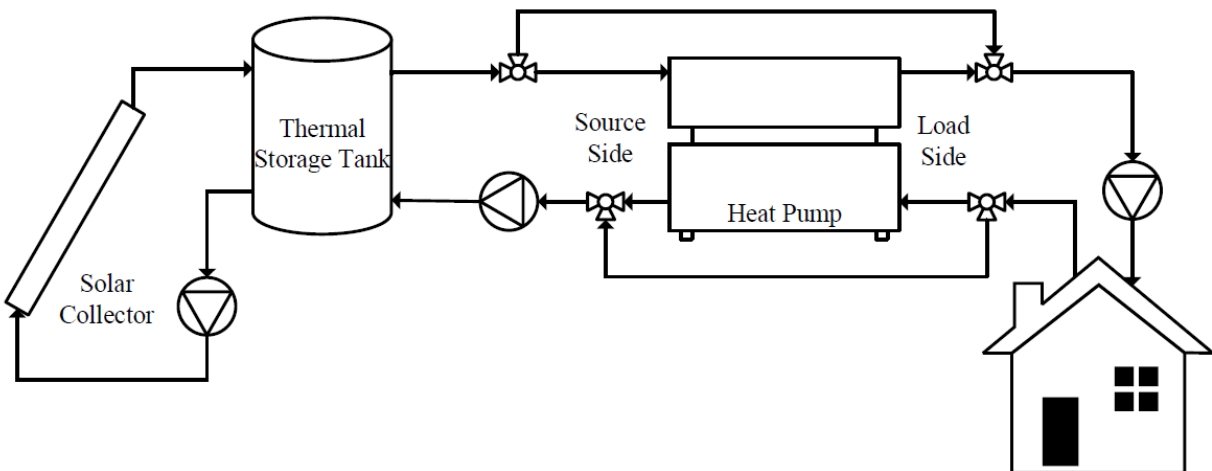


Figure 2-12: Schematic diagram of a Parallel/Series SAHP system

2.3 Applications of solar-assisted heat pump systems

SAHP systems can be applied in residential buildings to have a single or multiple functionalities, including DHW production, space heating, space cooling, and electricity generation. Many studies have been conducted on the development, design, testing, techno-

economic analysis, and optimization of SAHP systems for different applications. Most previous studies on SAHP systems have concentrated on using solar thermal collectors as the heat pump's source for heating. In this section, different applications of indirect SAHP systems are reviewed with a focus on the systems that use PVT collectors and have more than one functionality.

2.3.1 SAHP systems for domestic hot water heating

Sterling and Collins (2012) performed a simulation study using TRNSYS software to investigate the performance of an indirect expansion SAHP for DHW. The SAHP system has two tanks: one tank on the source side of the heat pump for energy storage and one DHW tank on the load side of the heat pump. Solar thermal collectors are used to charge the storage tank. Depending on the storage tank temperature, the storage tank can be used to heat the DHW tank via a heat exchanger or used as the heat pump's source. Therefore, the system has a parallel-series configuration. Banister and Collins (2015) further developed a test apparatus to validate the component parameters used in the TRNSYS model. Based on the validated simulation model, they compared the dual-tank SAHP with a standard electric DHW system and a traditional solar domestic hot water system. Their TRNSYS simulation results showed that for a 7.5 m² solar collector area, the dual tank SAHP system reduced electricity consumption by 69% relative to the non-solar system and 23% relative to the conventional solar DHW system. The savings could be greater for systems with a larger collector area.

PVT collectors have been used in SAHP systems for DHW production as well. Bai et al. (2012) used TRNSYS to simulate a series SAHP system for sports center water heating in Hong Kong. Their simulation results indicated that the SAHP saved 67% energy consumption than a conventional electric DHW system. Wang et al. (2015) made an experimental study of a series

SAHP system for DHW heating. A salient feature of the system lies in the use of a composite evaporator that can accommodate both ambient air and the water from a solar tank as the source of the heat pump. The experiments indicated that the system COP was 2.24 for the case of using the dual heat source evaporator, while it was 1.31 for the case of using the air source only. Qu et al. (2016) tested a series dual-source heat pump water heating system in Shanghai, China. The dual sources include an air-cooled evaporator and a water-cooled evaporator that are parallelly connected and can be independently used. The water in the water-cooled evaporator circulates from a storage tank heated by PVT collectors. They examined the impact of source temperature on DHW heating, but the investigation was conducted individually for each of the two sources instead of the simultaneous use of the dual sources. Fine, Friedman and Dworkin (2017) examined a series SAHP system with two cascaded heat pumps. The simulation results showed that the cascaded heat pump system had 37%-68% more annual thermal energy output than the evacuated tube heating system. Dannemand, Perers, and Furbo (2019) developed and tested a SAHP system for DHW. The system had two tanks: a cold buffer storage tank and a hot storage tank located respectively on the source side and the load side of the heat pump. PVT collectors could directly charge both tanks. They showed that PVT collectors could solely cover hot water demand on sunny summer days and add a substantial amount of energy to the buffer tank on days with low solar irradiation. More studies of SAHP systems for DHW production are presented in Table A-1 in Appendix A.

2.3.2 SAHP systems for space heating

Space heating is one of the main applications of SAHP systems that have been extensively studied in the literature. Table A-2 in appendix A lists the reviewed studies but only several

representative ones are presented here. Bellos et al. (2016) performed an energetic and financial evaluation of four SAHP systems, namely, an air-source heat pump system with PV modules, a water-source heat pump system with conventional flat solar thermal collectors, a water-source heat pump system with PVT collectors, and a water-source heat pump with PV modules and solar thermal collectors. Each system was examined with different PV or collector areas (no less than 20 m²). The solutions with minimum total costs were compared. It was concluded that the air-source heat pump system with PV modules had the lowest cost if the electricity rate is less than 0.23€/kWh, and otherwise, the water-source heat pump system with PVT collectors had the lowest cost. Plytaria et al. (2018, 2019) extended the work by Bellos et al. (2016) further by adding a PCM layer to the floor for underfloor heating. Adding the PCM layer resulted in an electricity consumption reduction by more than 40%. With the reduced electrical load, they found that the water-source heat pump system with PVT collectors became the most appropriate option with respect to the total cost. However, the simple payback was increased from 10.2 years to 18.3 years after the PCM layer was added. Vallati et al. (2019) used Matlab simulation to investigate the potential benefits of a series SAHP system for space heating in three European cities. With 40 m² PVT collectors and a 4 m³ storage tank, the proposed system could cover up to 70%, 62%, and 47% of the space heating demand in Rome (12.41 MWh), Milan (14.99 MWh), and Cracow (16.94 MWh). Simonetti, Molinaroli, and Manzolini (2019) proposed a series dual-source SAHP system. The composite evaporator could absorb energy from the ambient air and the water circulated from PVT collectors. The system concept was validated in the laboratory, and then a numerical model was developed in Matlab for the optimal design of the composite evaporator. Their results showed that the system COP was increased 14% compared to the standard air-source heat pump system. Del Almo et al. (2020) used TRNSYS simulation to look into the technical and economic

feasibility of a series SAHP system for an educational building in Spain. The system integrated 75 PVT collectors (1.96 m² per panel) and 200 PV modules, a water-to-water heat pump, a seasonal storage (300 m³) on the source side of the heat pump, and a secondary storage on the load side of the heat pump. Their results showed that the heat produced by the PVT collectors could cover 60% of the heating demand of the building, and the simple payback period was 15.4 years.

All aforementioned SAHP systems for space heating have series configuration. Parallel/series configuration is also used in a few studies. For example, Li et al. (2015) developed and implemented model-predictive control algorithms for a SAHP system installed at Purdue's Living Laboratory. Building-integrated PVT collectors were used for preheating the ventilation air, and the warm air was also used as the source of an air-to-water heat pump. The hot water generated by the heat pump was then used for radiant floor heating. Based on the TRNSYS simulation results for a period of one month during the heating season, the SAHP system with model-predictive controls had ~45% energy savings than the baseline none-solar radiant floor heating system.

2.3.3 SAHP systems for both DHW and space heating

SAHP systems for DHW and space heating were extensively studied by IEA SHC Task 44 (Hadorn 2015). Some representative studies are briefly presented below, while the reviewed SAHP studies for DHW and space heating are presented in Table A-3 in Appendix A.

Haller and Frank (2011) used simulation models to compare the performance between series configuration and parallel configuration for space heating and DHW. Based on the simulation results, they developed the criterion to determine whether switching from parallel configuration to series configuration was beneficial. However, the criterion was not

straightforward for use because it required the heat pump COP and collector efficiency for the cases of air and water being the sources of the heat pump. Dott, Genkinger, and Afjei (2012) used the Polysun software to compare nine different SAHP systems for space heating and DHW. The systems varied with the use of solar panel types (e.g., solar thermal collectors, PV modules, and PVT collectors), heat pump sources, and building types. The simulation results showed the main characteristics of the respective systems, but it was challenging to conclude which one was the best. Lerch, Heinz, and Heimrath (2015) used TRNSYS to compare five SAHP systems with a conventional air-to-water heat pump system for space heating and DHW. The five SAHP systems had different configurations, heat storage use, and heat pump sources. The seasonal performance factor (SPF) of the system was one of the major metrics used to compare all systems. The system that enabled the direct use of solar collectors as the additional source for refrigerant evaporation had the highest SPF. Carbonell et al. (2015, 2016) proposed and modeled a SAHP system with an ice storage tank for space heating and DHW. The simulated system was validated with one-year measurements from a pilot project installed in Switzerland with a monitored yearly SPF of 4.6.

In addition to the work related to IEA SHC Task 44, there are many other studies on SAHP systems for space heating and DHW. Poppi et al. (2016) used TRNSYS simulation to investigate the influence of component sizing on energy consumption for two parallel SAHP systems: one with ambient air and the other with borehole as the heat source of the heat pump. Different sizing options were considered for the collector area, the heat exchanger size for DHW preparation, and the heat pump. Emmi, Zarrella, and De Carli (2017) compared four different dual-source SAHP systems for a single-family house in Vicenza, Italy. All systems combined an air-to-water heat pump and a water-to-water heat pump in parallel. The water-to-water heat pump used different sources (e.g., PVT collectors, borehole, and the combination of them) in the four systems. Their

TRNSYS simulation results showed that 1) recharging the borehole in heating-dominated buildings was not an economical solution if there were a few borehole fields; and 2) the solar-air source combination appeared to be the most advantageous one if adequate roof surfaces and storage were available. Sakellariou et al. (2019) modeled a solar-assisted ground source heat pump system for a single-family house in Birmingham, UK. An earth energy bank (EEB) of 47 m³ volume was employed to store thermal energy. The heat pump's source-side loop had a ground heat exchanger and a plate heat exchanger used to couple with the EEB and the solar subsystem with PVT collectors, respectively. The solar heat always contributed to the heat pump operation via the ground heat exchanger. Solar heat could be stored in the EEB in case of no heating load. Sommerfeldt and Madani (2019) conducted a techno-economic analysis of ground source heat pump systems with series-connected PVT collectors for a multi-family building of 2000 m² floor area in Stockholm, Sweden. They found that integrating PVT collectors of 236 m² could reduce the borehole length by 18% or the borehole spacing by 50% while maintaining an equivalent seasonal performance factor of the system without PVT collectors. Simonetti et al. (2020) performed an energetic and economic assessment of three different SAHP systems for a single-family house in Milan, Italy. The three assessed systems included an air-to-water heat pump plus PV modules, a water-to-water heat pump with PVT collectors as the source, and a water-to-water heat pump with dual sources (ambient air and PVT collectors). The analysis was performed for a different number of solar modules and battery sizes. They concluded that the dual-source heat pump system with the largest battery size achieved the highest energy savings (77%) compared to a conventional boiler-based system.

2.3.4 Multifunctional SAHP Systems

A universal definition of multifunctional SAHP systems does not exist in the literature. The desired multiple functionalities can be specified differently for different applications. For residential buildings, it is reasonable to include space heating, space cooling, and DHW when referring to multifunctional heat pump systems. Therefore, a multifunctional SAHP system can be designed by extending from one of the SAHP systems for space heating and SHW, as discussed in Section 2.3.3, to cover space cooling as well. More specifically, the kind of multifunctional SAHP systems of particular interest to this research have the following characteristics:

- A single heat pump contributes to space heating, space cooling, and DHW. Thus, those systems that use non-heat pump equipment (e.g., absorption chillers) or one more heat pump for space cooling are not counted.
- Solar modules (e.g., conventional solar thermal collectors and PVT collectors) are used as the source of the heat pump at least for some of its operational modes. This means that the SAHP system should have series or parallel/series configurations. Simple parallel configurations are excluded because they usually have low solar utilization when low-temperature solar collectors are used.

A number of SAHP systems meeting the above characteristics have been found from the literature review, and they are presented below with an emphasis on the system description.

Chu et al. (2014) presented a multifunctional SAHP system for space heating, space cooling, dehumidification, and DHW in a high-performance house that participated in the 2013 Solar Decathlon. As shown in Figure 2-13, the SAHP system consisted of conventional solar collectors, two thermal storage tanks, and a liquid-to-liquid heat pump. An air-handling unit was

used to heat, cool, and dehumidify the supply air. In the winter, the cold tank was charged with the solar collectors and used as the heat pump's source to maintain the temperature at the bottom of the hot water tank no less than 40°C. The water in the hot tank was used for DHW and space heating needs. In the summer, the heat pump operation is reversed to maintain the temperature at the top of the cold tank no greater than 6°C. To avoid overheating of the hot water tank in the summer, if the temperature at the bottom of the hot tank was above 40°C, the refrigerant flow would bypass the hot water tank, and the heat would be dissipated to the ambient via an outdoor radiator.

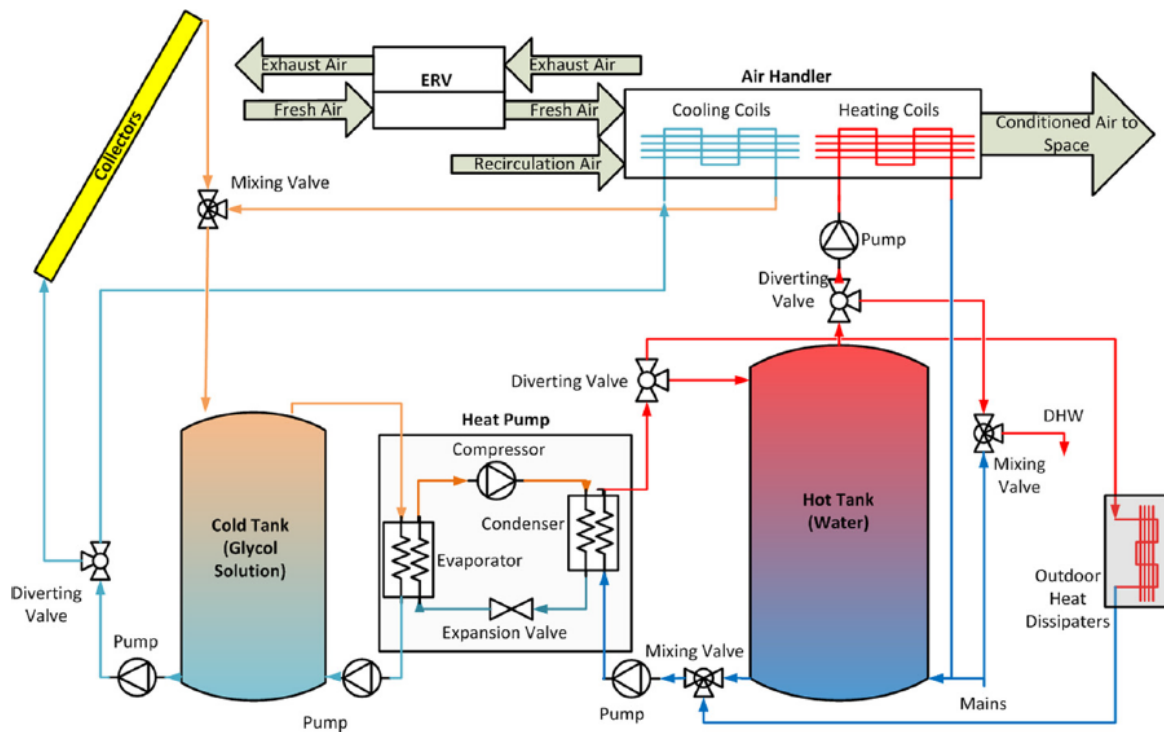
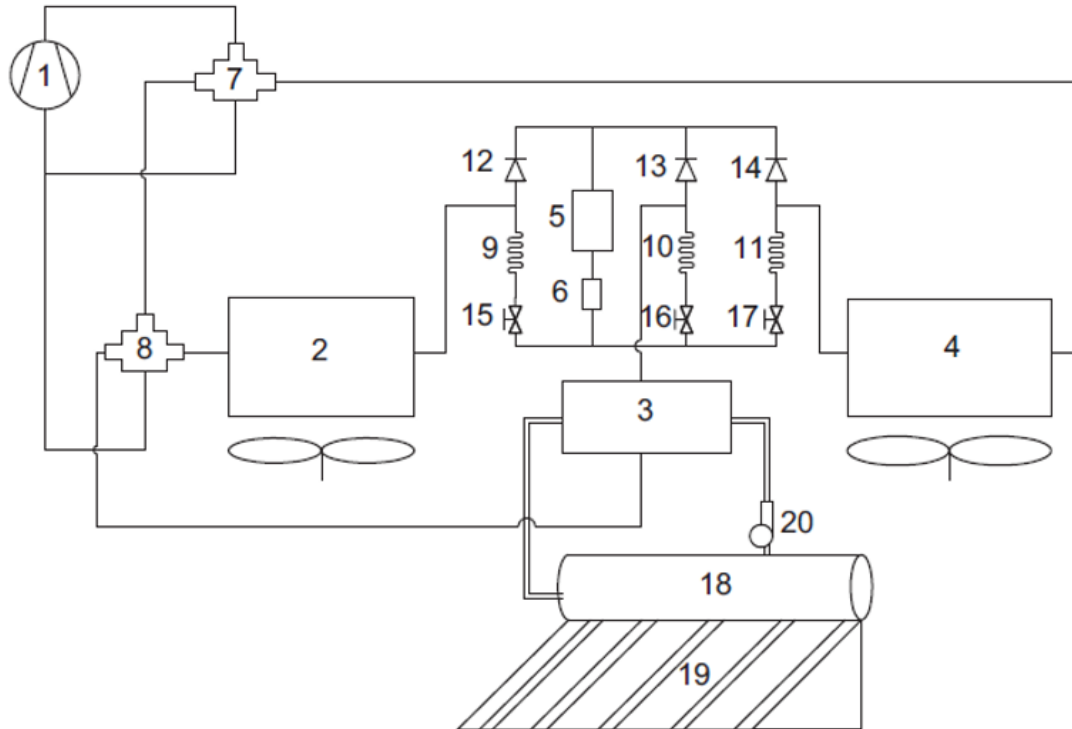


Figure 2-13: The schematic diagram of the SAHP system presented by Chu et al. (2014)

Wang et al. (2011) presented a dual-source multifunctional SAHP system for space heating, space cooling, and DHW heating. Figure 2-14 shows the schematic diagram of the

proposed system. Table 2-2 lists the seven operational modes and the corresponding refrigerant flow paths, where component indices in the flow paths can be found in Figure 2-14. Figure 2-14 and Table 2-2 indicate that 1) the heat pump had ambient air (Modes 1 and 4) and solar-heated water (Mode 5) as its alternative source for heating; 2) the heat pump had dual evaporators (the air heat exchanger and the water heat exchanger) as well, which was used depending on the operational mode; 3) the system provided a defrosting mode using tank water as the source to defrost the outdoor air exchanger (Component 4 in Figure 2-14). An experimental setup was built to verify the system could work in all seven operational modes. However, no details were given on how to determine which source should be used at what conditions. In addition, it is not clear whether the water tank had an auxiliary heating device to maintain the tank temperature setpoint and, if so, whether the system operation would end up using the auxiliary heat as the source of the heat pump at low solar radiation conditions.



1: compressor; 2: indoor air-cooled heat exchanger; 3: water-cooled heat exchanger; 4: outdoor air-cooled heat exchanger; 5: receiver; 6: dry filter; 7–8: four-way valves; 9–11: capillary tubes; 12–14: check valves; 15–17: solenoid valves; 18: insulated water tank; 19: solar collector; 20: water pump.

Figure 2-14: The schematic diagram of the SAHP system presented by Wang et al. (2011)

Table 2-2: Operational modes and corresponding refrigerant circulations in the SAHP system presented by Wang et al. (2011)

Mode number	Operation mode	Refrigerant circulation
1	Space heating	1→7→8→2→12→5→6→17→11→4→7→1
2	Common space cooling	1→7→4→14→5→6→15→9→2→8→1
3	Common solar water heating	The refrigeration circulation stops.
4	Heat pump water heating	1→7→8→3→13→5→6→17→11→4→7→1
5	Solar-assisted space heating	1→7→8→2→12→5→6→16→10→3→8→1
6	Space cooling and heat pump water heating	1→7→8→3→13→5→6→15→9→2→8→1
7	Energy-saving defrosting	1→7→4→14→5→6→16→10→3→8→1

Cai et al. (2016, 2017) proposed and studied the operation of a dual-source multifunctional heat pump system for space heating, space cooling, and DHW. As shown in Figure 2-15, the system consisted of solar thermal collectors, two air heat exchangers (one indoor and one outdoor), two water tanks (one DHW tank and one solar water tank), a compressor, capillary throttling devices, water pumps, and a plate heat exchanger coupling the water loop and the refrigerant loop. The system could support the following five operational modes: 1) air source for DHW heating, 2) solar water source for DHW heating, 3) air source for space heating, 4) solar water source for DHW heating, and 5) air source for space cooling. They developed a numerical model for the system and verified the model with laboratory tests. Through simulations, Cai et al. (2017) found that using the air source was superior to the solar water source for space heating when the ambient temperature was above 4°C, and the solar water source was more efficient for DHW heating when the ambient temperature was below 3°C.

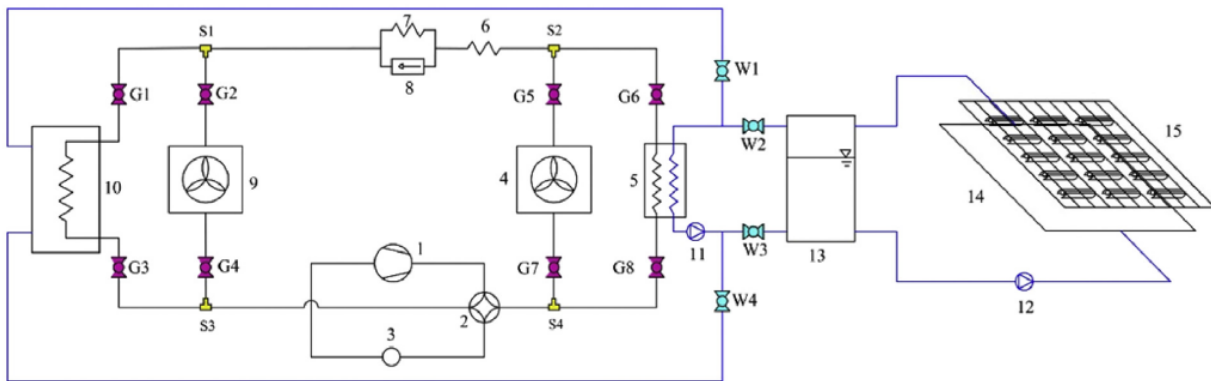


Figure 2-15: The schematic diagram of the SAHP system presented by Cai et al. (2016)

Entchev et al. (2014) proposed a solar-assisted ground source heat pump system for space heating, space cooling, DHW, and electricity generation. As Figure 2-16 shows, the system

consisted of PVT collectors, a solar tank, a hot water tank, a cold water tank, and a ground source heat pump with boreholes. The solar tank was used to preheat the city water before entering the hot water tank and transfer heat energy to the hot water tank at applicable conditions. The hot water tank had two immersed heat exchangers for space heating and DHW. The cold water tank was used to provide chilled water for cooling in the summer season. The ground source heat pump was equipped with a desuperheater to preheat the city water for DHW use. The SAHP system was compared with a reference system having a boiler and a chiller for space conditioning and DHW in Ottawa, Canada. TRNSYS simulation results showed that the multifunctional SAHP system had 58% energy saving than the reference system.

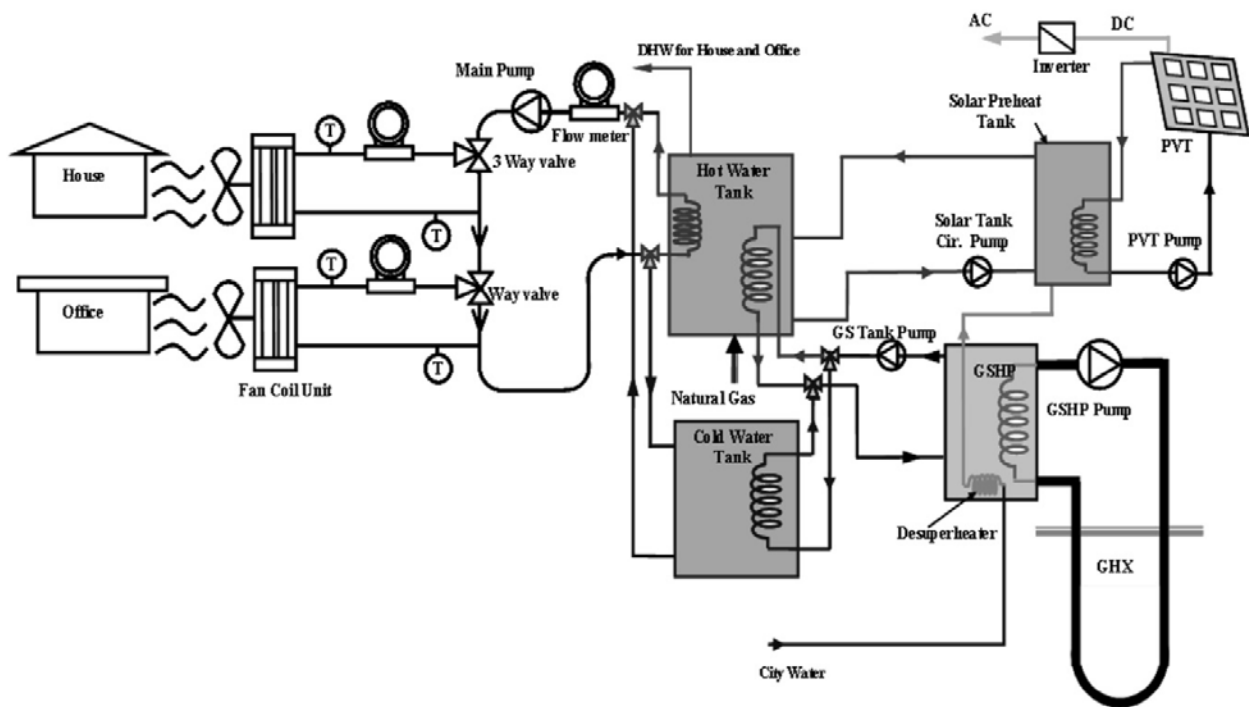


Figure 2-16: The schematic diagram of the SAHP system presented by Entchev et al. (2014)

Kang et al. (2016) investigated an air-based multifunctional SAHP system and evaluated its performance for residential buildings located in Incheon, Korea, and Ottawa, Canada. As Figure

2-17 shows, the system consisted of a horizontal ground-to-air heat exchanger, an air-to-water heat pump, a hot water storage tank, and PVT collectors. The hot water tank was used for space heating and DHW. In summer, the chilled water from the heat pump was directly circulated to the fan coil units. In winter, the heat pump was turned on when the temperature at the bottom of the tank was lower than 40°C and was turned off when the temperature was above 45°C. Generally, the ambient air was preheated or precooled by the ground-to-air heat exchanger before entering the heat pump's outdoor coil. In winter, the PVT collectors were used to preheat the ambient air when the average air temperature behind the PVT collectors was 5°C higher than the air temperature near the outlet of the ground heat exchanger. The PVT collectors would not be used for preheating after the temperature difference between the air behind the PVT collectors and the air near the outlet of the ground heat exchanger fell below 2°C. Based on the simulation results, Kang et al. (2016) found that the SAHP system had 45% (in Incheon) and 42% (in Ottawa) energy savings than a reference conventional system using a boiler for space heating and DHW and chiller for space cooling.

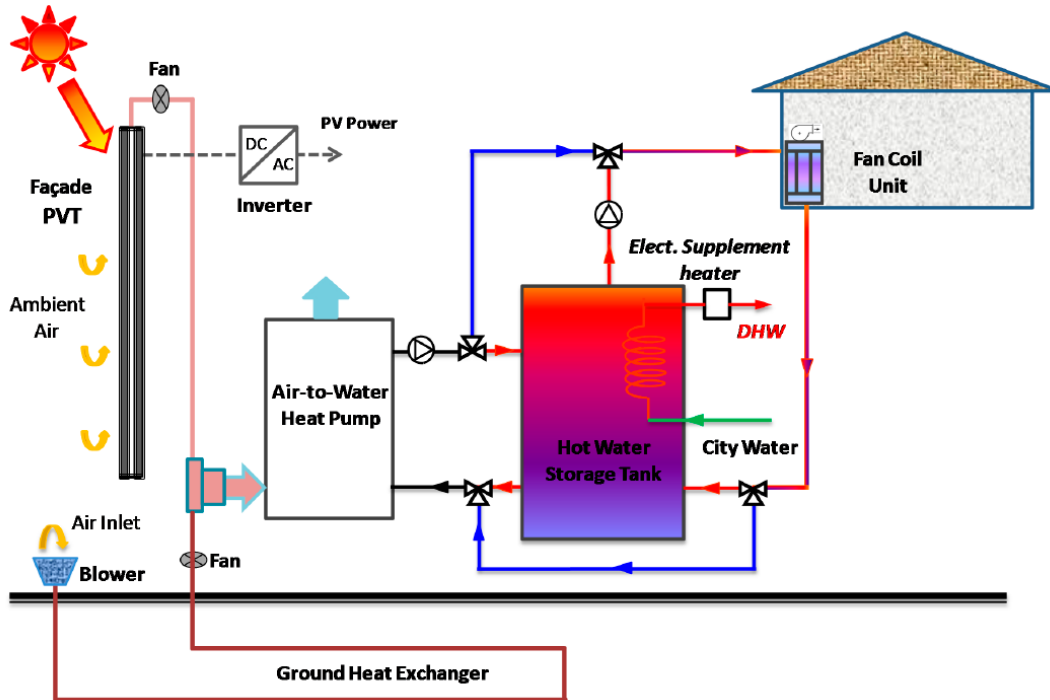


Figure 2-17: The schematic diagram of the SAHP system presented by Kang et al. (2016)

Besagni et al. (2019) experimentally investigated a multifunctional SAHP system for a detached house in Milan. As Figure 2-18 shows, the SAHP system had PVT collectors, a DHW tank, an intermediate-temperature storage tank used as the water source of the heat pump, an intermediate storage tank used to provide water to fan coils, and a heat pump. The heat pump was equipped with an air-source evaporator and a water-source evaporator connected in series. The glycol-water solution in the PVT collector loop could be circulated through the DHW tank or the intermediate-temperature storage tank, depending on the two tank temperatures. The heat pump was used to provide space heating, space cooling, and DHW. In the space heating mode, the water source was used if the tank water temperature was higher than the ambient air. In the space cooling mode, only the air source was used for the heat pump operation. However, the glycol-water solution was circulated between the intermediate storage tank and the PVT collectors at night to

reduce the tank temperature in the coldest hours of the day while the air source was used at other times. Besagni et al. estimated that their SAHP system had 15.4% lower daily-averaged energy consumption than the baseline air-to-water heat pump system.

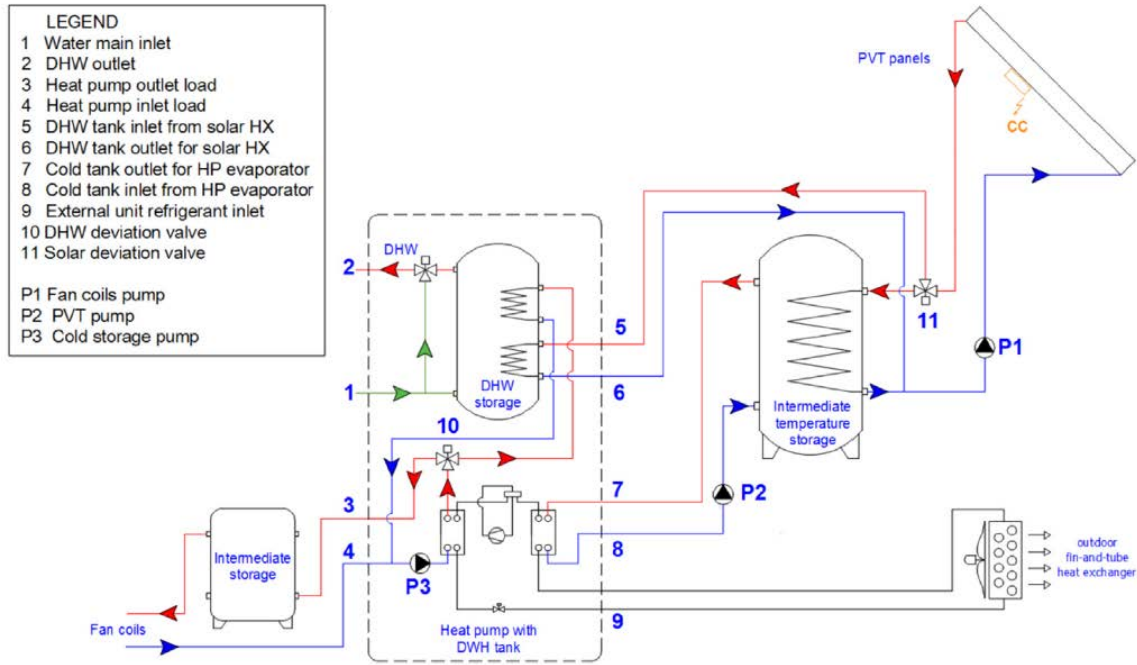


Figure 2-18: The schematic diagram of the SAHP system presented by Besagni et al. (2019)

2.4 Studies on using PVT collectors for radiative cooling

At the University of Applied Sciences in Stuttgart, Germany, Eicker and Dalibard (2011) used uncovered PVT collectors to generate cold water, which was then used to charge either the PCM ceiling or the storage tank. The concept was implemented in a residential zero energy building and tested under the climate conditions of Madrid, Spain. The measured radiant cooling power was in the range between 60 and 65 W/m² when the PVT collectors were used to cool the storage tank and in the range between 40 and 45 W/m² when the collectors were used to cool the PCM ceiling directly. Eicker and Dalibard also performed a simulation analysis, and they found

that the simulated summer cooling energy production per m² of PVT collector was 51 kWh in Madrid, Spain, and 55 kWh in Shanghai, China. Palla et al. (2014) investigated the potential of using a new prototype of PVT collectors for space heating, space cooling, and electricity production in six different locations using TRNSYS simulation. They concluded that the highest radiative cooling potential could be achieved in cold and moderate climates where cooling was required temporarily. Cremes et al. (2015) conducted experiments to investigate the impact of backside insulation on the performance of two differently design PVT collectors. They determined that backward insulation improved the PVT collector efficiency by 20-30% for both heating and radiative cooling applications. Gurlich, Dalibard, and Eicker (2017) compared the use of PVT collectors and the combined use of thermal collectors and PV modules via TRNSYS simulations. The PVT collectors had triple roles: electricity generation, thermal energy collection, and nighttime radiative cooling. Based on the simulations for three residential buildings in Portugal, Italy, and England, they found that PVT collectors using PVT collectors had ~6% higher exergetic efficiency than the combined use of thermal collectors and PV modules. However, from the economic point of view, using PVT collectors was more economically favorable if the additional cooling and electricity production was sufficient to compensate for the loss of heat gains.

Researchers at the Technical University of Denmark have also investigated the radiative cooling aspect of water-based PVT collectors. Pean et al. (2016) investigated the impact of environmental parameters on the nighttime radiative cooling potential of unglazed PVT collectors based on experiments. They indicated that the cooling output was affected most by the air temperature. Relative humidity, wind speed, and cloudiness were other parameters with a substantial impact on the cooling output. Bourdakis et al. (2016) experimentally tested a system

integrating PCM panels and PVT collectors. The cold water from PVT collectors was used to charge PCM ceiling panels at night.

At the University of Wollongong in Australia, Lin et al. (2014) studied an air-based ceiling ventilation system consisting of PVT collectors and a PCM ceiling. The PVT collectors were used to generate electricity, solar heating during winter days, and radiative cooling during summer nights. The system was evaluated with TRNSYS simulation based on a Solar Decathlon house. They showed that the average temperature reduction of air flowing through the PVT collectors was 2.4°C during the nighttime. On summer nights, the air temperature was decreased as much as 3°C by passing through the PVT panels. In a subsequent study, Fiorentini, Cooper, and Ma (2015) combined a standard reverse-cycle heat pump with air-based PVT collectors and PCM thermal storage. The PVT collectors were used to warm the fresh air during the heating season and to cool the fresh air during the cooling season. After being heated or cooled, the fresh air was supplied to space directly if ventilation was needed; and otherwise, the air was sent to the PCM for thermal storage. The thermal storage could be used either directly to condition the space or precondition the air entering the air-handling unit.

2.5 Summary of literature review

SAHP systems have been commonly used for space heating and DHW generation. By expanding the functionality to include space cooling, a multifunctional SAHP system can be developed. Once developed, the multifunctional SAHP system is expected to have a couple of major advantages: 1) reduce the number of equipment by using the heat pump for multiple purposes, and 2) increase the energy efficiency by coupling the heat pump with renewable energy components. A few multifunctional SAHP systems have been proposed. The functionality of space

cooling has been mostly achieved with the use of two sources: using ambient air and water from the collectors (Cai et al. 2016, Besegni et al. 2019) or using ground and air (or water) from the collectors (Wang et al. 2011, Entchev et al. 2014). In addition, some of the previous work on multifunctional SAHP systems focused on the demonstration of individual operational modes at laboratory conditions. However, much research is needed on the system operation with different modes at dynamic load conditions.

Using PVT collectors for radiative cooling is a relatively new concept. A number of studies, either numerical or experimental, have been performed to estimate the nighttime radiative cooling potential of PVT collectors. Because the cooling power is low and dependent on climate conditions, coupling radiative cooling of PVT collectors with heat pump seems to a promising approach because it shares the similar principle of SAHP for heating. However, no research has been found on the development of a multifunctional SAHP system for space heating, space cooling, and DHW based on PVT collectors. This research aims to fill in the knowledge gap by proposing a novel multifunctional SAHP system and evaluating its performance with TRNSYS simulations.

CHAPTER 3: SYSTEM DESIGN

3.1 Multifunctional solar-assisted heat pump system prototype design

Figure 3-1 shows the schematic of the multifunctional solar-assisted heat pump system prototype. Major components of the system include unglazed PVT collectors, a liquid-to-liquid heat pump, a thermal storage tank for space conditioning, a DHW tank, two instantaneous electric water heaters (for space heating and DHW production), four circulating pumps, and a number of valves for flow direction controls. Because of the need for freezing protection in cold climates, a mixture of propylene glycol and water in the ratio of 30% to 70% by volume is used as the heat transfer medium between the PVT collectors, the storage tanks, and the heat pump. Though it is possible to circulate glycol solution directly through the plastic tubes embedded in the floor, a plate heat exchanger is used between the PVT-HP plant and the radiant floor, which has both positive and negative impacts. The advantage comes from the reduction of pressure drop across the radiant floor as water is less viscous than glycol. However, on the other hand, using the heat exchanger introduces effectiveness losses.

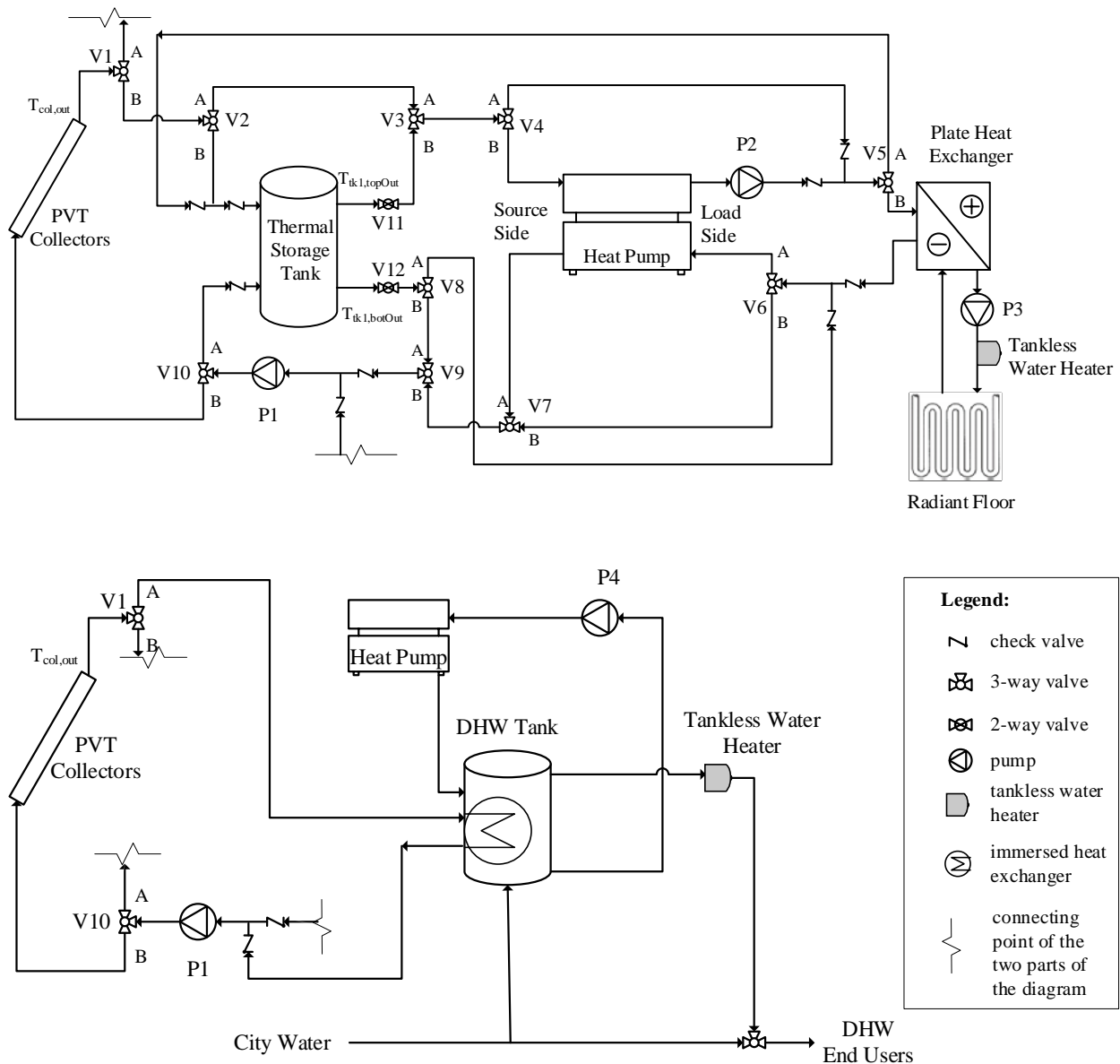


Figure 3-1: Schematic diagram of the proposed multifunctional SAHP system: the upper part for space conditioning and the lower part for DHW production

There exist different types of PVT collectors. Unglazed flat PVT collectors are used in this study because they not only serve the purpose of solar energy collection for heating but also act as radiative cooling panels to dissipate thermal energy to the sky in the cooling season. Glazed

collectors are favorable for solar collection, but they are less effective for radiative cooling (Lämmle et al. 2020, Eicker and Dalibard 2011). In addition, as will be discussed later, the collectors are sometimes used in the system as a heat exchanger for convective heat transfer from the ambient air to the glycol solution. In this respect, unglazed PVT collectors are preferable to glazed ones. Unglazed PVT collectors can generate low-temperature water up to 50°C (Lämmle et al. 2020), which is a major reason behind the use of hydronic radiant floor systems in the building. Even so, it is not reasonable to expect the PVT collectors to fully meet the heating load. Therefore, a liquid-to-liquid heat pump is used. When the heat pump is used for space conditioning, its source side connects to either the PVT collectors or the thermal storage tank, and its load side connects to the radiant floor system via the heat exchanger. The DHW tank water is heated by PVT collectors and the heat pump's desuperheater. The desuperheater uses superheated gases from the heat pump's compressor to heat the water circulated from the DHW tank. In addition, an instantaneous electric heater is placed after the DHW tank to ensure the hot water temperature has reached 49°C before being tempered with the city water.

3.2 Sequence of system operation

The seemingly complex piping (Figure 3-1) results from the system's high flexibility to support many operational modes. Figure 3-2 sketches the sequence of system operation. All operational modes are briefly described as follows.

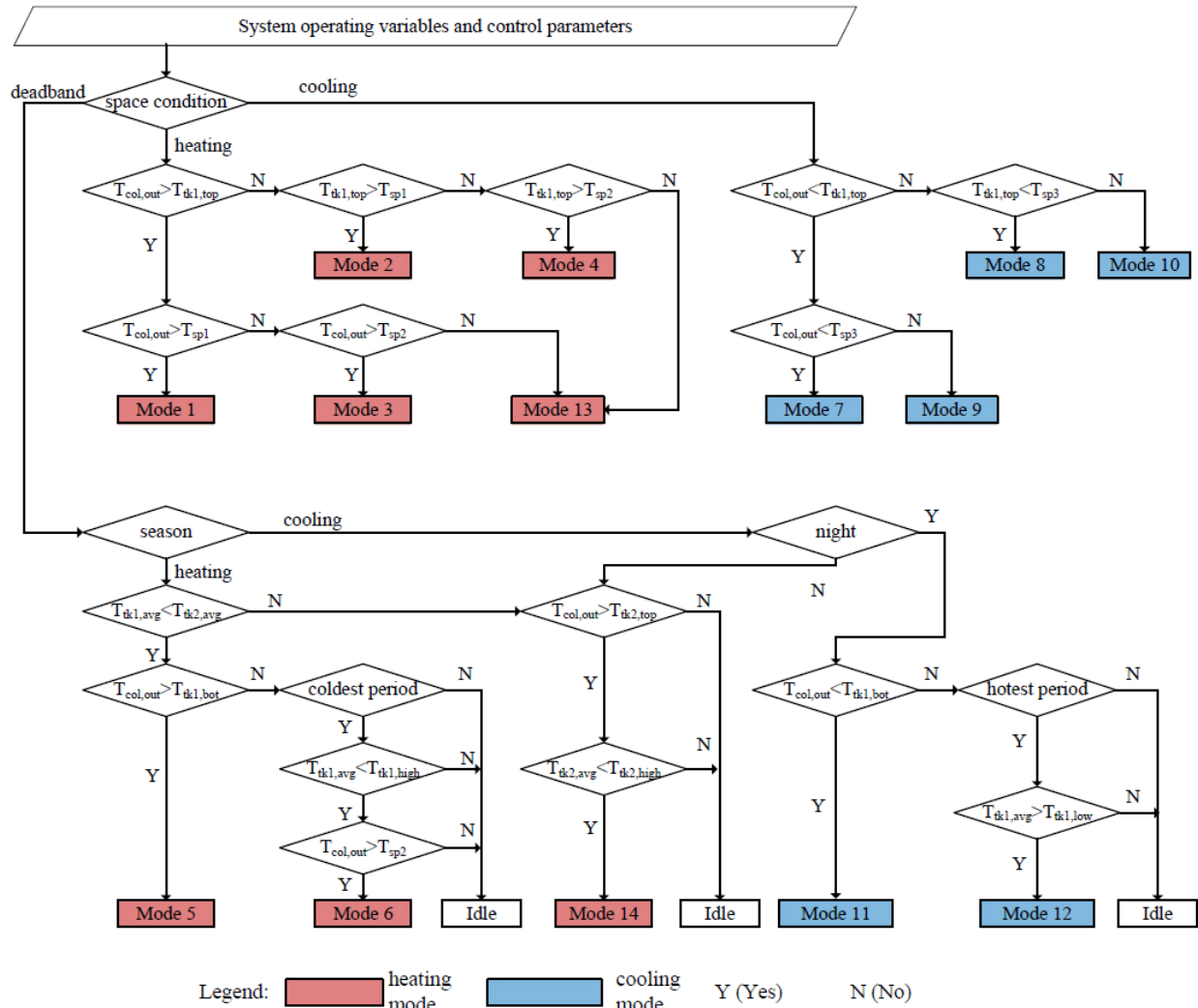


Figure 3-2: Flowchart diagram showing the system control sequence

Mode 1: PVT collectors for space heating. Under this mode, Pump P1 is on, and it drives the glycol solution flowing from the PVT collectors to the plate heat exchanger. Mode 1 operates when 1) the space calls for heating, 2) the glycol outlet temperature ($T_{col,out}$) from the PVT collectors is greater than the temperature limit (T_{sp1}) acceptable for space heating, and 3) $T_{col,out}$ is dead greater than the thermal storage tank's top outlet temperature ($T_{tk1,top}$, see Figure 3-1). The third condition is used because the system has two alternative sources (PVT collectors and the storage tank), and the source with a higher temperature is applied first.

Mode 2: Thermal storage tank for space heating. Under this mode, Pump P1 is on, and it drives the glycol solution flowing from the thermal storage tank to the plate heat exchanger. Mode 2 operates when 1) the space calls for heating, 2) $T_{tk1,top} > T_{sp1}$, and 3) $T_{tk1,top} > T_{col,out}$.

Mode 3: PVT-HP for space heating. In this mode, Pump P1 circulates the glycol solution between the collectors and the heat pump, while Pump P2 circulates the glycol between the heat pump and the plate heat exchanger. Because PVT collectors are located on the source side of the heat pump, the low temperature of the glycol from the heat pump's evaporator enhances solar utilization. Mode 3 operates when 1) the space calls for heating, 2) $T_{sp1} \geq T_{col,out} > T_{tk1,top}$, and 3) $T_{col,out}$ is greater than the low-temperature limit (T_{sp2}) for heat pump running. It is worth noting that this mode works independently of solar radiation. At times of no solar radiation (e.g., cloudy days and nights), the collectors simply play the role of a convective heat exchanger to transfer energy from the ambient air to the glycol solution.

Mode 4: Tank-HP for space heating. In contrast to Mode 3, this mode uses the thermal storage tank as the heat pump's source. Mode 4 operates when 1) the space calls for heating, 2) $T_{sp1} \geq T_{tk1,top} > T_{col,out}$, and 3) $T_{tk1,top} > T_{sp2}$.

Mode 5: PVT for storage tank water heating. By running Pump P1, this mode uses the collectors to charge the storage tank for heating. This mode operates when 1) the space does not call for heating, 2) the system runs in the heating season, and 3) $T_{col,out}$ is greater than the storage tank's bottom outlet temperature ($T_{tk1,bot}$, see Figure 3-1). The second condition is needed because the system has only one thermal storage tank that is used to store warm water in the heating season and cold water in the cooling season. Therefore, a seasonal changeover point is required to determine the usage of the storage tank.

Mode 6: PVT-HP for storage tank heating. In literature, it is common to use the storage tank as the source of the heat pump for heating, as described in Mode 4. Up to our best knowledge, the storage tank has never been charged by the heat pump in previous studies of solar-assisted heat pump systems. Mode 6 is proposed in our work for the following two reasons. Firstly, because the storage tank has a small capacity intended for daily cycling, the depletion of the tank (i.e., $T_{tk1,top} < T_{sp2}$) would occur in many days if Mode 5 was merely relied on for tank charging. Secondly, using collectors as the heat pump's source increases solar utilization, as explained in Mode 3. Mode 6 is used under the following conditions: 1) $T_{col,top} > T_{sp2}$, 2) neither of Mode 1 to Mode 5 is activated, 3) the system runs in the predefined coldest period of time, and 4) the average tank water temperature ($T_{tk1,avg}$) is less than the high limit for heat pump charging ($T_{tk1,high}$). Note that in the third condition, the coldest period is only part of the heating season when the storage tank is likely depleted.

In addition to Modes 1 to 6 for space heating, the system has another 6 modes (Modes 7 to 12) for space cooling. The modes for space cooling correspond to those for space heating but with the following major changes:

- The space calls for cooling in Modes 7-10, and the tank is charged for cooling storage in Modes 11 and 12.
- The heat pump runs in the cooling mode in Modes 9, 10, and 12.
- Instead of using T_{sp1} , a new control parameter T_{sp3} is used in Modes 7 and 8 to indicate the upper boundary to circulate the glycol from the collectors or the storage tank directly for space cooling.

- When comparing $T_{tk1,top}$ with $T_{col,out}$ in Modes 7-10, their relations are reversed from those in Modes 1-4. In addition, the conditions based on T_{sp2} are not used.
- Modes 11 and 12 are used in the cooling season, and they are considered only at nighttime when radiative cooling is possible for conventional PVT collectors. Mode 11 has the condition $T_{col,out} < T_{tk1,bot}$, which differs from Mode 5. Mode 12 has a low limit for the average tank water temperature ($T_{tk1,low}$) instead of the high limit as used in Mode 6.

As discussed earlier, the heat pump uses either PVT collectors (Mode 3) or the storage tank (Mode 4) as the source for space heating. Both modes have a low-temperature limit setting for the glycol entering the heat pump's evaporator. If neither of the collectors and the storage tank can work as the heat pump's source, an instantaneous electric water heater is relied on for space heating, which is labeled as Mode 13 in Figure 3-2.

Relative to space conditioning, DHW heating is much simpler. If PVT collectors are not used in any of the modes for space conditioning, they are used to heat the water in the DHW tank when the following two conditions are satisfied: 1) $T_{col,out}$ is greater than the DHW tank temperature at the glycol inlet ($T_{tk2,top}$), and 2) the DHW tank water average temperature ($T_{tk2,avg}$) is less than a predefined high limit ($T_{tk2,high}$), the purpose of which is to avoid overheating the DHW tank. The operation of using collectors to heat the DHW tank is regarded as Mode 14 in Figure 3-2. In this mode, the heated glycol solution flows through the immersed heat exchanger in the DHW tank to heat the cold makeup water from the city mains. An instantaneous electric water is then used to ensure the desired water temperature setpoint at 49°C.

As Figure 3-1 shows, the system has many valves, including 3-way diverting valves, 3-way mixing valves, 2-way valves, and check valves. Of the 3-way valves, V3, V7, and V9 are mixing valves while all others are diverting valves. Wherever a 3-way mixing valve is used, it is functionally equivalent to the use of two check valves on the two branch ports, as illustrated in several places in Figure 3-1. All 3-way and 2-way valves are used as two-position valves for the purpose of flow direction controls. Their positions and the status of four circulating pumps are listed in Table 3-1 for all operational modes that have been presented. In Table 3-1, the 3-way valve position is indicated by specifying which branch port (A or B) is fully open, while the 2-way valve position is indicated by specifying whether it is open or close. The status of P4, the pump used for circulating water between the DHW tank and the heat pump's desuperheater, is marked as on/off when the heat pump runs because the pump status also depends on the DHW tank water temperature.

Table 3-1: The schedule of pumps and valves of the multifunctional SAHP system

Pump and Valve Status		Operational Mode								
		1 & 7	2 & 8	3 & 9	4 & 10	5 & 11	6 & 12	13	14	Idle
Pump	P1	on	on	on	on	on	on	off	on	off
	P2	off	off	on	on	off	on	off	off	off
	P3	on	on	on	on	off	off	on	off	off
	P4	off	off	on/off	on/off	off	on/off	off	off	off
Valve	V1	B	B	B	B	B	B		A	B
	V2	A	-	A	-	B	A		-	-
	V3	A	B	A	B	-	A		-	-
	V4	A	A	B	B	-	B		-	-
	V5	B	B	B	B	-	A		-	-
	V6	B	B	A	A	-	A		-	-
	V7	B	B	A	A	-	A		-	-
	V8	-	-	-	-	B	A		-	-
	V9	B	B	B	B	A	B		-	-
	V10	B	A	B	A	B	B		B	-
	V11	close	open	close	open	close	close		close	close

Table 3-1 cont: The schedule of pumps and valves of the multifunctional SAHP system

Pump and Valve Status		Operational Mode								
		1 & 7	2 & 8	3 & 9	4 & 10	5 & 11	6 & 12	13	14	Idle
Valve	V12	close	close	close	close	open	open		close	close

3.3 Reference system

A reference is needed in this research to facilitate the performance evaluation of the multifunctional SAHP system. Some performance metrics (e.g., the percentage energy savings and the simple payback period, to be discussed in Chapter 5) cannot be quantified without a reference system. There are many options for the reference system definition. However, it makes more sense to define one common system in the field as a reference. According to the Residential Energy Consumption Survey (EIA 2018), a central system with a warm-air furnace and an air conditioner is the most common system type for space heating and cooling. A natural gas-fired water heater is also the most common equipment for DHW production. Considering that the multifunctional SAHP system uses a heat pump and electricity as the only fuel type, the reference system is defined to have a split air-source heat pump (ASHP) system for space heating and cooling and an electric water heater for DHW production. Electric resistance is used as auxiliary space heating.

The ASHP may operate in one of the following modes if it is on: the cooling mode, the compressor heating mode only, the compressor heating plus auxiliary heating mode, and the auxiliary heating mode only. The cooling mode is triggered on whenever the space temperature is above the cooling setpoint. Which heating mode is used depends on the space temperature and the outdoor air temperature. The compressor heating mode only is used if 1) the space temperature is below the heating setpoint, and 2) the outdoor air temperature is above the auxiliary heater lockout temperature, beyond which the auxiliary heater is disabled. The auxiliary can be used together with

compressor heating if 1) the space temperature is below the heating setpoint minus 0.5°C , and 2) the outdoor air temperature is above the compressor lockout temperature but below the auxiliary heater lockout temperature. The auxiliary heating only mode is used if 1) the space temperature is below the heating setpoint, and 2) the outdoor air temperature is no greater than the compressor lockout temperature.

A 60-gallon (227 L) electric water heater is used in the reference system for DHW production. The tank has its thermostat setpoint at 49°C .

3.4 Boundary considerations for the system design

The system presented in Section 3.1 is called a prototype because it considers a comprehensive set of possible operations. The system prototype can be customized for different conditions. Two boundary conditions that will probably affect the system design are the climate and the building.

3.4.1 Climate conditions

The climate affects solar radiation, building thermal loads, and radiative cooling. Therefore, the operational modes discussed in Section 3.2 may play different roles, and the system performance will vary in different climates. This work considers two locations (i.e., Baltimore, MD, and Las Vegas, NV) with quite different climate conditions. Baltimore has a mixed climate, cold in winter and hot in summer, and it has annual heating degree days (HDDs) of 2495°C-day and cooling degree days (CDDs) of 704°C-day . In contrast, Las Vegas has a milder and dryer climate (HDDs= 1097°C-day , CDDs= 1929°C-day) (ASHRAE 2017). All degree days are calculated with a base temperature of 18.8°C . Figure 3-3 shows the monthly average temperature

profiles for the outdoor dry-bulb temperature and the effective sky temperature for the two locations. The temperature profiles are based on the Typical Meteorological Year (TMY-2) weather database, which offers daily values of the outdoor dry-bulb temperature, humidity ratio, wind speed, solar irradiance, cloud coverage and so on. The outdoor dry-bulb temperatures are directly available from the TMY-2 weather database, but the effective sky temperatures are calculated from TMY-2 weather data fields using the TRNSYS software.

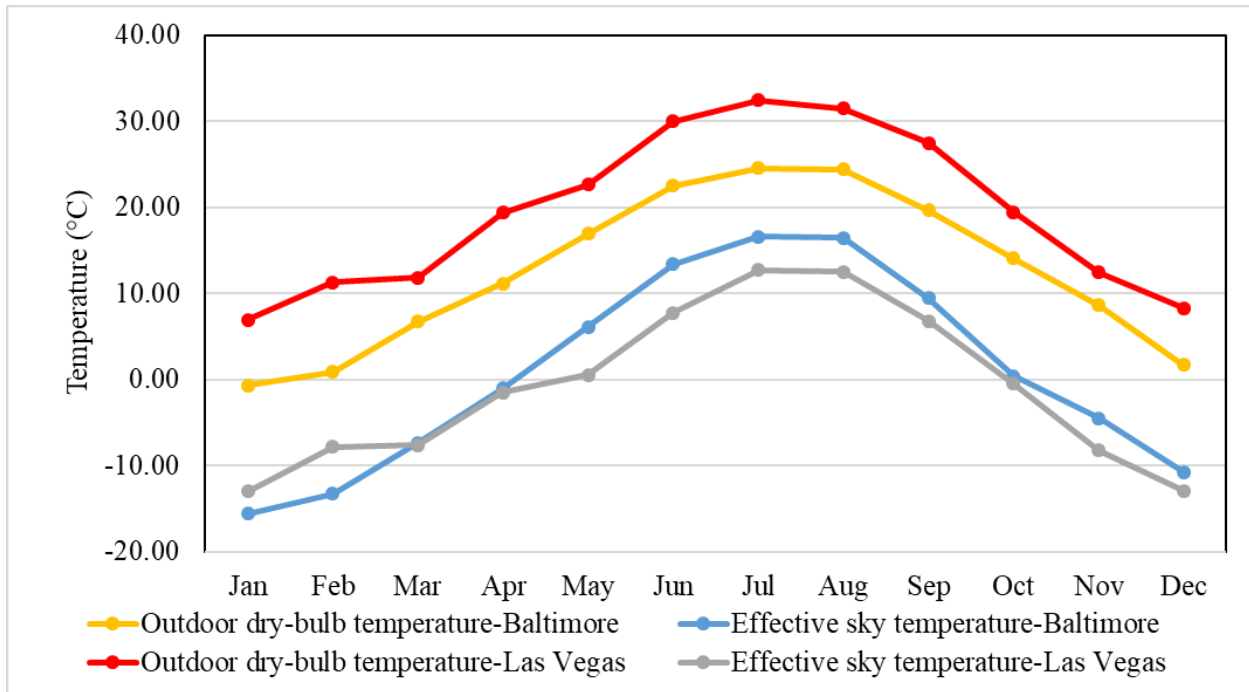


Figure 3-3: Profiles of the monthly average outdoor dry-bulb temperature and the monthly average effective sky temperature

3.4.2 Building description

The multifunctional SAHP system can be used for both residential and commercial buildings. Because this study has its focus on residential buildings, a hypothetical single-family house is created to investigate the system performance. The house has one floor with a total area of 200 m². The floor has a rectangular shape with an aspect ratio of 0.86. A slab-on-grade floor

and wood-frame constructions are assumed. The house has a flat roof with a floor-to-ceiling height of 2.44 m. On each façade, windows occupy 2 m². Note that the house geometry and construction are more simplified than real buildings. This simplification does not sacrifice the value of this research because building thermal loads are the primary concerns.

Regarding the thermal performance of exterior building envelope, Table 1 lists the U-factors and R-values that meet the minimum code requirement of the International Energy Conservation Code for residential buildings (IECC 2006). The U-factor refers to the heat loss coefficient, including the construction and the air films on both sides of the envelope. The R-value refers to the thermal resistance of the insulation layer only. Because the code requirement may vary with climates, Table 3-2 provides the thermal performance of the building envelope for both Baltimore, MD and Las Vegas, NV, the two locations chosen for studying the impact of climate on system operation and performance.

For the reference system, the house has conventional slab-on-grade floor. However, for the multifunctional SAHP system, the house has hydronic radiant floors constructed with an embedded surface system (Babiak, Dusan, and Olesen 2007). With this construction, water tubes are embedded in the surface of the building floor, and the surface layer with embedded water tubes is insulated from the concrete slab.

An air change rate of 10 at 50 Pa is assumed for the air infiltration. Based on European Standard SIA 2024, internal heat gains from lights, electrical equipment, and people are 9.72 kJ/(m²h), 28.80 kJ/(m²h), and 5.04 kJ/(m²h), respectively (SIA 2006).

Table 3-2: Thermal performance of exterior building envelope

Building Envelope	Thermal Performance	
	Baltimore	Las Vegas
Roof	U-factor=0.170 W/(m ² K)	U-factor=0.199 W/(m ² K)
Ground Floor	R-value=2.64 m ² K/W	R-value=0.88 m ² K/W
Exterior Walls	U-factor =0.465 W/(m ² K)	U-factor =0.465 W/(m ² K)
Windows	U-factor =1.69 W/(m ² K) SHGC=0.66	U-factor =1.12 W/(m ² K) SHGC=0.4

3.5 Component sizing

Components are sized on the basis of load calculation and sensitivity analysis. Space heating and cooling loads are determined by pre-running the annual simulation of the building while keeping the space air temperature in the desired range. The peak heating and cooling loads are used to size the heat pumps. Load calculation, engineering judgments, and the residential code requirements (IECC 2006) are used to size other components such as the pumps and the fan. Sensitivity analysis is performed to size the PVT collectors and the thermal storage tank, as to be discussed in Chapter 5.

CHAPTER 4: SYSTEM SIMULATION

In the present, there exist a large number of building energy simulation programs, which may vary in different aspects, such as modeling features and capabilities, ease of use, validation effort, and source availability (Crawley et al. 2008). The TRNSYS software is selected for this research mainly because of the following considerations. First, the TRNSYS software has a rich library of validated component models (e.g., solar collector, PV, and energy storage) commonly found in solar-based thermal and electrical energy systems. The strong capability of modeling solar systems has made TRNSYS the most suitable choice in this study. Secondly, the TRNSYS software is featured with its open and modular structure, which means that 1) each component, representing either a real physical device or a utility tool (e.g., data reader, printer, and plotter), is implemented as an individual subroutine; and 2) the source code of the component models in the library is available to the user. The open modular feature of TRNSYS facilitates the creation of new components and the modification of existing components, which are essential to simulate novel systems. Thirdly, the TRNSYS software has a graphical user interface, through which components can be dragged, dropped, and connected to form a whole system. This graphical user interface significantly eases the use of the TRNSYS software.

TRNSYS components are usually referred to as Types. A Type is defined with its PARAMETERS, INPUTS, OUTPUTS, and DERIVATIVES. Theoretically, both PARAMETERS and INPUTS are the inputs of a TRNSYS component, but they are distinguished according to whether their values change with time. PARAMETERS are time-independent inputs such as the volume of a water storage tank and the area of solar collectors, whereas INPUTS are time-dependent inputs such as the ambient air temperature and the water flow rate of a tank connection.

During simulation, a TRNSYS component model turns the current values of PARAMETERS and INPUTS into OUTPUTS, some of which may be used as the inputs for the downstream components. For those components that solve differential equations numerically, DERIVATIVES are needed to specify the initial values, such as the initial temperatures of various nodes in a thermal storage tank or the initial zone temperatures in a multi-zone building. More details about the aforementioned TRNSYS terminologies can be found in Klein et al. (2018). Major components used to model the multifunctional SAHP system in TRNSYS are presented in this chapter.

4.1 Type 560: PVT solar collectors

TRNSYS Type 560 intends to model unglazed sheet-and-tube PVT solar collectors, the schematic of which is shown in Figure 4-1. The collector comprises of PV cells, a thin adhesive layer, an absorber plate in thermal contact with water tubes, and a layer of thermal insulation at the back of the PVT collector. Because the heat collected by the PV cells is transferred to the absorber plate by conduction, the adhesive layer needs to be thermally conductive but electrically insulative materials such as Silicon adhesive and epoxy glue.

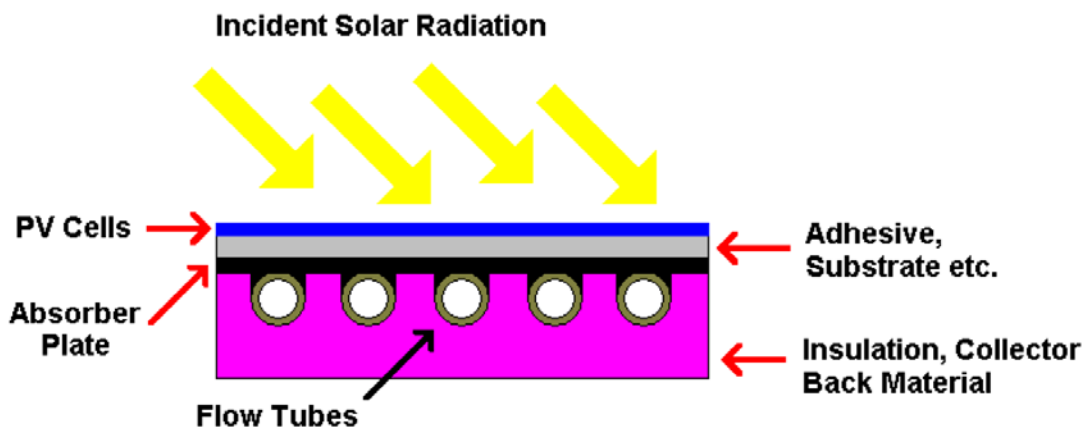


Figure 4-1: PVT schematic (Klein et al. 2018)

In TRNSYS Type 560, the PVT collector is modeled by establishing the energy balance equations respectively for the PV cells, the absorber plate and the tube, and the fluid in the tube. These energy balance equations are briefly described next, and detailed discussions of the model can be found in Klein et al. (2018).

For the PV cells, the energy balance equation is written as:

$$S - h_c(T_{PV} - T_a) - h_r(T_{PV} - T_{sky}) - \frac{T_{PV} - T_{abs}}{R_1} = 0 \quad (4-1)$$

where, S is the absorbed solar radiation for thermal energy collection (W); T_{PV} , T_a , T_{sky} , and T_{abs} represent the cell temperature (°C), the ambient air temperature (°C), the effective sky temperature (°C) and the absorber plate temperature (°C), respectively; h_c is the convective heat transfer coefficient (W/m²-°C) between the PV cells and the ambient air; h_r is the radiative heat transfer coefficient (W/m²-°C) between the PV cells and the sky; R_1 is the thermal resistance of the adhesive layer, which is a user-defined parameter of the model.

In Equation (4-1), the absorbed solar radiation S is for thermal energy collection, after accounting for the solar energy used for electricity generation. Thus, S is expressed as:

$$S = (\tau\alpha)_n K_{\tau\alpha} G_T (1 - \eta_e) \quad (4-2)$$

where, $(\tau\alpha)_n$ is the solar transmittance-absorptance product of PV module at normal incidence, $K_{\tau\alpha}$ is the incidence angle modifier to consider the impact of incident angle on optical properties, G_T is the total solar radiation on the tilted collector surface (W/m²), and η_e is the electrical efficiency of PV cells.

The value of $(\tau\alpha)_n$ in Equation (4-2) is determined from the PV reflectance, ρ , with $(\tau\alpha)_n = 1 - \rho$. The incidence angle modifier $K_{\tau\alpha}$ is based on the following equation:

$$K_{\tau\alpha} = \frac{(\tau\alpha)}{(\tau\alpha)_n} = 1 - b_0\left(\frac{1}{\cos\theta} - 1\right) \quad (4-3)$$

where, θ is the angle of incidence and b_0 is a constant called the incidence angle modifier coefficient.

The electrical efficiency of PV is a function of the cell temperature and the incident solar radiation:

$$\eta_e = \eta_{STC}[1 + \beta_T(T_{PV} - 25)][1 + \beta_G(G_T - 1000)] \quad (4-4)$$

where, η_{STC} is the PV efficiency at the Standard Test Conditions (cell temperature at 25°C and solar radiation at 1000 W/m²), β_T and β_G refer to the temperature coefficient and the radiation coefficient of PV electrical efficiency, with the unit of 1/°C and m²/W, respectively.

Many correlations are available to estimate the convective heat transfer coefficient h_c , an overview of which is provided by Mirsadeghi et al. (2013). Test, Lessmann, and Johary (1981) developed a linear correlation between h_c and the wind speed (V , in m/s) based on an experimental study using a collector-resembled plate on a building's roof. The linear correlation is shown in Equation (4-5), and its validity was further demonstrated in the experimental work by Sharples and Charlesworth (1998). Because Equation (4-5) is developed specifically for solar collectors, it is used in our research.

$$h_c = 8.55 + 2.56V \quad (4-5)$$

The radiative heat transfer coefficient is expressed as:

$$h_r = \varepsilon\sigma(T_{PV} + 273 + T_{sky} + 273)\left\{(T_{PV} + 273)^2 + (T_{sky} + 273)^2\right\} \quad (4-6)$$

where, ε is the PV surface emissivity, σ is the Stefan-Boltzmann constant, and T_{sky} is the effective sky temperature (°C).

The effective sky temperature is a critical variable that could have a large impact on the system performance because of the consideration of radiative cooling. There exist many sky temperature models (Evangelisti, Guattari, and Asdrubali et al. 2019). TRNSYS Type 15, a component for weather data processing, is used to calculate the sky temperature. Type 15 calculates the effective sky temperature based on the model from Martin and Berdahl (1984).

The absorber plate and the tube are modeled in the same manner as classical flat-plate thermal collectors (Duffie and Beckman 2006). By assuming the sheet above the tube is well bonded and is at a local base temperature T_{base} , the sheet between the centerline separating the tubes and the tube base can be considered a fin. For a differential element of the fin (Figure 4-2) with unit length along the fluid flow direction, its energy balance is expressed as:

$$k\delta \frac{d^2 T_{abs}}{dx^2} = \frac{T_{abs} - T_{back}}{R_{back}} - \frac{T_{PV} - T_{abs}}{R_1} \quad (4-7)$$

where, k is the absorber plate's thermal conductivity (W/m-°C), δ is the plate's thickness (m), T_{back} is the temperature (°C) of the ambient air at the back of the collectors, R_{back} is the thermal resistance (°Cm²/W) between the absorber plate and the back ambient air. The thermal resistance R_{back} is calculated from the thermal resistance of back insulation (R_{ins}) and the convective heat transfer coefficient:

$$R_{back} = R_{ins} + 1/h_c \quad (4-8)$$

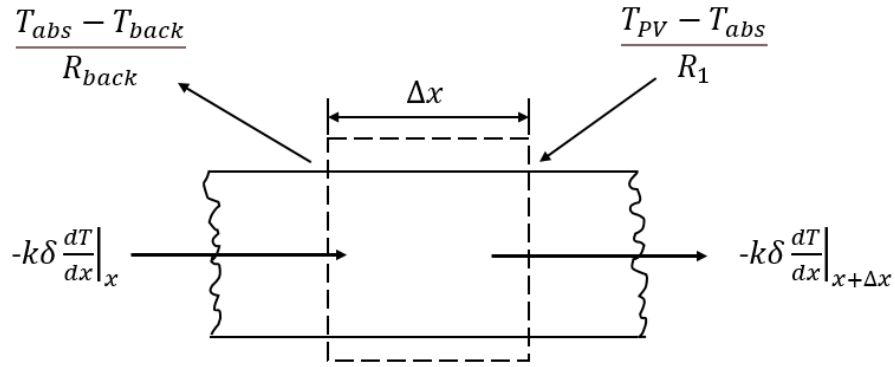


Figure 4-2: Energy balance on fin element (Duffie and Beckman 2006)

For typical PVT collector installations on the roof, it is reasonable to expect that the ambient conditions in the front of collectors are somewhat different from those in the back. However, because of the lack of information, the convective heat transfer coefficients are used the same and T_{back} is assigned the same value of the ambient air temperature (T_a in Equation (4-1)) in our research.

The differential equation (Equation (4-7)) has the following two boundary conditions:

- at the centerline separating the adjacent tubes ($x=0$), $\frac{dT_{abs}}{dx} = 0$; and
- at the base ($x = \frac{W-D}{2}$), $T(x) = T_{base}$.

Based on the above two boundary conditions, Equation (4-7) can be solved analytically to obtain the temperature distribution along the plate as a function of the base temperature. With plate temperature distribution function $T_{abs}(x)$, the energy conducted from the fin to the base (q_{fin} , in W) can be calculated per unit length in the fluid flow direction as:

$$q_{fin} = -k\delta \frac{dT_{abs}(x)}{dx} \quad (4-9)$$

For the base above the tube, the energy balance is established as:

$$q_{fluid} = 2q_{fin} + D \frac{T_{PV} - T_{base}}{R_1} - D \frac{T_{base} - T_{back}}{R_{back}} \quad (4-10)$$

where, q_{fluid} is the heat transferred to the fluid per unit length of the collector (W).

In addition, q_{fluid} can be expressed as the following:

$$q_{fluid} = \frac{T_{base} - T_{fluid}}{\frac{1}{h_{fluid}\pi D} + \frac{1}{C_b}} \quad (4-11)$$

where, T_{fluid} is the fluid temperature in °C, h_{fluid} is the heat transfer coefficient (W/m²-°C) between the fluid and the tube wall, C_b is the bond conductance (W/°C). The bond conductance per unit length in the fluid flow direction be calculated from the bond thermal conductivity k_b (W/m-°C), the bond thickness δ_b (m), and the bond width b (m) as follows:

$$C_b = \frac{k_b b}{\delta_b} \quad (4-12)$$

The energy balance on the fluid flowing through a single tube is expressed as:

$$q_{fluid} = c_p \frac{m}{n} \frac{dT_{fluid}}{dy} \quad (4-13)$$

where, c_p is the specific heat (J/kg-°C) of the fluid, m is the fluid mass flow rate (kg/s) for the entire collector array, n is the number of parallel tubes, y indicates the length in the fluid flow direction.

Combining Equation (4-11) and Equation (4-13), the fluid temperature can be solved to have:

$$T_{fluid}(y) = \left(T_{fluid,in} + \frac{C_1}{C_2} \right) \exp\left(\frac{n}{mc_p} \frac{C_2}{C_3} y \right) - \frac{C_1}{C_2} \quad (4-14)$$

where, $T_{fluid,in}$ is the temperature of the fluid entering the collectors, C_1 , C_2 , and C_3 are complicated expressions as shown below.

$$C_1 = DF' \left(S + h_r T_{sky} + h_c T_a + \frac{T_{back}}{R_{back} F'} \right) + 2k\delta\psi \tanh \left(\psi \frac{W-D}{2} \right) \left(\frac{S + h_r T_{sky} + h_c T_a + \frac{T_{back}}{R_{back} F'}}{\frac{1}{R_1 F'} + \frac{1}{R_{back} F'} - \frac{1}{R_1}} \right) \quad (4-15)$$

$$C_2 = -DF' \left(h_r + h_c + \frac{1}{R_{back} F'} \right) - 2k\delta\psi \tanh \left(\psi \frac{W-D}{2} \right) \quad (4-16)$$

$$C_3 = 1 + DF' \left(\frac{1}{h_{fluid} \pi D} + \frac{1}{C_b} \right) \left(h_r + h_c + \frac{1}{R_{back} F'} \right) + 2k\delta\psi \tanh \left(\psi \frac{W-D}{2} \right) \left(\frac{1}{h_{fluid} \pi D} + \frac{1}{C_b} \right) \quad (4-17)$$

$$F' = \frac{1}{h_r R_1 + h_c R_1 + 1} \quad (4-18)$$

$$\psi = \sqrt{\frac{F' \left(\frac{1}{R_1 F'} + \frac{1}{R_{back} F'} - \frac{1}{R_1} \right)}{k\delta}} \quad (4-19)$$

Based on Equation (4-14), the fluid outlet temperature at the collector length of L is the following:

$$T_{fluid,out} = \left(T_{fluid,in} + \frac{C_1}{C_2} \right) \exp \left(\frac{n}{m c_p} \frac{C_2}{C_3} L \right) - \frac{C_1}{C_2} \quad (4-20)$$

The above equation shows that for a given mass flow rate through the entire collector array, the fluid outlet temperature does not change with array connections, because both series and parallel connections have the same product of n and L .

As indicated in Equations (4-15)-(4-17), C_1 , C_2 , and C_3 are related to S and h_r , both of which depend on the PV cell temperature. Therefore, the numerical model is solved by guessing an initial value of T_{PV} . Then, the fluid out temperature, the mean fluid temperature, the mean base temperature, the mean fin temperature, and the mean absorber plate temperature can be calculated. Finally, Equation (4-10) is used to calculate a new value of the PV cell temperature T_{PV} . The above process is iterated until convergence is reached by comparing the values of T_{PV} from the current iteration and the previous iteration. More detailed discussion is provided in Klein et al. (2018).

Table 4-1 provides the parameters of unglazed PVT collectors used in this study. Nearly all these parameter values are from Grossule (2015). Each collector has a dimension of 1m x 1.3m. Twenty-three collectors are serially connected with a total collector area of about 30 m². The length in Table 4-1 indicates the length of the collector array instead of an individual collector.

Table 4-1: Parameters of unglazed PVT collectors

Parameter	Value	Unit
Collector length (L)	30	m
Collector width	1	m
Collector slope	45	degree
Absorber plate thickness (δ)	0.001	m
Absorber plate thermal conductivity (k)	380	W/m-°C
Number of tubes (n)	15	-
Tube diameter (D)	0.036	m
Bond width (b)	0.01	m
Bond thickness (δ_b)	0.001	m
Bond thermal conductivity (k_b)	380	W/m-°C
Adhesive thermal resistance (R_1)	0.001	m ² *°C/W
Back insulation thermal resistance (R_{back})	2.8	m ² *°C/W
PV surface reflectance (ρ)	0.15	-
PV surface emissivity (ϵ)	0.89	-
Incident angle modifier coefficient (b_0)	0.1	-
PV nominal electrical efficiency (η_e)	0.184	-
Temperature coefficient of PV efficiency (β_T)	-0.005	1/°C
Radiation coefficient of PV efficiency (β_G)	0.00009	m ² /W

4.2 Type 927: Liquid-to-liquid heat pump

TRNSYS Type 927 represents a single-stage liquid-to-liquid heat pump, whose performance is based on two external data files containing catalog data for normalized capacity and normalized power consumption at different operating conditions (i.e., liquid flow rates and entering liquid temperature at both the source side and the load side). One data file is for heating, and the other data file is for cooling. In this work, the data files are developed based on a 3.3-ton (11.7 kW) geothermal heat pump from WaterFurnace (model NSW040), which has its rated capacity and power consumption shown in Table 4-2. The normalized data files are attached in Appendix B.

Table 4-2: Parameters of the liquid-to-liquid heat pump

Rating Condition	Capacity (kW)	EER for Cooling (Btu/h/W)	COP for Heating (-)
Cooling (30°C source, 12°C load)	10.5	15.5	-
Heating (15°C source, 40°C load)	14.0	-	4.8

Type 927 does not have the functionality of modeling desuperheater that uses superheated gases from the heat pump's compressor for hot water generation. Therefore, TRNSYS Type 927 is modified to support the use of desuperheater in the PVT-HP system. In the modified version of Type 927, the heat transfer rate from the desuperheater to the water is calculated as:

$$q_{despr} = UA(T_{despr} - T_{dhw,in}) \quad (4-21)$$

where, q_{despr} is the heat transfer rate in W, UA is the heat transfer coefficient between the refrigerant and the water stream (W/°C), T_{despr} and $T_{dhw,in}$ represent the average refrigerant temperature and the water inlet temperature (°C), respectively. Because the WaterFurnace product

manual does not specify the desuperheater coil size and the refrigerant temperature, the values of UA and T_{despr} are estimated to be $100 \text{ W/}^\circ\text{C}$ and 49°C .

After q_{despr} is known, the same magnitude of heat transfer rate is deducted from the condenser. Apparently, the use of desuperheater is favorable when the heat pump works in its cooling mode because 1) the energy of superheated refrigerant gas is reclaimed instead of dissipating to the heat sink, and 2) if the storage tank is used as the heat sink, using desuperheater slows down the rise of the tank temperature. However, if the heat pump works in its heating mode, using desuperheater will produce less energy for the targeted heating.

4.3 Types 156 & 158: Thermal storage

TRNSYS offers a number of component models (e.g., Types 39, 153, 156, etc.) for thermal storage using tanks. These models vary with respect to the number of ports for liquid (water) inlet and outlet, the number of immersed heat exchangers, and whether and what type of auxiliary heaters are supported. In our simulation model, TRNSYS Type 158 is used for the storage tank, and Type 156 is used for the DHW tank. Both tanks are cylindrical. The storage tank has two pairs of ports but no immersed heat exchangers. One pair of ports is configured to have its inlet fluid stream on the top and the outlet stream at the bottom, whereas the other pair of ports have the opposite configuration. The DHW tank has one pair of ports for makeup water heating and another pair for connection to the heat pump desuperheater. Whenever there is hot water consumption at end use points, the cold water from city mains enters the DHW tank at the bottom and leaves the tank at the top. In contrast, the desuperheater-related ports have the opposite configuration. The DHW tank also has an immersed heat exchanger (i.e., a coiled tube) used to heat the water from

PVT collectors when conditions permit. The heat exchanger is needed because glycol solution is used in the collector loop, but water is in the DHW tank.

To support the modeling of thermal stratification in both Type 156 and Type 158, the tank volume is evenly divided into a number of vertical layers. Each layer, normally called a node, is assumed to be isothermal, and its energy balance is established by considering the following mechanisms: heat transfer between the tank and the ambient through the tank surfaces, fluid thermal condition between neighboring nodes through nodes, fluid movement due to inlet and outlet flow streams, the heat convection between the tank fluid and the fluid in the immersed heat exchanger, and the mixing effects in case the nodes in the storage tank become thermally unstable. Increasing the number of nodes leads to more refined modeling of thermal stratification in the tank but also increases the computation time.

Table 4-3 summarizes the major parameters of the two storage tanks. The surface heat loss coefficient is derived from the work (Furbo 2004), which investigated the characteristics of water storage tanks for solar heating systems in the Denmark market. The height fraction is calculated in reference to the tank height: a value of 0 refers to the bottom of the tank, and a value of 1 refers to the top of the tank.

Table 4-3: Parameters of the thermal storage and DHW tanks

Parameter	Storage tank (Type 158)	DHW tank (Type 156)
Fluid in the tank	propylene glycol	water
Tank volume (m ³)	2	0.23
Tank height (m)	1.8	1.8
Number of tank nodes	6	6
Surface heat loss coefficient (W/m ² -°C)	1	1
Height fraction of inlet 1	1	0
Height fraction of outlet 1	0	1
Height fraction of inlet 2	0	1

Table 4-3 cont: Parameters of the thermal storage and DHW tanks

Parameter	Storage tank (Type 158)	DHW tank (Type 156)
Height fraction of outlet 2	1	0
Height fraction of HX inlet	-	0.67
Height fraction of HX outlet	-	0

4.4 Type 114: Pump

TRNSYS Type 114 models constant-speed pumps with several simple parameters, including the rated flow rate, the rated power, and the fraction of motor heat loss transferred to the fluid stream. The pump status is determined by an external control signal. If the pump is on, it delivers the rated flow rate and consumes the rated power. The impact of the resistance of piping systems on pump operation and the efficiency losses due to pump starting and stopping are not modeled.

Figure 3-1 shows that the multifunctional SAHP system uses a total of four pumps to circulate the fluids: Pump 1 is on the heat pump's source side, Pump 2 is on the heat pump's load side, Pump 3 is used to move water between the plate heat exchanger and the radiant floor, and Pump 4 is used for the heat pump's desuperheater. Of the above four pumps, Pumps 1 & 2 circulate the glycol solution while the other two pumps circulate water.

As Figure 3-1 shows, the piping length and the number of fittings vary with circuits served by different pumps and even with different operating modes for the same pump. It is highly reasonable to expect that the pumps are sized differently depending on the flow rate and the pressure requirement. Because of the lack of actual piping dimensions, Pumps 1-3 are sized the same for simplification, and they have the rated power of 75 W at the rated flow rate of 0.63 L/s

(10 gpm). Pump 4 is much smaller, with the rated power of 15 W at the rated flow rate of 0.076 L/s (1.2 gpm).

4.5 Type 91: Plate heat exchanger

The plate heat exchanger between the PVT-HP system and the house is modeled with TRNSYS Type 91, which takes a constant, user-defined heat exchanger effectiveness as the major parameter. The heat transfer rate is calculated based on the heat exchanger effectiveness and the inlet flow conditions (i.e., temperature and capacity rate) of the two fluid streams of the heat exchanger. A value of 70% is used in this work for the heat exchanger effectiveness.

4.6 Type 138: Fluid heater

TRNSYS Type 138 is used to model two components in the system: one is the instantaneous water heater for DHW heating, and the other is the auxiliary heater for space heating. When the heater is on, Type 138 adds heat to the water stream and elevates the water temperature at the heater outlet to the desired setpoint if the heater has sufficient capacity. Both heaters are electric. The DHW heater has a capacity of 0.83 kW, and its setpoint temperature is 49°C. The auxiliary heater for space heating has a capacity of 8 kW, and its setpoint temperature is 40°C.

4.7 Type 119: Air-to-air heat pump

The air-source heat pump in the reference system is modeled with TRNSYS Type 119, which relies on the manufacturer's catalog data to predict heat pump performance. Specified in two text files (one for heating and one for cooling) external to TRNSYS, the catalog data includes the heating/cooling capacity and the electric power consumption at different operating conditions

(i.e., the air flow rate, the dry-bulb (DB), and wet-bulb (WB) temperature of the air entering the indoor coil, and the outdoor air dry-bulb temperature). This performance map approach is similar to the one used to model liquid-to-liquid heat pumps (Type 927) discussed earlier. The major difference lies in that the performance data in the external data files are normalized for Type 927 but not normalized for Type 119.

The performance data are based on a 3-ton (10.6 kW) split air-source heat pump from Carrier (Model: 25HCE436). Table 4-4 lists the major technical parameters of the product. The rated conditions are based on the AHRI Standard 210/240 (AHRI 2017), which has 26.7°C dry-bulb (DB) and 19.4°C wet-bulb (WB) for air entering the indoor coil and 35°C DB for air entering the outdoor coil for rated cooling conditions and 21.1°C DB for air entering the indoor coil and 8.3°C for air entering the outdoor coil for rated heating conditions.

Table 4-4: parameters of the air-to-air heat pump

Parameter	Value	Unit
Air flow rate	0.57	m ³ /s
Rated total cooling capacity	9.67	kW
Rated sensible cooling capacity	7.77	kW
Power consumption at rated cooling conditions	2.87	kW
Rated heating capacity	9.90	kW
Power consumption at rated heating conditions	2.74	kW
Indoor fan power	0.56	kW
Auxiliary electric heating capacity	6	kW
Auxiliary heater lockout temperature	10	°C
Compressor lockout temperature	-6	°C

4.8 System simulation

After a system simulation model is built by connecting individual components together, TRNSYS employs the successive substitution method or Powell's method to solve the set of governing equations used in the program. At each simulation time step, the computation starts

from a known boundary condition and operates on the system components successively until convergence is reached. The convergence is determined when the changes of all input values between successive iterations have fallen below a predefined relative or absolute tolerance.

Figure 4-3 shows the TRNSYS simulation model developed for the multifunctional SAHP system. Each mode requires a different path for the water and glycol solution loops. The water and glycol solution flow paths are defined according to the control signals of the participating diverters and pumps. It is worth mentioning that loops and the number of pumps and valves are slightly different from the schematic diagram of Figure 3-1. The differences are resulted from the ease of modeling without affecting the controls. A new TRNSYS type is developed for controlling the system operation. This type determines the applicable operating mode based on the control sequence described in Section 3.2 and then determines the control signals of all diverters, pumps, and the heat pump corresponding to the operating mode.

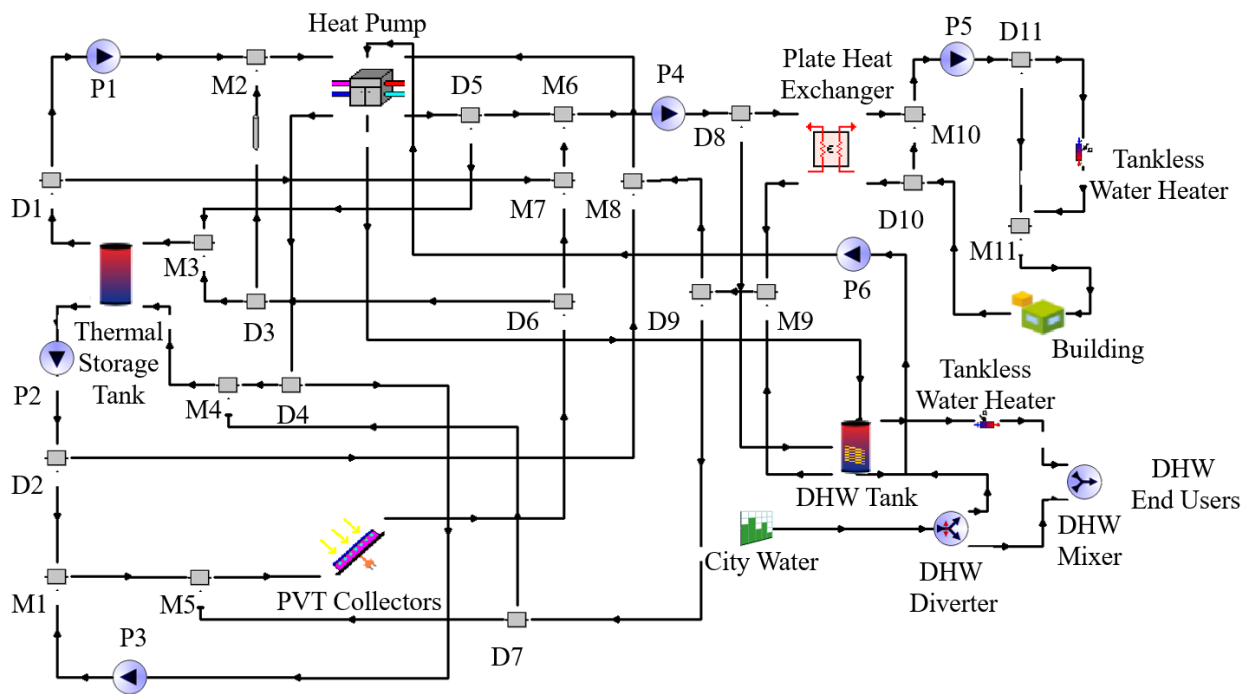


Figure 4-3: TRNSYS model of the multifunctional SAHP system

Table 4-5 lists the settings of controls parameters. As shown in the table, the SAHP system and the reference system have different heating setpoints and cooling setpoints. The difference between the setpoint temperatures in the two systems is coming from the employment of different methods for providing space conditioning (radiant floor conditioning for the SAHP system versus forced air conditioning for the reference system).

Table 4-5: Control parameters of the proposed and reference systems

Control Parameter	Value (°C)
T_{sp1}	30
T_{sp2}	-3
T_{sp3}	20
$T_{tk1,high}$	45
$T_{tk1,low}$	5
$T_{tk2,high}$	52
Thermostat heating setpoint (proposed system)	19
Thermostat cooling setpoint (proposed system)	26
Thermostat heating setpoint (reference system)	21
Thermostat cooling setpoint (reference system)	24

The building model has been developed in Google Sketchup and subsequently imported into the TRNSYS package. TRNSYS Type 56 is used to model the house, and Type 166 is used to monitor the space air temperature.

CHAPTER 5: SYSTEM PERFORMANCE ANALYSIS

The SAHP system is simulated with TRNSYS using a two-minute time step and the typical meteorological year weather data (TMY-2) for the considered locations (Baltimore, MD, and Las Vegas, NV). The implementation of system controls is verified first by checking whether the mode changes correctly following the control logics described in Section 3.2. After the verification, the operational modes are summarized with respect to their running time. The SAHP system performance is then evaluated using utilization ratios, solar fractions, fractional energy savings, and seasonal performance factors. Then, the results on sensitivity analysis are presented to investigate the impact of collector area, storage tank volume, and certain modes on system performance. The simplification of control strategy and its impact on system performance is discussed at the end of this chapter.

5.1 Verification of control implementation

As seen from the control strategies described in Section 3.2, the SAHP system operates differently with weather conditions. The effort of verifying control implementation needs to cover all possible system operational modes. Therefore, a typical day is selected to represent each of the winter season (November to April), the summer season (June to September), and the shoulder season (May and October) for the Baltimore location. For each typical day, the ambient temperature (T_{air}), the space air temperature (T_{space}), the PVT collector output temperature ($T_{col,out}$), the thermal storage tank output temperature ($T_{tk1,top}$) and the system operational modes are investigated to verify the system operation.

5.1.1 System operation in the winter season

February 5 is the day selected to represent the winter season. As Figure 5-1 shows, at the beginning of the day, the space temperature is around 19°C. The system runs for space heating because the thermostat initiated space heating before the start of the day, and the space temperature has not reached the upper bound (i.e., 19.5°C) to stop space heating. Based on the flowchart diagram of the control strategy (Figure 3-2), Mode 4 (Tank-HP for space heating) is the operational mode for space heating because 1) the storage tank output temperature ($T_{tk1,top}$) is higher than the collector outlet temperature $T_{col,out}$; and 2) $T_{tk1,top}$ is in between the temperature limit (T_{sp1}) acceptable for space heating (30°C), and low-temperature limit (T_{sp2}) for heat pump running (-3°C). The system continues running on Mode 4 until the space temperature (T_{space}) reaches 19.5°C at around 2:30 am when the system enters its idle mode. At about 6 am, T_{space} drops to 18.5°C and space heating is required again. Because the conditions for running Mode 4 are still satisfied, the heat pump uses the storage tank as its source for space heating. Using Mode 4 leads to the gradual decrease of the thermal storage tank temperature. At around 7 am, $T_{tk1,top}$ drops below T_{sp2} , which deactivates Mode 4 but activates Mode 13 (backup electric heater for space heating). Mode 13 is used until around 9 am when the following conditions are met 1) $T_{col,out}$ is higher than $T_{tk1,top}$; and 2) $T_{col,out}$ is in between T_{sp1} and T_{sp2} . Thus, Mode 3 (PVT-HP for space heating) is activated, and this mode continuously runs until the space temperature reaches 19.5°C at around 10 am. At this time, Because $T_{tk1,avg}$ is lower than $T_{tk2,avg}$ and $T_{col,out}$ is higher than $T_{tk1,bot}$, Mode 5 starts to use PVT collectors directly for heating the storage tank. This mode runs continuously until around 2 pm, when $T_{col,out}$ drops below $T_{tk1,bot}$ and PVT collectors are no longer able to directly charge the thermal storage tank. During the period of running Mode 5 from

10 am to 2:00 pm, the storage tank temperature has been increased from -3°C to 12°C . Because February is regarded as one of the coldest months, using the heat pump to charge the storage tank with PVT collectors being the source (Mode 6) is a possible operational mode according to Figure 3-2. Therefore, after Mode 5, Mode 6 is used until around 4:30 pm when $T_{col,out}$ drops below T_{sp2} . During the period of running Mode 6, the storage tank temperature has increased from 12°C to 30°C . By comparing the trajectories of storage tank temperature between Mode 5 and Mode 6, one can find that the thermal storage is charged at a higher rate in Mode 6 because the heat pump provides a higher heating capacity than the collectors. After 4:30 pm, the system has been idle except for the period from 6 pm to 8:30 pm when Mode 4 is used for space heating.

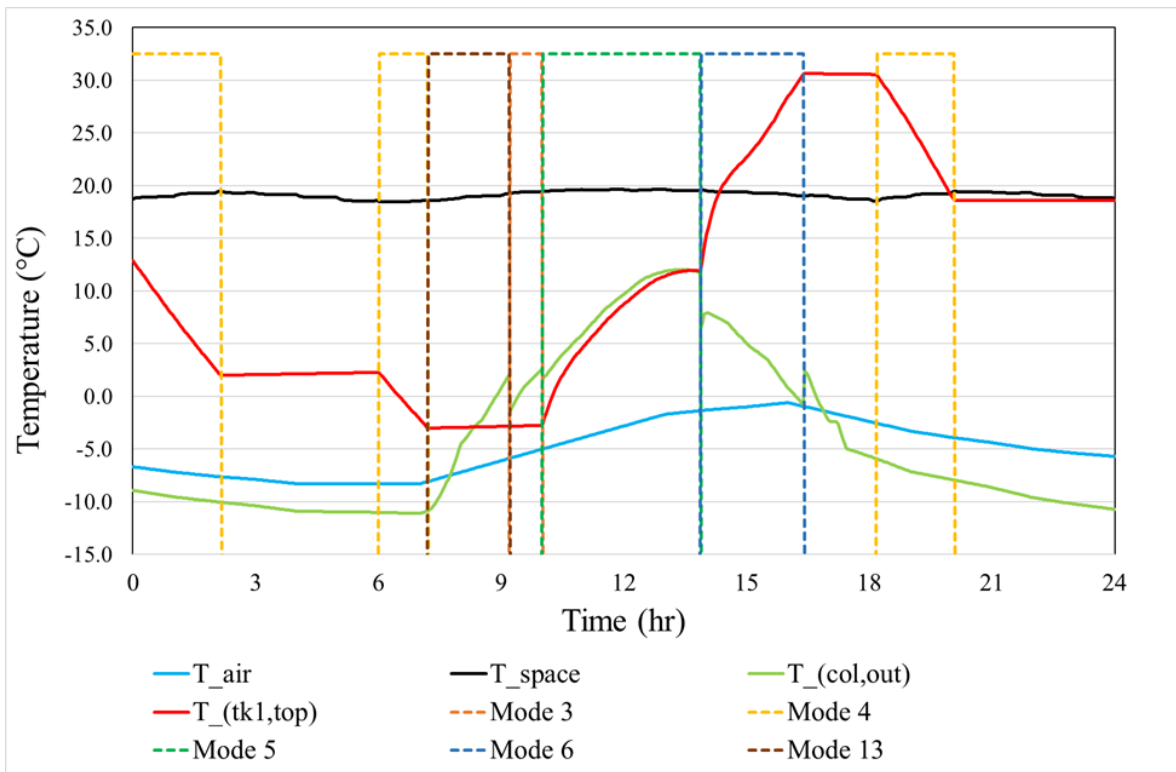


Figure 5-1: System operation on February 5

5.1.2 System operation in the summer season

July 4 is the day selected to represent the summer season. This day has outdoor air temperature ranging from 18°C to 32°C. As Figure 5-2 shows, the first active mode occurs around 9:30 am, and it is a DHW heating mode. Because the collector outlet temperature ($T_{col,out}$) exceeds the DHW tank top water temperature ($T_{tk2,top}$) and the DHW tank average temperature ($T_{tk2,avg}$) is lower than $T_{tk2,high}$ (i.e., 52°C), Mode 14 is activated to use PVT collectors to heat the DHW tank. The operation of Mode 14 runs continuously until around 11:30 am when $T_{col,out}$ is not higher than $T_{tk2,top}$ after accounting for the applicable deadband. The space temperature reaches 26.5°C around the noontime, and hence the thermostat calls for space cooling. Because $T_{tk1,top}$ is lower than T_{sp3} (20°C), the storage tank water is used directly for space cooling (Mode 8). As the system operates in Mode 8, $T_{tk1,top}$ increases to 20°C around 1:30 pm. Then the system switches to Mode 10, which uses the heat pump for space cooling. Because the storage tank is the source of the heat pump in Mode 10, the storage tank temperature continuously increases. At about 6 pm, because $T_{col,out}$ becomes lower than $T_{tk1,top}$, the system switches from Mode 10 to Mode 9 that uses the collectors as the source of the heat pump for space cooling. The system operates in Mode 9 for approximately 30 minutes until the space temperature drops below 25.5°C and the space cooling is no longer needed. After 8 pm (the starting point of nighttime), PVT collectors are used to cool the thermal storage tank (Mode 11) because $T_{col,out}$ is lower than $T_{tk1,bot}$. The capability of using collectors to charge the storage tank for cooling comes from the combined effect of radiative sky cooling and convective heat losses to the ambient. Mode 11 is active for the rest of the day, and the storage tank temperature has decreased from 35°C to 26°C.

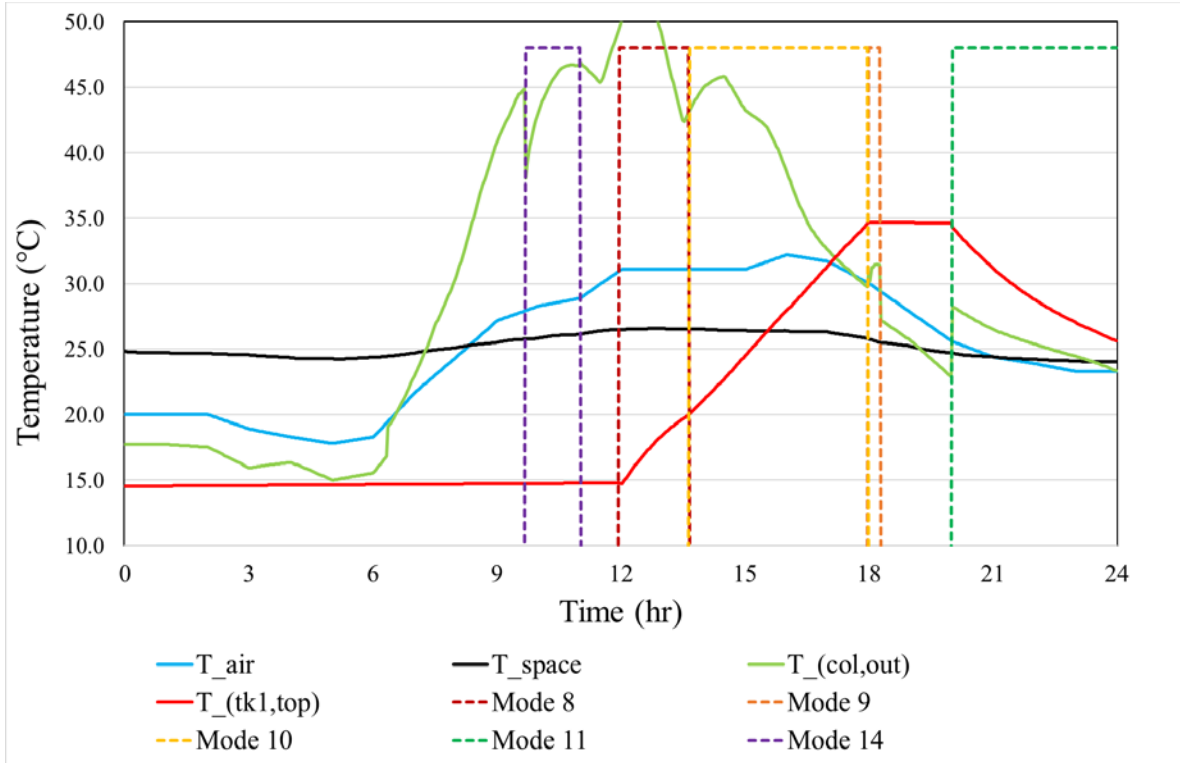


Figure 5-2: System operation on July 4

5.1.3 System operation in the shoulder season

May 9 is the day selected to represent the shoulder season. This day has outdoor air temperature ranging from 4°C to 19°C. As Figure 5-3 shows, space heating is required from 3 am to 5 am. During this period, the storage tank is used as the source directly for space heating (Mode 2) because $T_{tk1,top}$ is higher than T_{sp1} (30°C). The tank temperature decreases with the system operation in Mode 2. At about 4:30 am, the storage tank temperature drops below T_{sp1} , which triggers the switch of system operation from Mode 2 to Mode 4 (Tank-HP for space heating). Mode 4 runs for about half an hour until the space temperature reaches 19.5°C and the space heating ends around 5 am. From 9 am to 2:30 pm, $T_{col,out}$ is higher than $T_{tk1,bot}$ and $T_{tk2,top}$, which enables the PVT collectors to charge either the storage tank or the DHW tank. According

to the control sequence (Figure 3-2), which tank is charged depends on the comparison of $T_{tk1,avg}$ and $T_{tk2,avg}$. If $T_{tk1,avg}$ is lower than $T_{tk2,avg}$, the storage tank is charged with the collectors (Mode 5); otherwise, the DHW tank is charged (Mode 14). This control logic leads to the alternative operations of Mode 5 and Mode 14 from 9 am to 2:30 pm. After 2:30 pm, $T_{col,out}$ is lower than $T_{tk1,bot}$ and $T_{tk2,top}$, so the collectors are not used for charging either of the two tanks. The system keeps at the idle mode for the rest of the day because the space temperature lies between the heating and cooling setpoints.

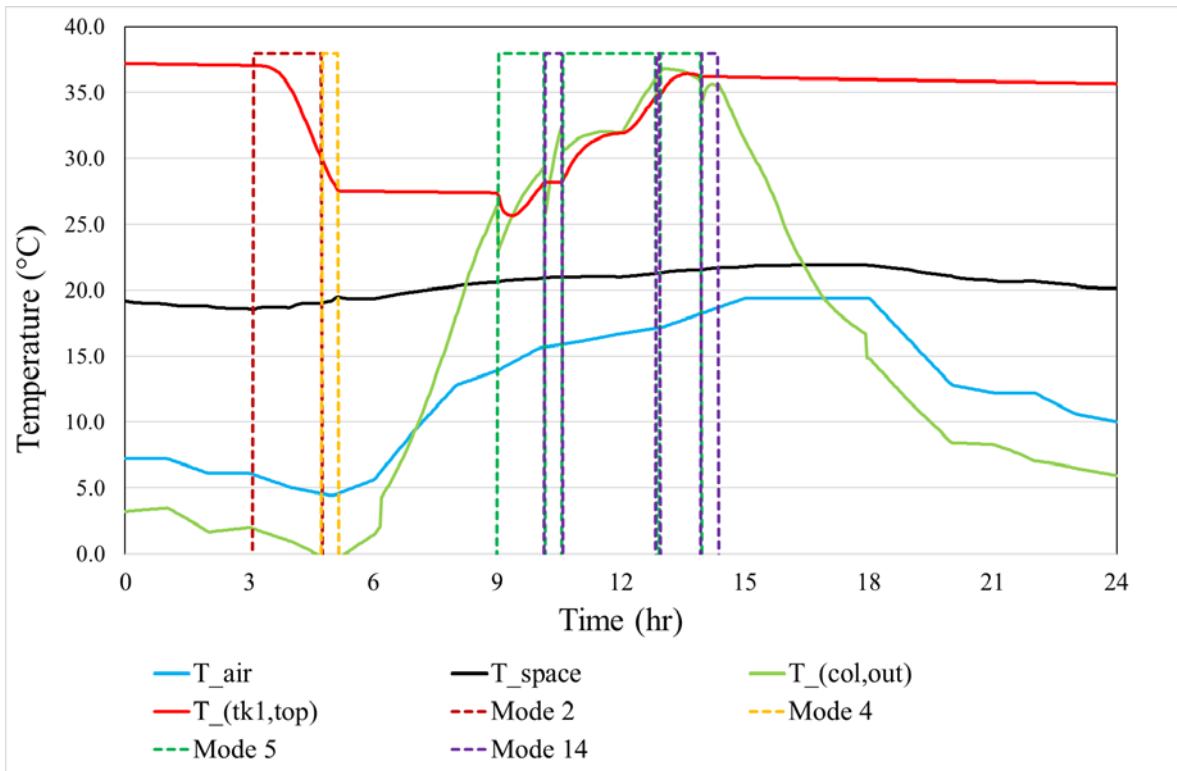


Figure 5-3: System operation on May 9

By investigating the system operation in three typical days with different weather conditions, we have verified that the controls work properly.

5.2 Statistical analysis of system operational modes

The three single days of system operation in Figure 5-1 to Figure 5-3 have shown that the length of time on different modes varies. It will be valuable to perform a statistical analysis of the running time of all modes in different months. Such a statistical analysis serves two purposes: 1) to facilitate the analysis of results later on when performance metrics are presented, and 2) to set the foundation of simplifying controls for system operation. It needs to be noted that in the following analysis, the heating season, the cooling season, and the shoulder season are defined with minor differences in Baltimore and Las Vegas, as Table 5-1 shows.

Table 5-1: Seasons defined in the two locations

Location	Heating Season	Cooling Season	Shoulder Season
Baltimore	November to April	June to September	May, October
Las Vegas	December to February	April to October	March, November

5.2.1 Run time analysis of modes related to space heating and cooling

Figure 5-4 and Figure 5-5 are the stacked bar charts showing the hours of system operation in different modes for each month. These two figures indicate the following:

- Different climates in the two considered locations lead to different patterns of system running hours. For Baltimore with a cold climate, the system operates longer time in the heating season than in the cooling season. In the heating season, the total run time on modes related to space heating and cooling ranges from 80 hrs (April) to 355 hrs (January) in the heating season, while it is from 150 hrs (September) to 280 hrs (July) in the cooling season. The system's lowest operational time is 50 hrs (May) in the shoulder season. In contrast, for Las Vegas with a warm climate, the total run time ranges from 90 hrs in April to 425

hrs in July for the cooling season, from 80 hrs in February to 200 hrs in January for the heating season, and the lowest operational run time (35 hrs in November) occurs in the shoulder season.

- Of all modes related to space heating, Mode 1 (PVT-SH, PVT for space heating), Mode 2 (TSG-SH, Thermal storage tank for space heating), and Mode 3 (PVT-HP-SH, Heat pump for space heating with the PVT collectors being the source) have played very minor roles because of their limited time of use. Mode 1 is not used at all, demonstrating that unglazed plate PVT collectors can provide low-temperature heat only. In Baltimore, Mode 4 (TSG-HP-SH, Heat pump for space heating with the storage tank being the source), Mode 5 (PVT-TSG Heat, Storage charging with the PVT collectors), Mode 6 (PVT-HP-TSG Heat, Heat pump for storage charging with PVT collectors being the source), and Mode 13 (Backup heater) are predominately used. Note that Mode 6 is allowed only in the four coldest months (January, February, November, and December). In Las Vegas, only Mode 4 and Mode 5 are predominately used, while Mode 13 is occasionally used (5 hrs in January and not used in other months) because of the mild weather conditions.
- Of all modes related to space cooling, Mode 7 (PVT-SC, PVT for space cooling) and Mode 8 (TSG-SC, Thermal storage tank for space cooling) are rarely used in both locations, while Mode 10 (TSG-HP-SC, Heat pump for space cooling with the storage tank being the source) and Mode 11 (PVT-TSG Cool, Storage charging with the PVT collectors) are predominately used. Mode 9 (PVT-HP-SC, Heat pump for space cooling with the PVT collectors being the source) usage is also significant in Las Vegas, but it is used much less in Baltimore.

- If the heat pump is used for space heating or cooling, the source can be either PVT collectors (Modes 3 and 9) or the thermal storage tank (Modes 4 and 10). As indicated earlier, it is more common to use the thermal storage instead of collectors as the source because the thermal storage has a more favorable temperature for the heat pump operation than the collectors.

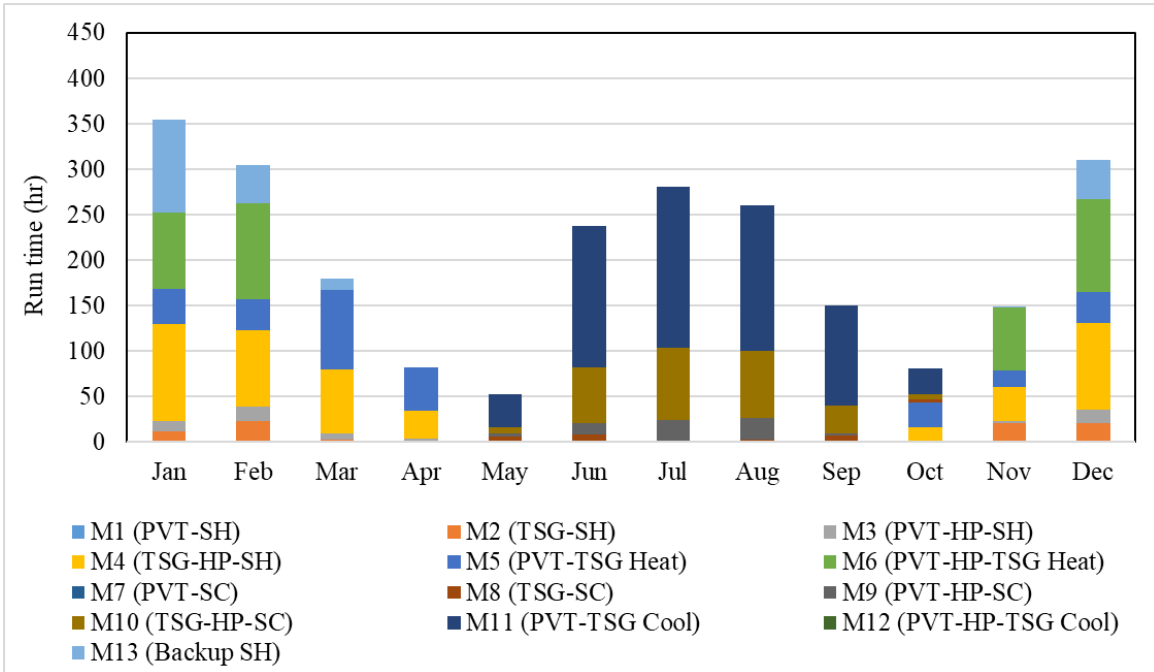


Figure 5-4: Monthly running time of operational modes related to space conditioning in Baltimore

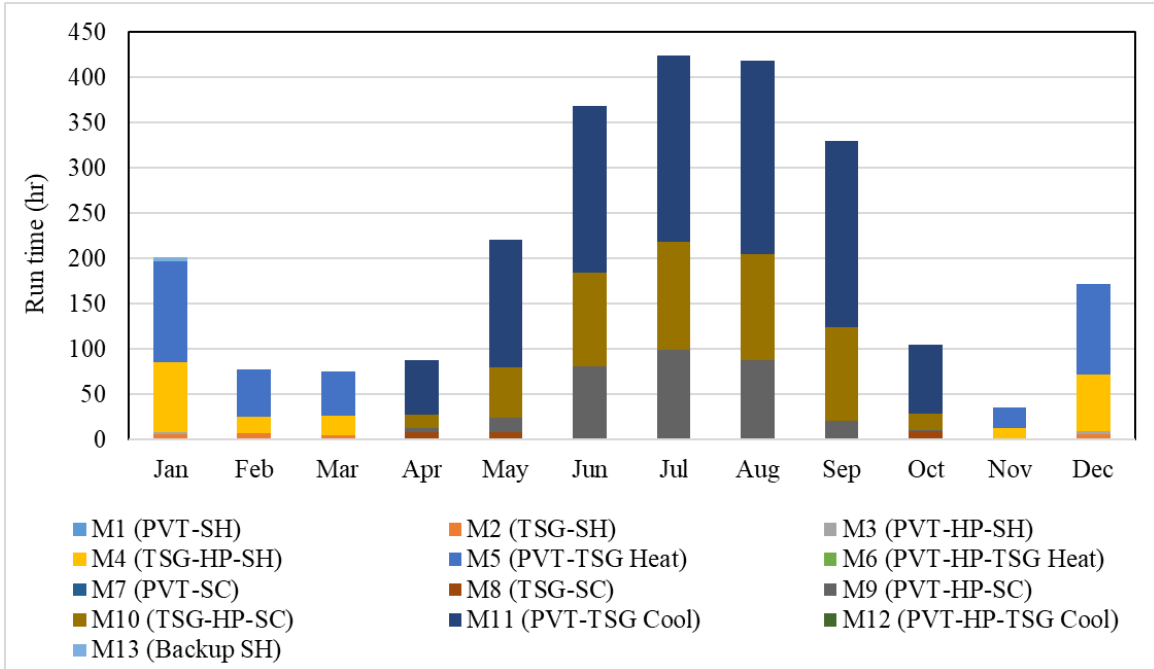


Figure 5-5: Monthly running time of operational modes related to space conditioning in Las Vegas

5.2.2 Run time analysis of modes related to DHW heating

DHW is heated by PVT collectors (Mode 14) and the heat pump's desuperheater. An auxiliary electric heater is placed after the DHW tank to ensure the water temperature leaving the DHW tank has reached 49°C before being tempered with the city water. The auxiliary instantaneous water heater is used quite often since the temperature of the water leaving the DHW tank is usually less than 49°C. However, using Mode 14 and desuperheater results in a leaving water temperature from the DHW tank higher than the city water, and therefore, instantaneous water heater consumes less energy than the case without the use of Mode 14 and desuperheater. Figure 5-6 and Figure 5-7 show the monthly running time of DHW-related modes for Baltimore and Las Vegas, respectively. From these figures, the following can be concluded:

- In the heating season, PVT collectors are used to charge the thermal storage tank and DHW tank when space heating is not needed. The average temperatures of the thermal storage tank and the DHW tank are compared, and the one with the lower temperature is charged. Because the thermal storage tank is often used as the source for space heating, resulting in a lower temperature in the thermal storage tank than the DHW tank, the run time of Mode 14 is related to the space heating needs. In Baltimore, Mode 14 is not activated in December and January. The run time of Mode 14 is slightly increased in other months with lower heating loads (i.e., 10 hrs in March and November and 25 hrs in April). A similar trend is observed in Las Vegas though the run time of Mode 14 is longer than that in Baltimore. Because the desuperheater is used whenever the heat pump runs, the months with higher space heating loads lead to a longer running time of the heat pump and the desuperheater.
- Relative to the heating season, the system operates in Mode 14 more often in the cooling season because of favorable weather conditions. Similarly, the desuperheater is used significantly in both locations in the cooling season because of the need of running the heat pump for space cooling.
- The shoulder season has low space heating and cooling loads, and therefore, it generally has much less time of DHW heating with the desuperheater than both the heating season and the cooling season. In contrast, Mode 14 is used more often for DHW production. In both locations, the run time of Mode 14 is more than 50 hours in all months of the shoulder season.

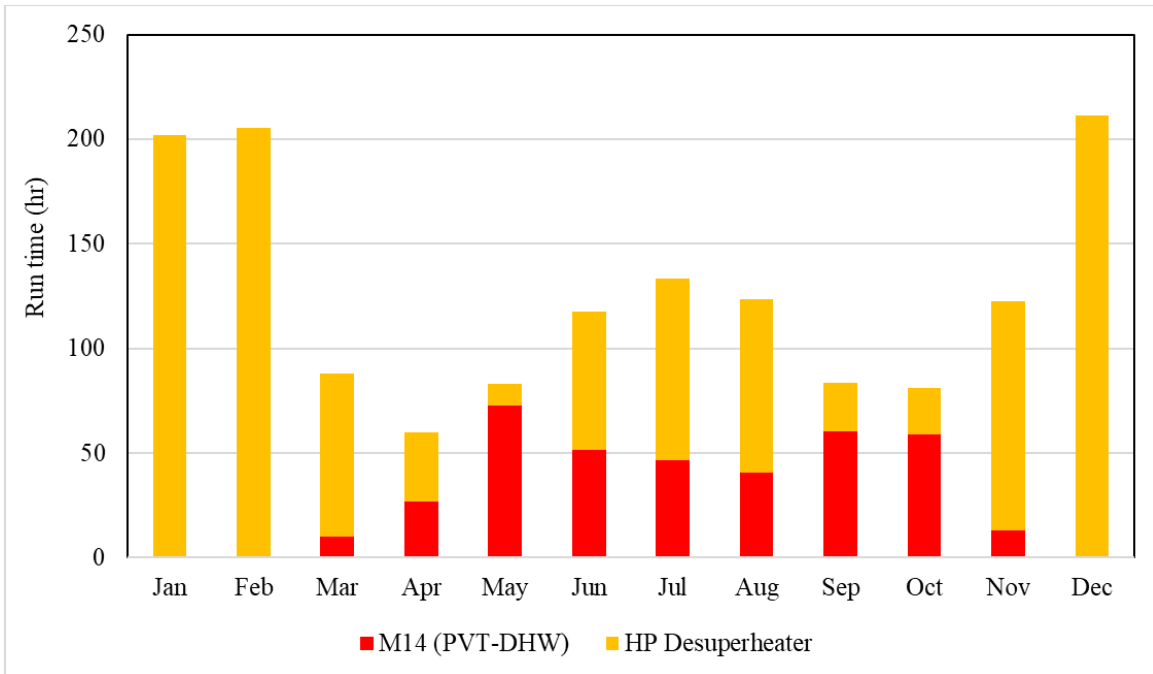


Figure 5-6: Monthly running time of operational modes related to DHW production in Baltimore

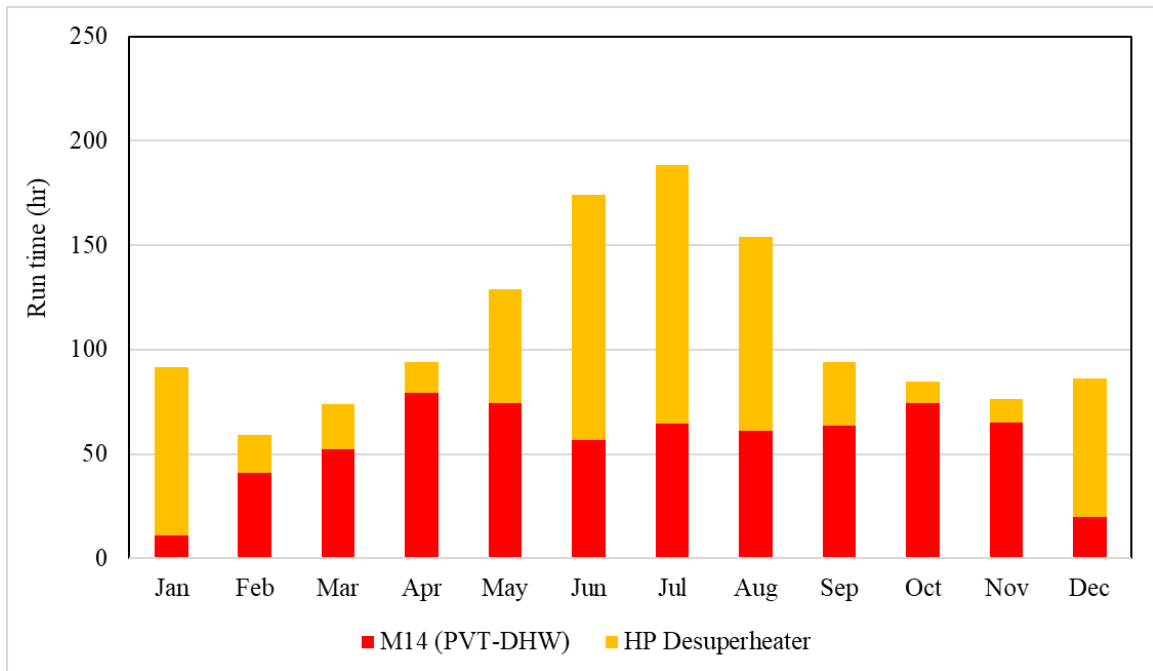


Figure 5-7: Monthly running time of operational modes related to DHW production in Las Vegas

5.3 System performance evaluation and analysis

Meaningful metrics are needed to evaluate the performance of the multifunctional SAHP system or to compare its performance with any reference systems such as the one presented in Section 3.3. IEA SHC Task 60 has a subtask dedicated to developing key performance indicators (KPIs) for PVT systems. SHC Task 60 defined KPIs related to energy performance, environmental performance, and economic performance. Energy-related KPIs are defined at the component level and the system level. Selective energy-related KPIs from Zenhäusern (2020) are used in this research for the purpose of performance analysis.

5.3.1 Solar utilization ratios

The utilization ratios define the performance of PVT collectors over a specific period of time. Since PVT collectors generate both heat and electricity, thermal, electrical, and energy utilization ratios can be defined in Equations (5-1)-(5-3).

$$\omega_{PVT,th} = \frac{\int Q_{PVT} dt}{\int G_{PVT} dt} \quad (5-1)$$

$$\omega_{PVT,el} = \frac{\int E_{PVT} dt}{\int G_{PVT} dt} \quad (5-2)$$

$$\omega_{PVT,en} = \frac{\int Q_{PVT} dt + \int E_{PVT} dt}{\int G_{PVT} dt} \quad (5-3)$$

where, $\omega_{PVT,th}$, $\omega_{PVT,el}$, and $\omega_{PVT,en}$ indicate the thermal, electrical, and energy utilization ratios, respectively, G_{PVT} , Q_{PVT} , and E_{PVT} are the solar irradiance (J/m^2) on the collector surface, the heat generation (J/m^2), and the electricity generation (J/m^2) per unit area of the PVT collector. Because the values of G_{PVT} , Q_{PVT} , and E_{PVT} vary with time, they are integrated for a specific period of time (e.g., a month and a whole year) in Equations (5-1)-(5-3).

The following needs to be noted regarding Equations (5-1)-(5-3):

- PVT collectors are used for cooling as well in this study. However, the thermal utilization ratio does not account for the usage of collectors for cooling because radiative cooling is not part of solar irradiation.
- Depending on weather conditions and system operation, it is possible that PVT collectors absorb energy from the ambient air, which occurs when the collectors are operated below the ambient air temperature.
- The energy utilization ratio is simply the sum of the thermal and electrical utilization ratios. Thus, the energy utilization ratio does not distinguish the different qualities of thermal and electrical energy. Although there are approaches, such as using primary energy efficiency as the conversion factor between electricity and thermal energy, they are not used in this work to make the energy utilization ratio more easily understandable.

Solar utilization ratios are shown in Figure 5-8 for Baltimore and Figure 5-9 for Las Vegas. In addition to solar utilization ratios (in dots), these figures also include the monthly area-specific solar radiation (the yellow bars), area-specific useful solar heat gains (the red bars), and area-specific solar electricity generation (the blue bars). The following observations can be made from Figure 5-8 and Figure 5-9:

- Though solar irradiation is the highest in summer, the useful solar heat gains and solar electricity generation have much different patterns. The useful solar heat gains are high in the winter months because of the existence of heating loads. Solar heat gains are not useful in summer because of the lack of heating needs. For example, in Baltimore, the useful solar heat gains have a peak value of $\sim 160 \text{ MJ/m}^2$ in February, while they have a value of ~ 13

MJ/m² in August. Relative to the useful solar heat gains, solar electricity generation is almost flat across different months. In Baltimore, the monthly area-specific electricity generation lies in the range from 504 MJ/m² (14 kWh/m²) in December to 777 MJ/m² (21.6 kWh/m²) in March.

- The thermal utilization ratio significantly changes across the year for both locations. In Baltimore, the thermal utilization ratio ranges from ~0.02 in summer months to 0.47 in December, with an annual average value of 0.19. In Las Vegas, the thermal utilization ratio ranges from ~0.02 in summer months to 0.20 in January, with an annual average value of 0.06.
- The solar electrical utilization ratio changes slightly from ~0.12 in summer to ~0.16 in winter for both locations. The solar electrical utilization ratio can be considered equivalent to the average electrical efficiency of PVT collectors. Because the electrical efficiency decreases with the operating cell temperature, the solar electrical utilization ratio takes lower values in summer.
- The energy utilization ratio is the sum of thermal and electrical utilization ratios. Therefore, it has higher values in winter than in summer. The energy utilization ratio ranges from 0.15 to 0.62 with an annual average of 0.28 in Baltimore, while it ranges from 0.15 to 0.35 with a yearly average of 0.20 in Las Vegas.

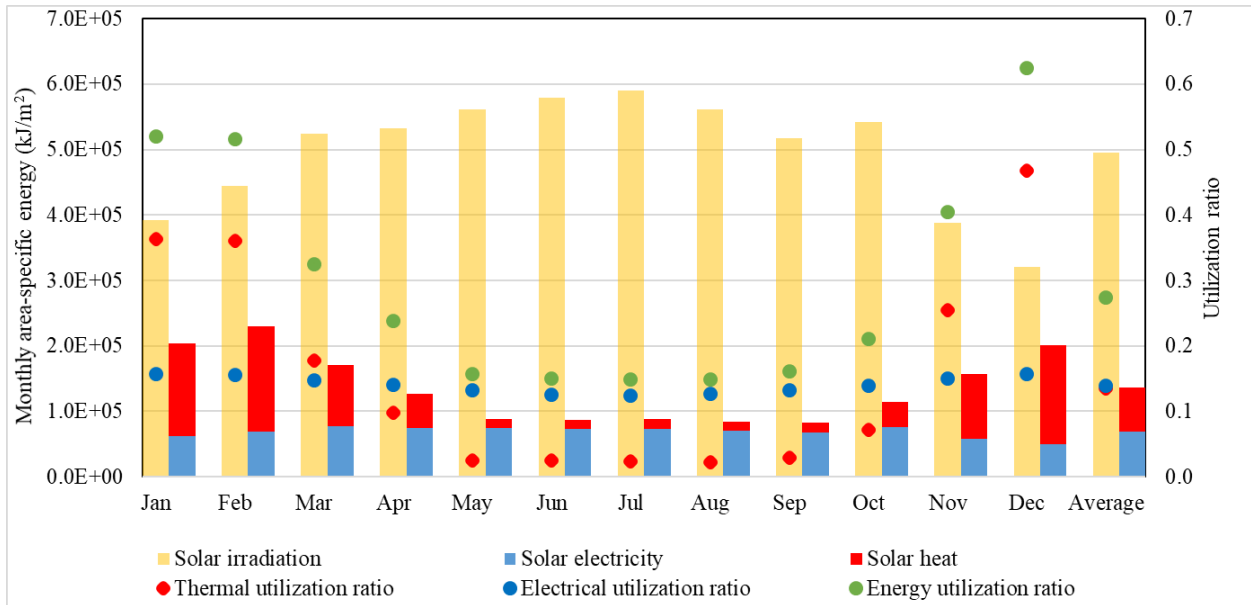


Figure 5-8: Solar yields and utilization ratios of the multifunctional SAHP system in Baltimore

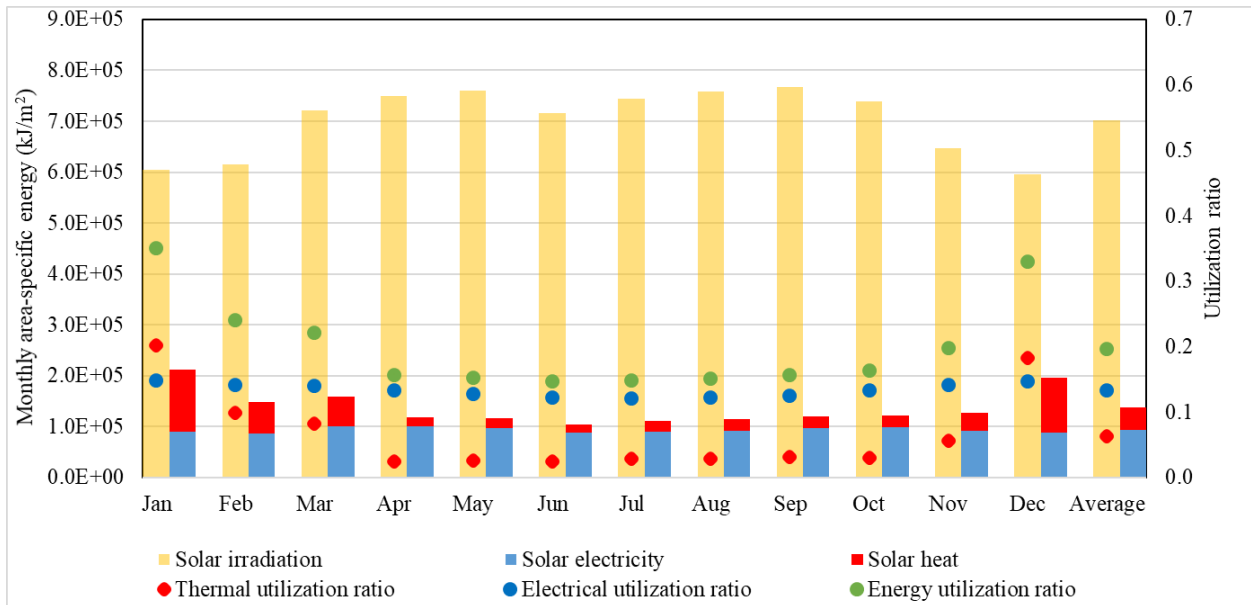


Figure 5-9: Solar yields and utilization ratios of the multifunctional SAHP system in Las Vegas

5.3.2 Solar fractions

According to SHC Task 60 (Zenhäusern 2020), for systems with PVT collectors, the solar fraction can be defined from the thermal and electrical perspectives as the solar thermal fraction and solar electrical fraction. The solar thermal fraction indicates the fraction of energy input into the system for heating provided directly by the collectors. For the system presented in Section 3.1, the solar thermal fraction can be defined as:

$$f_{sol,th} = \frac{\int (Q_{PVT,SH} + Q_{PVT,DHW}) dt}{\int (E_{HP,SH} + E_{heater,SH} + E_{heater,DHW} + Q_{PVT,DHW} + Q_{PVT,SH}) dt} \quad (5-4)$$

where, $Q_{PVT,SH}$ is the direct solar energy for space heating, $Q_{PVT,DHW}$ is the direct solar energy for DHW, $E_{HP,SH}$ is the heat pump electricity consumption for space heating, $E_{heater,SH}$ is the electricity consumption by the instantaneous water heater for space heating, $E_{heater,DHW}$ is the electricity consumption by the auxiliary heater in the DHW tank.

For the solar thermal fraction, the following needs to be noted: 1) it considers heating only (space and DHW) while space cooling is excluded; 2) it counts direct solar heating only while the solar energy input to the thermal storage and the primary source of the heat pump is not counted.

The solar electrical fraction can be defined differently depending on whether the household electricity (e.g., lighting, plug loads, and appliances) is considered. If the household electricity is not considered, the solar electrical fraction is defined as:

$$f_{sol,el}^{sys} = \frac{\int E_{PVT}^{AC} dt}{\int E_{sys} dt} \quad (5-5)$$

where, E_{PVT}^{AC} is the AC electricity generation (J) from PVT collectors, E_{sys} is the electricity consumed by the system (J). Both items are evaluated per time step.

In contrast, if the household electricity is included, the solar electrical fraction is defined as:

$$f_{sol,el}^{site} = \frac{\int E_{PVT}^{AC} dt}{\int (E_{sys} + E_{HE}) dt} \quad (5-6)$$

where, E_{HE} is the household electricity consumption (e.g., lighting and appliance).

Figure 5-10 shows the monthly and annual values of solar thermal fraction for Baltimore and Las Vegas. Because the mode using PVT collectors directly for space heating is not activated (see Section 5.2.1), the solar thermal fraction is just the result of using PVT collectors for DHW production (Mode 14). The solar thermal fraction ranges from 0% (January) to 72% (July) in Baltimore and from 2% (January) to 91% (September) in Las Vegas. As expected, the summer months have a significantly high solar thermal fraction. The annual solar thermal fraction is 9% in Baltimore and 34% in Las Vegas.

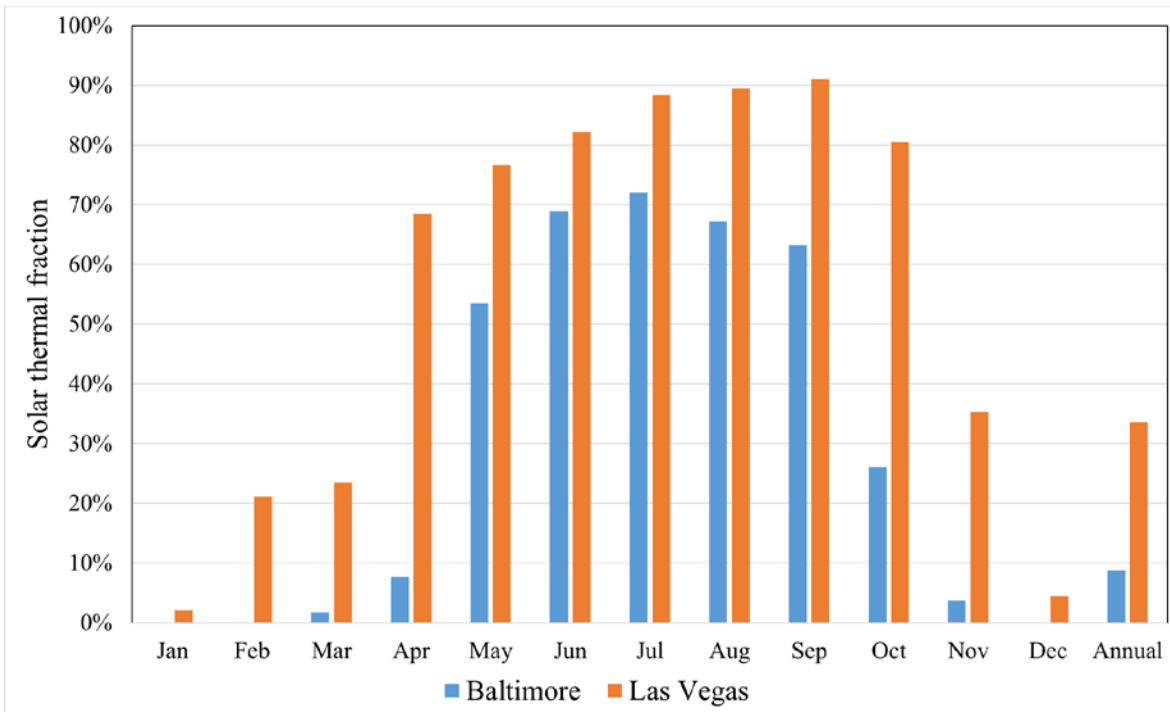


Figure 5-10: Solar thermal fraction

The system and site solar electrical fractions are presented in Figure 5-11 for Baltimore and Figure 5-12 for Las Vegas. Takeaways from these figures are as follows:

- The monthly system solar electrical fraction varies significantly across the year. It changes from 36% (January) to 435% (May) with an annual average of 118% in Baltimore, while it changes from 97% (July) to 746% (November) with a yearly average of 228% in Las Vegas. The monthly variation comes from two sources: 1) the solar electricity generation varies with months, and 2) the electricity consumption of the system also varies with months, with the latter one playing the prominent role. The pattern of monthly solar electrical fraction reflects the load changes. In Baltimore (cold climate), the load for space conditioning increases from the shoulder season, the cooling season, and then the heating season. Therefore, the solar electrical fraction generally increases from the heating season, the cooling season, and then the shoulder season. A similar explanation can be made for Las Vegas.
- After accounting for the non-HVAC electricity consumption of the building, the site solar electrical fraction takes much smaller values than the system solar electrical fraction. The site solar electrical fraction changes from 25% (January) to 83% (May) with an annual average of 53% in Baltimore, while it changes from 54% (July) to 115% (November) with a yearly average of 83% in Las Vegas.

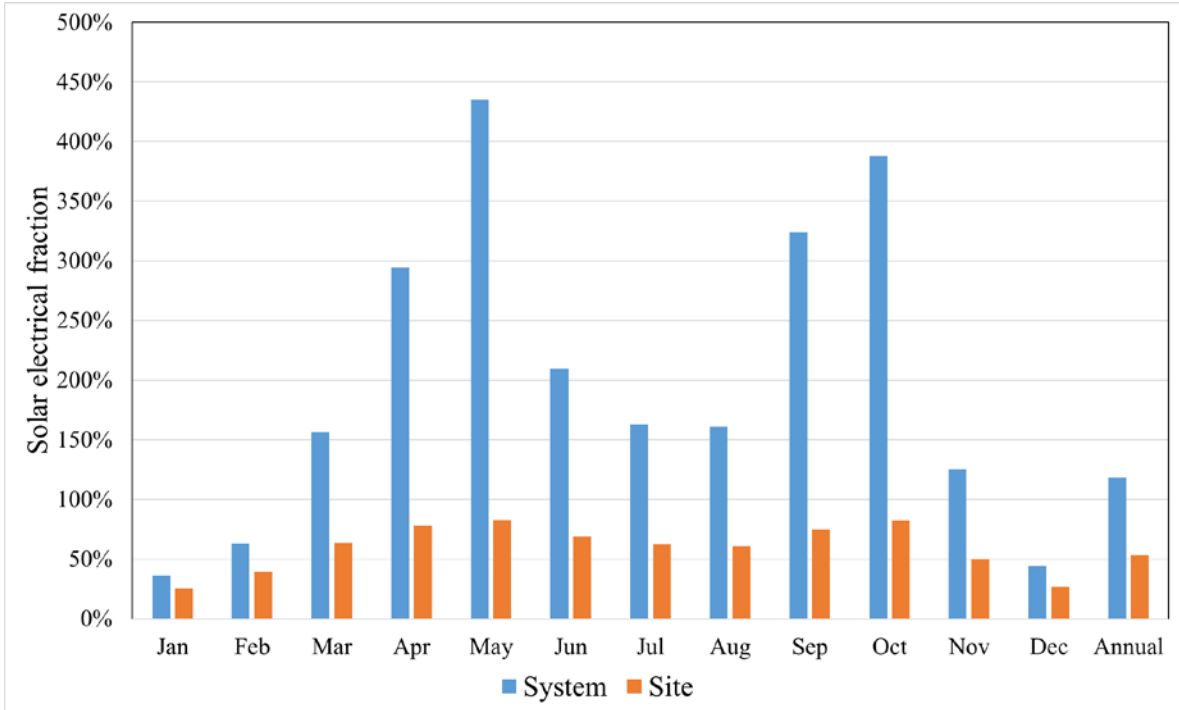


Figure 5-11: System and site solar electrical fractions in Baltimore

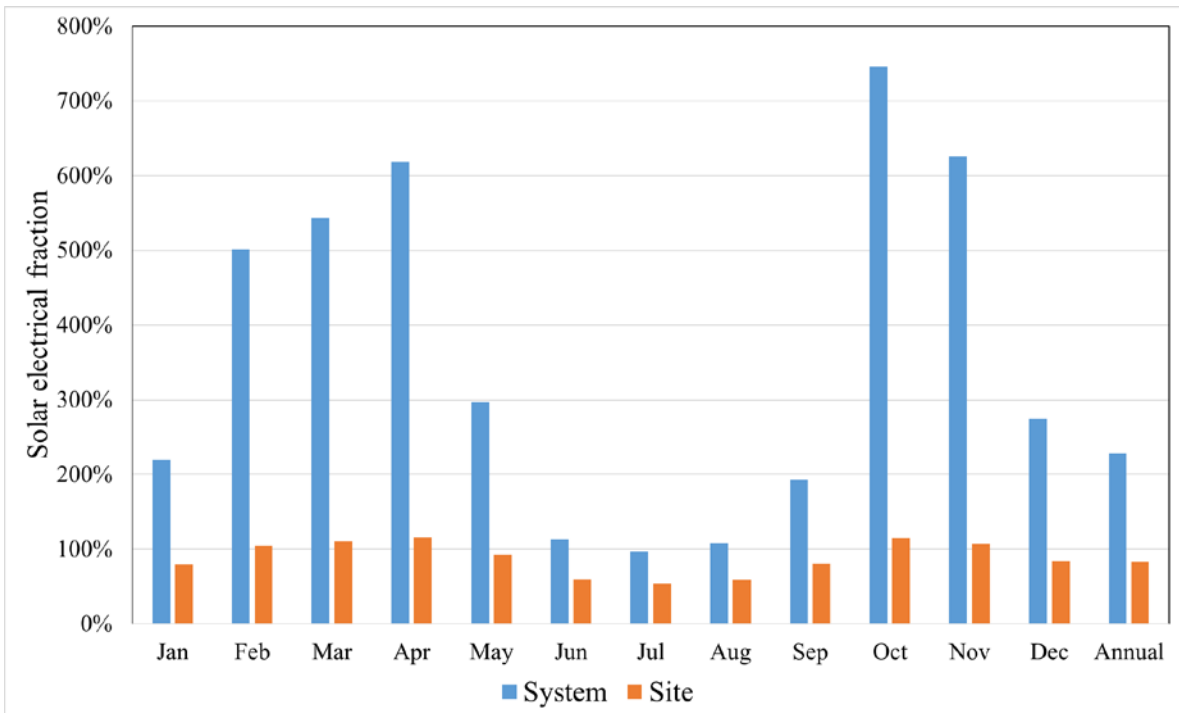


Figure 5-12: System and site solar electrical fractions in Las Vegas

5.3.3 Self-consumption

The solar electrical fraction metric does not distinguish between the portion of generated solar electricity consumed onsite and the portion exported to the grid. Therefore, self-consumption is defined as the ratio of solar electricity consumed onsite to the total solar electricity production. Similar to solar electrical fraction, self-consumption is defined over system and site boundaries depending on the inclusion of household electricity usage.

$$f_{sol,el}^{sys} = \frac{\int E_{PVT,sys}^{AC} dt}{\int E_{PVT}^{AC} dt} \quad (5-7)$$

$$f_{sol,el}^{site} = \frac{\int (E_{PVT,sys}^{AC} + E_{PVT,HE}^{AC}) dt}{\int E_{PVT}^{AC} dt} \quad (5-8)$$

In Equations (5-7) and (5-8), $E_{PVT,sys}^{AC}$ and $E_{PVT,HE}^{AC}$ denote the solar electricity (J) used by the SAHP system and other household usages, respectively.

Figure 5-13 and Figure 5-14 show the system and site self-consumption of onsite solar electricity generation in Baltimore and Las Vegas, respectively. These figures indicate the following:

- The system self-consumption of onsite solar electricity generation changes from 12% (October) to 51% (December) with an annual average of 27% in Baltimore, while it changes from 7% (March) to 46% (July) with a yearly average of 19% in Las Vegas.
- After including the non-HVAC electricity consumption of the building, the site self-consumption takes higher values than the system self-consumption. The site self-consumption changes from 32% (October) to 66% (December) with an annual average of 45% in Baltimore, while it changes from 24% (March) to 56% (July) with a yearly average of 35% in Las Vegas.

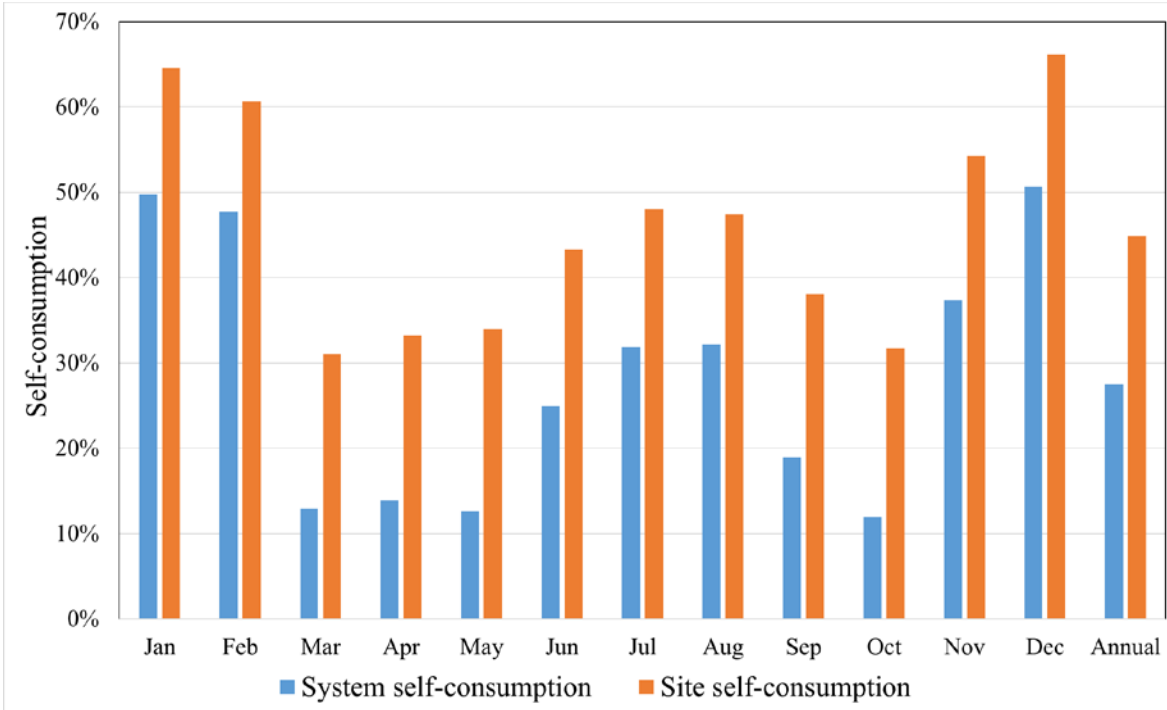


Figure 5-13: System and site self-consumption of onsite solar electricity generation in Baltimore

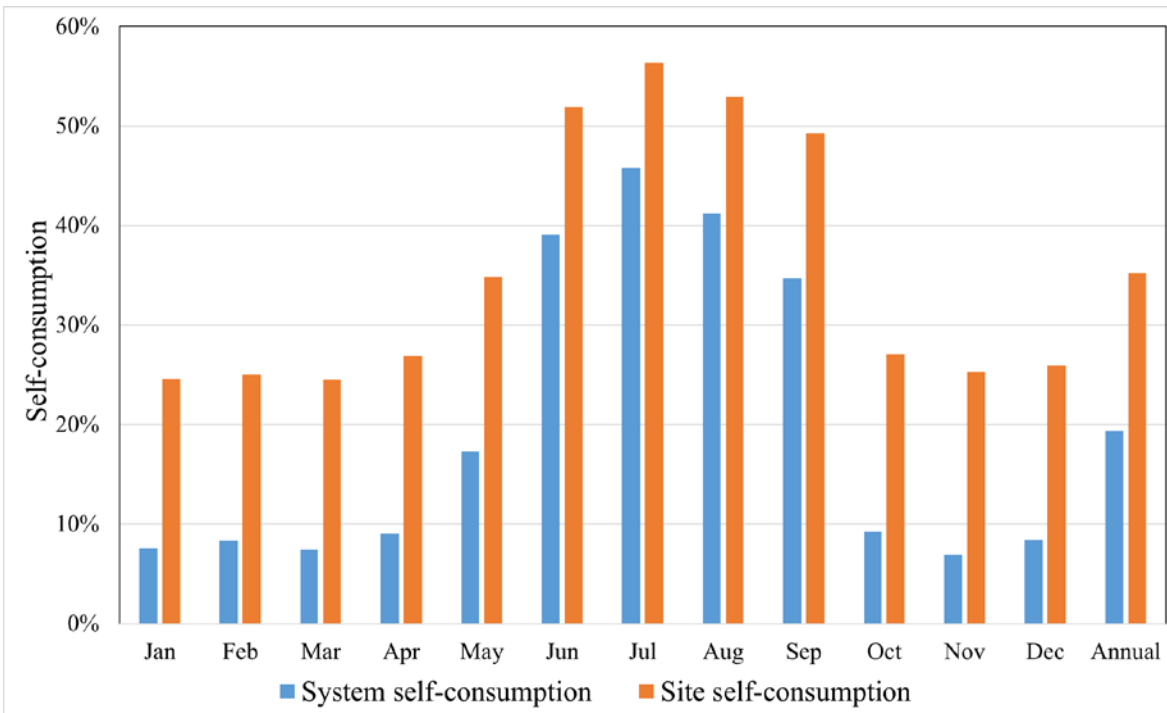


Figure 5-14: System and site self-consumption of onsite solar electricity generation in Las Vegas

5.3.4 Area-specific cooling power of PVT collectors

Considering that the solar thermal fraction addresses heating only, a similar metric can be defined for space cooling to measure the fraction of energy input into the system that is provided by PVT cooling directly. However, it is observed that direct space cooling using PVT collectors does not occur at all (Figure 5-4 and Figure 5-5). The collectors are used to charge the tank for cooling (Mode 11) and used as the source of the heat pump for cooling (Mode 9). The value will be 0 if a metric similar to the solar thermal fraction for heating is defined for cooling. Therefore, to evaluate the potential of PVT collectors for cooling, the metric called area-specific cooling power of PVT collectors (ASC_{PVT}) is defined as:

$$ASC_{PVT} = \frac{Q_{PVT,C}}{A_{PVT}} \quad (5-9)$$

where, $Q_{PVT,C}$ is the cooling energy (J, due to radiative and convective phenomena) of PVT collectors per time step and A_{PVT} is the total area of PVT collectors.

Based on Equation (5-9), the area-specific cooling power of PVT collectors is calculated at times that collector is used for cooling and then averaged for the summer months because PVT cooling (Mode 11) is used in summer only. Figure 5-15 shows the results. This figure indicates the following:

- Las Vegas has a higher average area-specific cooling power than Baltimore in all summer months. The major reason is that Las Vegas has a lower sky temperature in the summer months than Baltimore because of the arid and desert-like climate (Figure 3-3). The low sky temperature is beneficial for radiative cooling. Additionally, because of the high cooling load in Las Vegas, the thermal storage is used frequently as the source of the heat pump for space cooling. Therefore, the thermal storage tank temperature and the collector

temperature are higher in Las Vegas. As a result, the temperature differences between the PVT collector and its surroundings and sky are also increased, which causes increased cooling power.

- The area-specific cooling power of PVT collectors (kJ/h/m^2) ranges from 515 kJ/h/m^2 (October) to 835 kJ/h/m^2 (August) in Baltimore with an annual average of 730 kJ/h/m^2 , while it ranges from 595 kJ/h/m^2 (October) to 1110 kJ/h/m^2 (July) with a yearly average of 970 kJ/h/m^2 in Las Vegas.

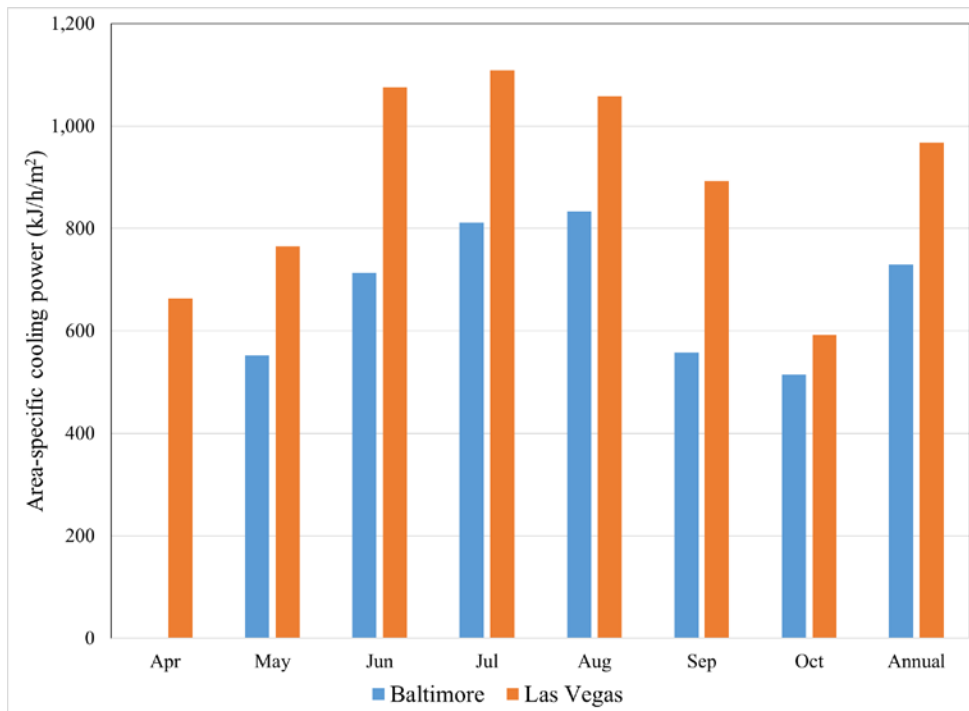


Figure 5-15: Monthly and annual average of the area-specific cooling power of PVT collectors

5.3.5 Fractional energy savings relative to the reference system

Percentage energy savings are used to compare the multifunctional SAHP system and the reference conventional split air-source heat pump system. Percentage savings can be computed with respect to the energy for space conditioning (both heating and cooling), the energy for DHW

production, and the total energy for both space conditioning and DHW production, as shown in Equations (5-10) to (5-12). Note that electricity is the only type of energy used in both the reference and the SAHP systems.

$$SavePer_{SHC} = \frac{E_{Ref,SHC} - E_{SAHP,SHC}}{E_{Ref,SHC}} * 100\% \quad (5-10)$$

$$SavePer_{DHW} = \frac{E_{Ref,DHW} - E_{SAHP,DHW}}{E_{Ref,DHW}} * 100\% \quad (5-11)$$

$$SavePer_{total} = \frac{E_{Ref,total} - E_{SAHP,total}}{E_{Ref,total}} * 100\% \quad (5-12)$$

where, *SavePer* stands for percentage savings, *E* stands for electrical energy consumption, the subscripts *SHC*, *DHW*, *total* respectively refer to the energy for space heating and cooling, the energy for DHW production, and the total energy is the combination of the above two end uses, the subscripts *Ref* and *SAHP* refer to the reference system and the multifunctional SAHP system, respectively.

The SAHP system and the reference system have different energy consumption in space heating, space cooling, and DHW, but the systems do not affect lighting, appliances, and plug loads. Therefore, the fractional energy savings are presented in this section with a focus on DHW and space heating and cooling, as shown in Figure 5-16 and Figure 5-17. When calculating the fractional energy savings, the DHW energy refers to the energy used by the auxiliary DHW electric heaters; the space heating and cooling energy refers to the energy used by the liquid-to-liquid heat pump, circulation pumps, and the backup electric water heater in the SAHP system and by the air-source heat pump, the supply fan, and the backup electric heater in the reference system; the total refers to the sum of energy used for DHW and space heating and cooling. Figure 5-16 and Figure 5-17 indicate the following:

- The SAHP system has significant energy savings on DHW, more than 80% for nearly all months in both locations, than the reference system. The major reason lies in the use of the desuperheater for DHW heating. In the SAHP system, the desuperheater is available for use as long as the heat pump operates. Therefore, longer heat pump running hours (in both winter and summer) means more desuperheater energy. Certainly, the use of the desuperheater reduces the energy provided by the heat pump for space heating in the winter months. In addition to the desuperheater, a secondary reason leading to significant DHW energy savings comes from the SAHP system operational Mode 14, which enables the direct use of solar collectors for DHW in the summer months.
- The fractional energy savings on space heating and cooling fluctuate over the year. In Baltimore, the SAHP system has positive energy savings up to 39% in all months except for January, in which the SAHP system turns out to consume 3% more energy. In Las Vegas, the SAHP system has positive energy savings (up to 74%) on space heating and cooling throughout the year. It looks that Baltimore has higher fractional energy savings in summer than in winter, while Las Vegas has the reverse trend. Several factors could affect the fractional energy savings on space heating and cooling. First, when the heat pump runs, the source temperatures and the corresponding efficiency may be different between the reference system (ambient air being the source) and the SAHP system (either thermal storage or PVT collectors being the source). Second, the reference air-source heat pump and the liquid-source heat pump of the SAHP system have different low-temperature limits (i.e., -6°C for the air-source and -3°C for the liquid-source), below which the backup electrical heaters must be used. Figure 5-4 has shown that Baltimore has the highest run

time of Mode 13 (backup heater) in January, which explains the negative energy saving in this month.

- The fractional savings on the total energy use for DHW and space heating and cooling are positive for all months. The savings range from 26% (January) to 74% (May) in Baltimore and from 44% (July) to 80% (October) in Las Vegas.

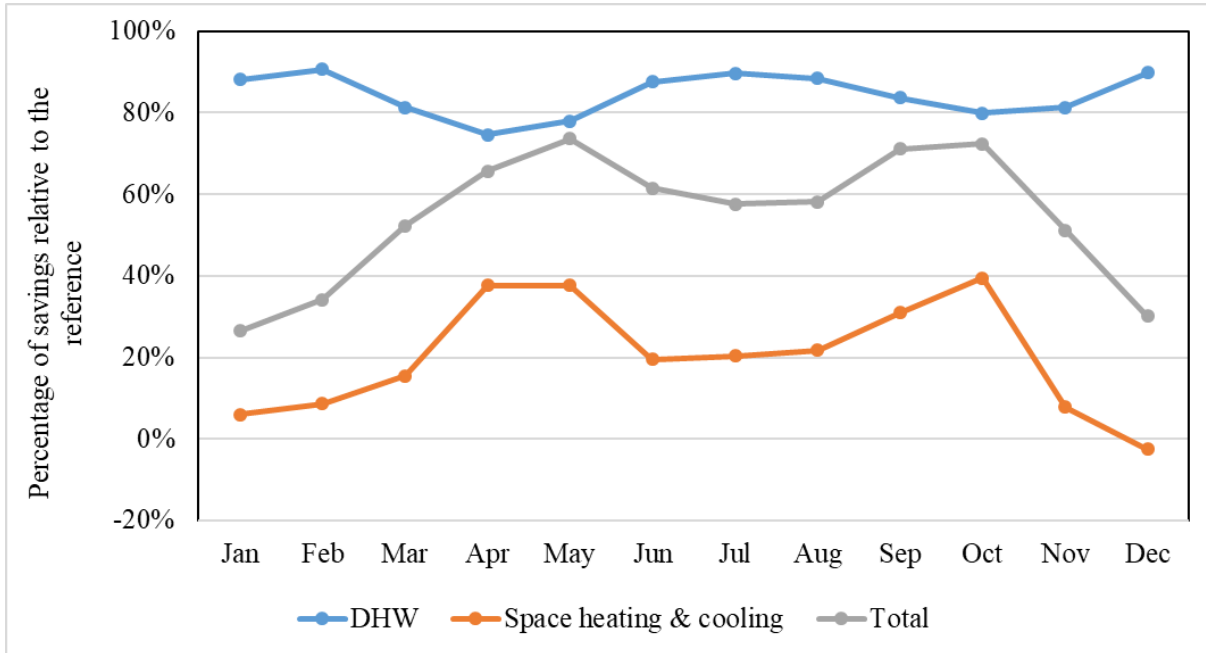


Figure 5-16: Monthly fractional energy saving of the proposed system compared to the reference system for Baltimore

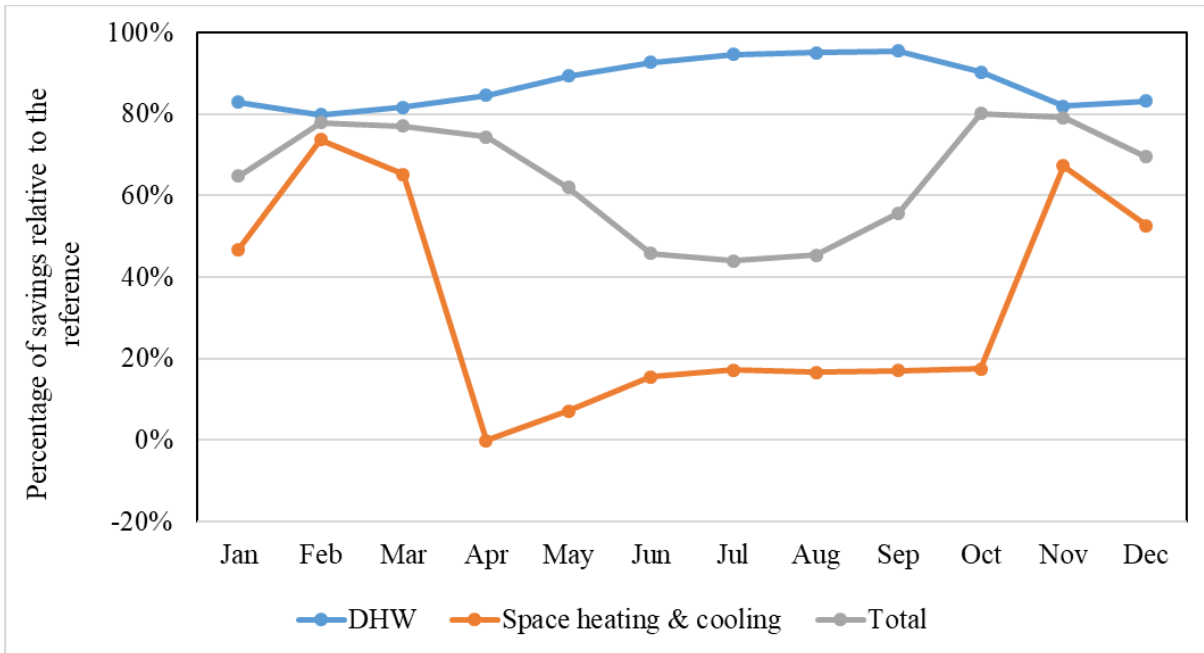


Figure 5-17: Monthly fractional energy saving of the proposed system compared to the reference system for Las Vegas

The annual energy use intensities of the reference system and the SAHP system are compared in Figure 5-18, where the numbers above the bars indicate the percentage of savings for each energy end use (i.e., DHW, space heating and cooling, and the total of the above two items). This figure shows that overall the SAHP system saves 48% energy in Baltimore and 61% energy in Las Vegas.

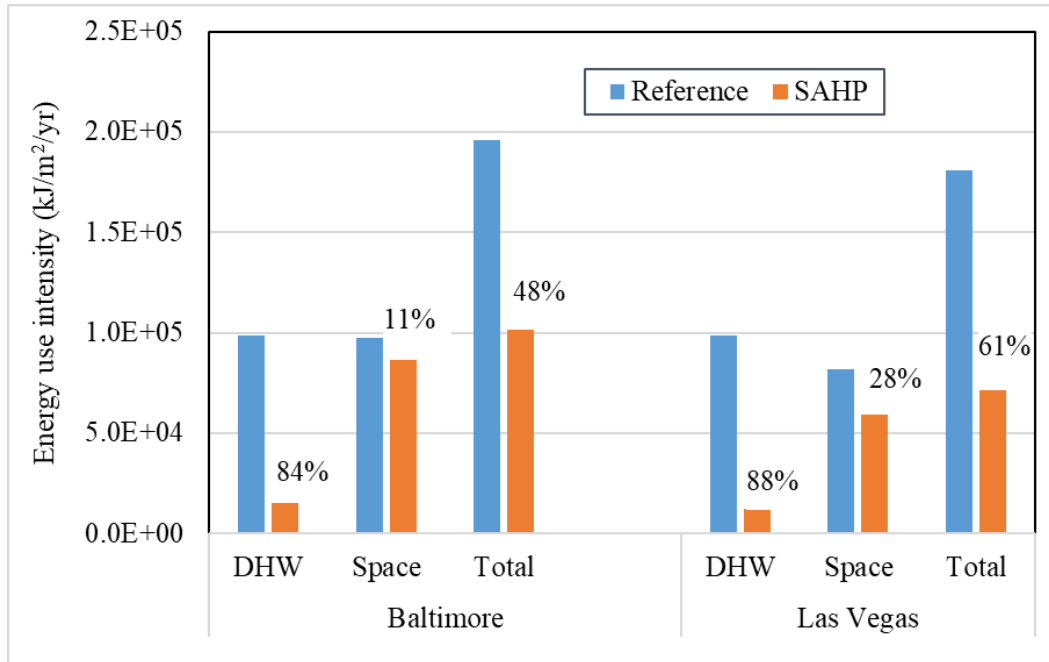


Figure 5-18: Annual energy consumption comparison between the proposed and reference systems and fractional energy saving of the proposed system compared to the reference system.

5.3.6 Seasonal performance factors

According to IEA SHC Task 60 (Zenhäusern 2020) and Task 44 (Hadorn 2015), Seasonal Performance Factor (SPF) is defined as the ratio between the amount of useful heat and/or cold (with positive sign) generation to the electricity consumption over a specified period of time. SPF can be defined over different system boundaries, but it is used for the whole SAHP system in this work. The amount of useful heat and cold energy generation are determined at the interfaces between the SAHP system and the distribution system to end uses. If energy losses of the heat distribution system are not considered, which is the case in this work, the amount of useful heat and cold energy is the energy delivered to the space for space conditioning and DHW end users. The electricity consumption comes from all components of the whole system, such as the heat pump, the auxiliary heater, and the pumps. In equation (5-13), SPF is expressed as

$$SPF = \frac{\int (Q_{SH} + Q_{SC} + Q_{DHW}) dt}{\int E_{sys} dt} \quad (5-13)$$

where, Q_{SH} , Q_{SC} , and Q_{DHW} represents the rate of energy delivered by the system for space heating, space cooling, and DHW, respectively, E_{sys} is the rate of electricity consumption of the system.

Figure 5-19 and Figure 5-20 compare the SPF between the reference system and the SAHP system, respectively, for the two locations. Both monthly and annual overall values are presented in the figures. Essentially, the SPF can be understood as the system COP for DHW and space heating and cooling. Therefore, the system with a higher SPF is more energy efficient. Major observations from Figure 5-19 and Figure 5-20 include the following:

- The SAHP system has higher SPFs than the reference system throughout the year for both locations.
- In Baltimore, the monthly SPF ranges from 1.87 (January) to 3.97 (June) for the SAHP system, while it is from 1.13 (January) to 1.87 (July) for the reference system. The annual SPF is 2.69 and 1.59, respectively, for the above two systems.
- In Las Vegas, the monthly SPF ranges from 3.24 (November) to 4.82 (October) for the SAHP system, while it is from 1.27 (April) to 2.13 (July) for the reference system. The annual SPF is 3.70 and 1.90, respectively, for the above two systems.

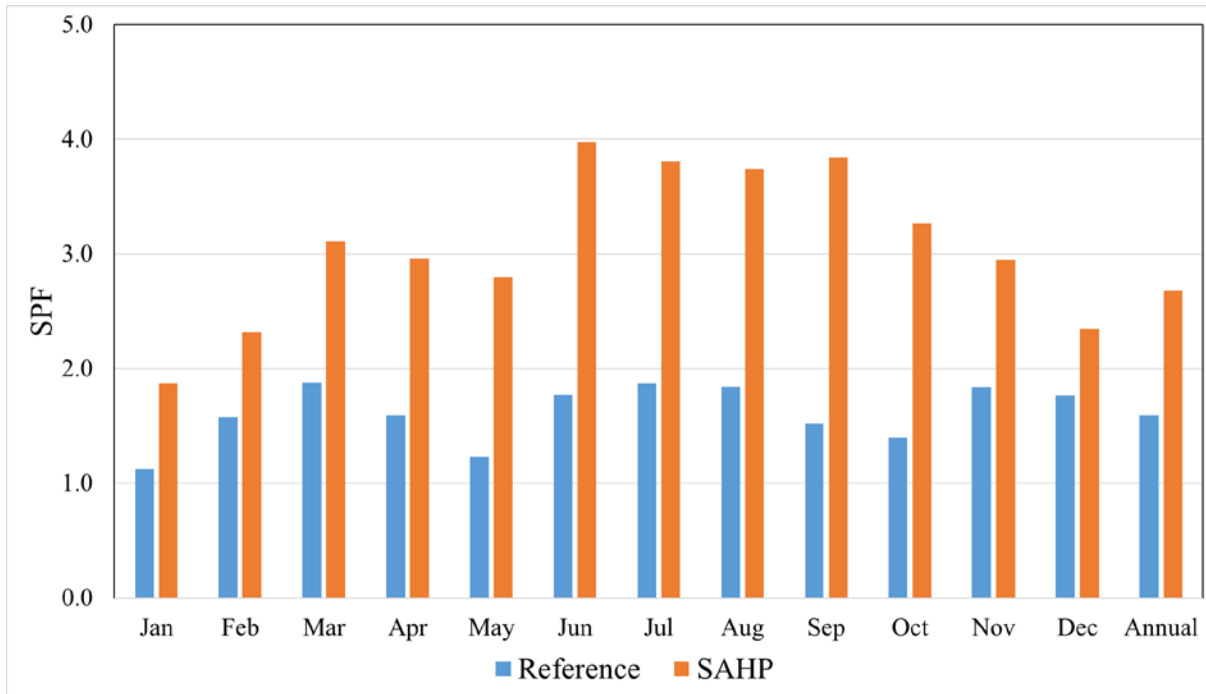


Figure 5-19: SPF comparison between the proposed and reference systems in Baltimore

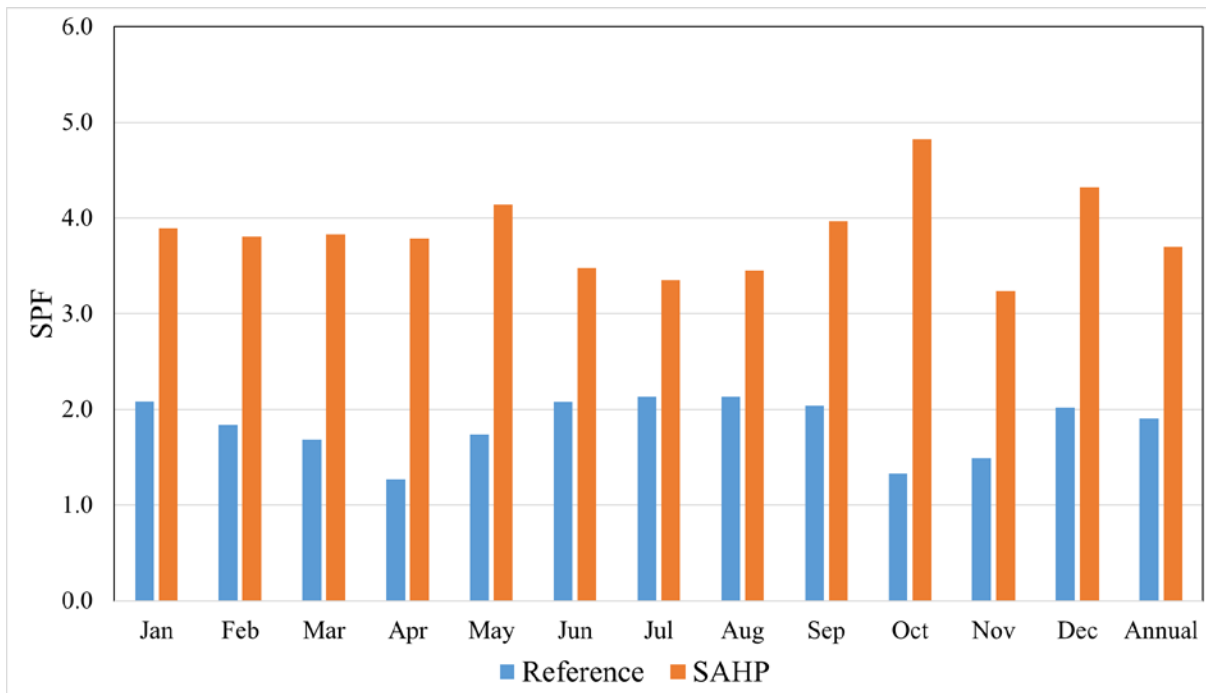


Figure 5-20: SPF comparison between the proposed and reference systems in Las Vegas

5.4 Sensitivity analysis

For the SAHP system studied in this work, the PVT collector area and the thermal storage tank volume are two important design parameters that could affect the energy performance significantly. The results presented earlier in this chapter are based on the collector area of 30 m^2 and the storage tank volume of 2 m^3 . The collector area is thus defined according to the typical favorable roof area for PVT collector installation, and the tank volume is thus defined mostly from engineering judgment by considering the tank footprint and cost. Therefore, it is worthwhile to perform a sensitivity analysis on collector area and storage tank volume. In addition, the impact of nighttime radiative cooling and using the heat pump to charge the storage tank is investigated because of their uniqueness in the SAHP system.

5.4.1 Sensitivity analysis of collector area and storage tank volume

In this sensitivity analysis, the PVT collector area is perturbed from 10 m^2 to 50 m^2 with an interval of 10 m^2 , and the storage tank volume is perturbed from 0.5 m^3 to 3.5 m^3 with an interval of 0.5 m^3 . All combinations of the collector area and tank volume are simulated to explore their impact on SPF.

Figure 5-21 and Figure 5-22 are the results, respectively, for Baltimore and Las Vegas. The SPF increases with the collector area and the storage tank volume, which is expected. The SPF tends to saturate at a smaller PVT area as the storage tank volume decreases. For example, in Baltimore, the SPF improves slightly for the case of tank volume of 0.5 m^3 as the collector area increases from 30 m^2 to 50 m^2 , while the SPF still shows a rapid increase for the case of tank volume of 3.5 m^3 . Similarly, the SPF tends to saturate at a smaller tank volume as the collector

area decreases. The above observations essentially imply the importance of matching collector area and storage tank volume: a big collector area needs a large tank volume and vice versa.

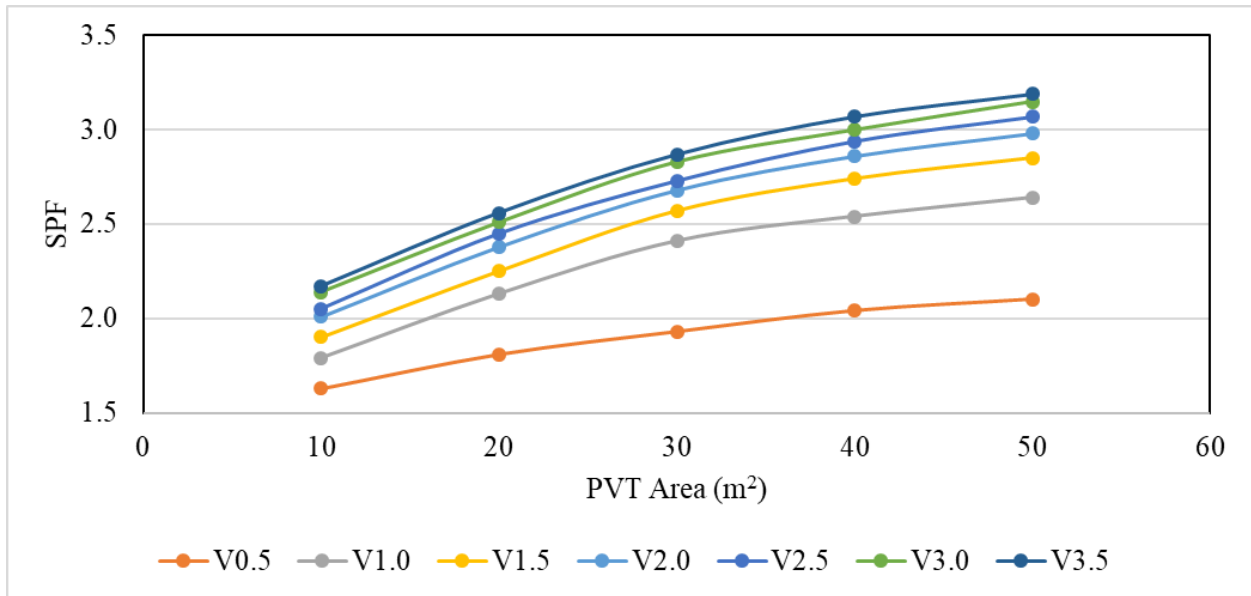


Figure 5-21: Sensitivity analysis on PVT area and storage tank volume for Baltimore

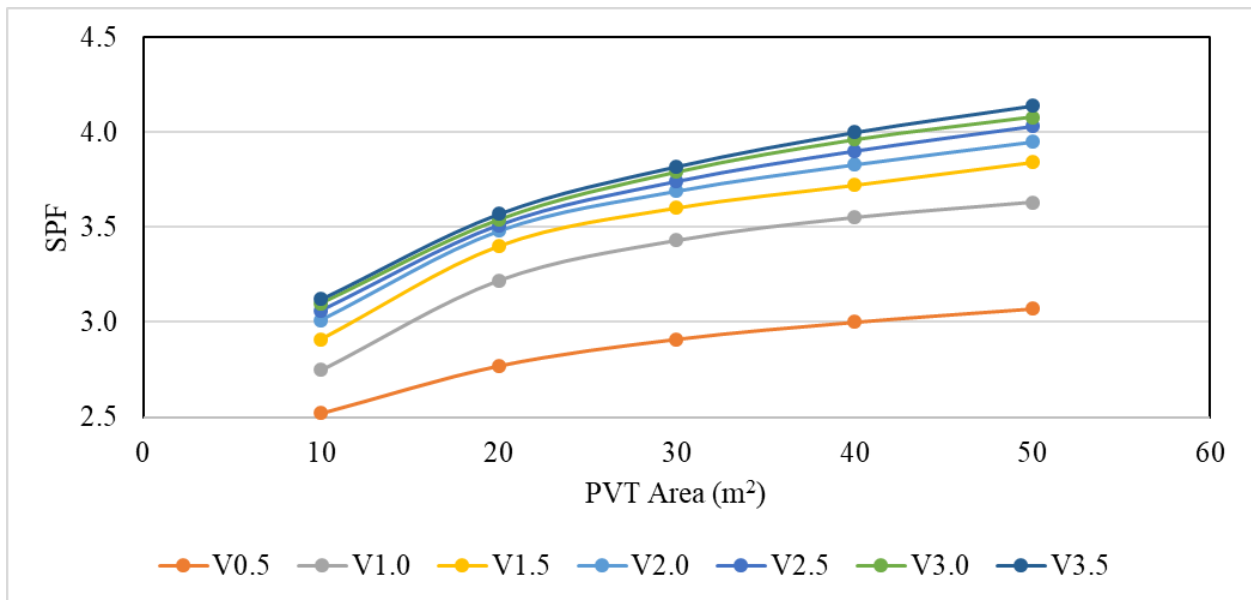


Figure 5-22: Sensitivity analysis on PVT area and storage tank volume for Las Vegas

5.4.2 Impact of nighttime radiative cooling

Recall that the system has a mode that uses PVT collectors to cool the storage at night (Mode 11). Actually, the cooling energy may come from both radiative cooling and the convective heat loss to the ambient (when the liquid temperature is higher than the ambient air temperature), but it is difficult to separate them out in the simulation. Additionally, radiative cooling also contributes to Mode 9 that uses PVT collectors as the source of the heat pump for cooling.

Investigating the impact of nighttime radiative cooling is simplified by excluding Mode 11 from the system operation and examining the resulted change in energy consumption. Figure 5-23 shows the results for the summer months because Mode 11 is used in summer only. Not using Mode 11 causes 11%-21% more energy consumption in Baltimore and 4%-31% more energy in Las Vegas.

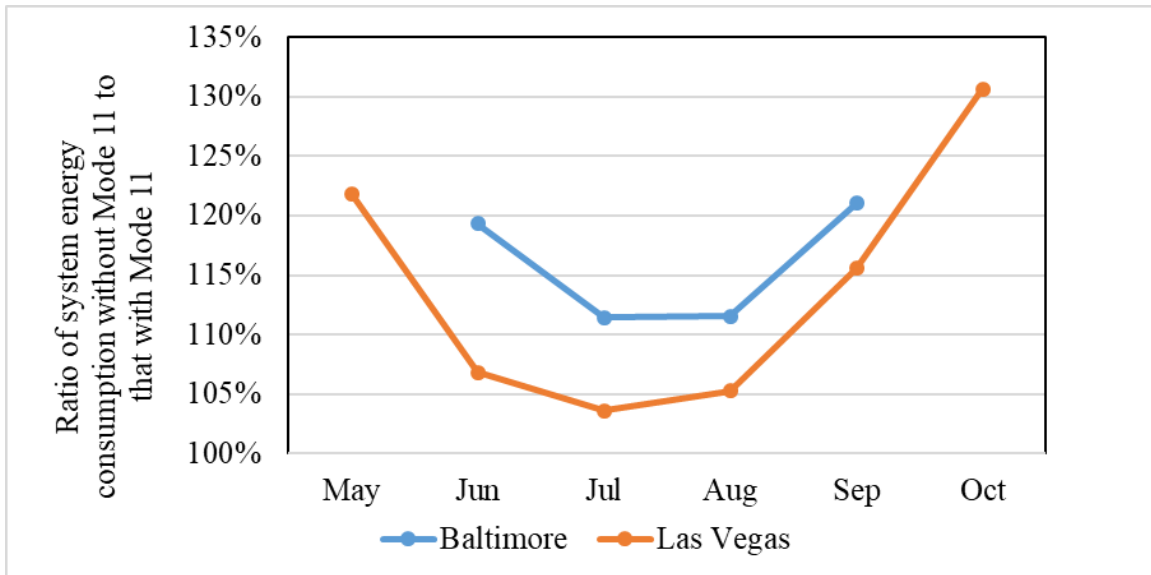


Figure 5-23: Impact of Mode 11 on the system energy consumption

5.4.3 Impact of thermal storage charging with the heat pump

The intent of using the heat pump to charge the thermal storage for heating (Mode 6) is to increase the storage temperature by using the collectors as the source. Increasing the storage temperature improves the capacity and efficiency when the heat pump runs for space heating. Certainly, having Mode 6 increases the heat pump running time. Recall that Mode 6 is used in the coldest months (January, February, November, and December) in Baltimore. The impact of Mode 6 is investigated by deactivating that mode in those four months and comparing the system energy consumption with that prior to the change. Figure 5-24 shows the results, which indicate that deactivating Mode 6 causes an 8%-34% increase in system energy consumption.

The following scenarios are also investigated: 1) using Mode 6 in March, April, and October in Baltimore; 2) using Mode 6 in December and January in Las Vegas; and 3) using the heat pump to charge the thermal storage for cooling in summer (Mode 12) in both locations. It is found that all the above scenarios consume more energy than the original one.

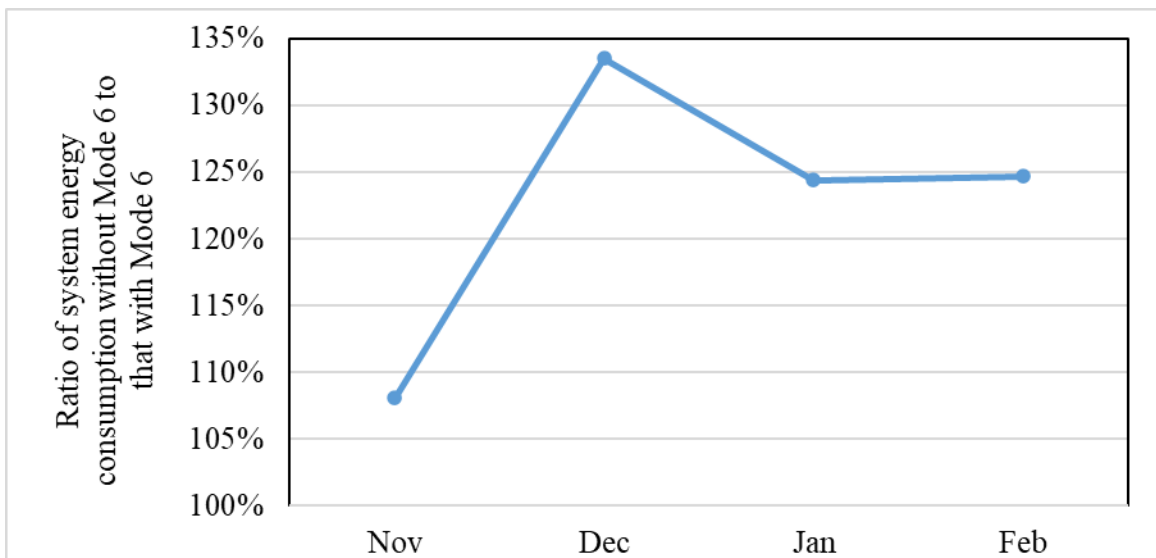


Figure 5-24: Impact of Mode 6 on the system energy consumption

5.5 Simplified control strategy

The multifunctional SAHP system presented in Section 3.1 consists of 14 operational modes. However, the runtime analysis (Figure 5-4 and Figure 5-5) reveals that several operational modes are rarely used. Therefore, the original system design and controls can be simplified by removing the unimportant operational modes. This section discusses simplification and its impact on system performance in the two considered locations: Baltimore and Las Vegas.

When analyzing the run time of different operational modes (Figure 5-4 and Figure 5-5) and investigating the impact of using the heat pump to charge the storage tank (Section 5.4.3), it has been found the following:

- The modes of using the PVT collectors directly for space heating (Mode 1) and space cooling (Mode 7) are never used for both locations. Therefore, Mode 1 and Mode 7 can be eliminated from the sequence of controls.
- The modes of using the storage tank directly for space heating (Mode 2) and cooling (Mode 8) are rarely used. Therefore, these two modes can be eliminated from the sequence of controls as well.
- Using the heat pump to charge the thermal storage tank for cooling (Mode 12) does not improve the system performance in both locations. Therefore, Mode 12 can be removed from the sequence of controls.
- The significance of Mode 6, which uses the heat pump to charge the thermal storage tank for heating) varies with the two locations. Mode 6 contributes to the system performance in Baltimore but not in Las Vegas (see Figure 5-24).

Consequently, after removing Modes 1, 2, 7, 8 & 12 in both locations, and additionally, Mode 6 in Las Vegas, the sequence of system controls is simplified to what Figure 5-25 shows. The system piping can be simplified accordingly, as shown in Figure 5-26 and Figure 5-27.

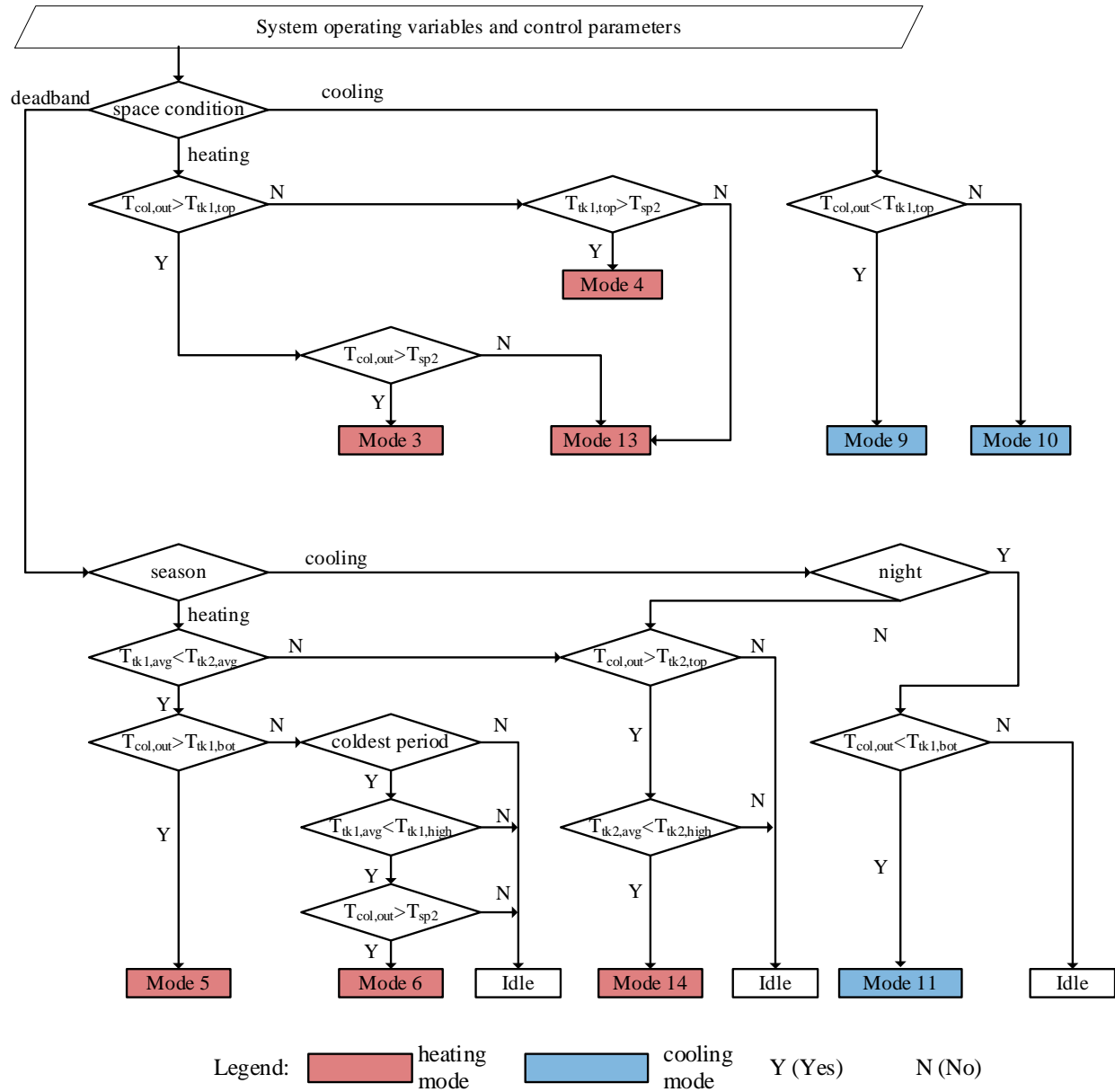


Figure 5-25: Flowchart diagram of the simplified control strategy for the proposed system.

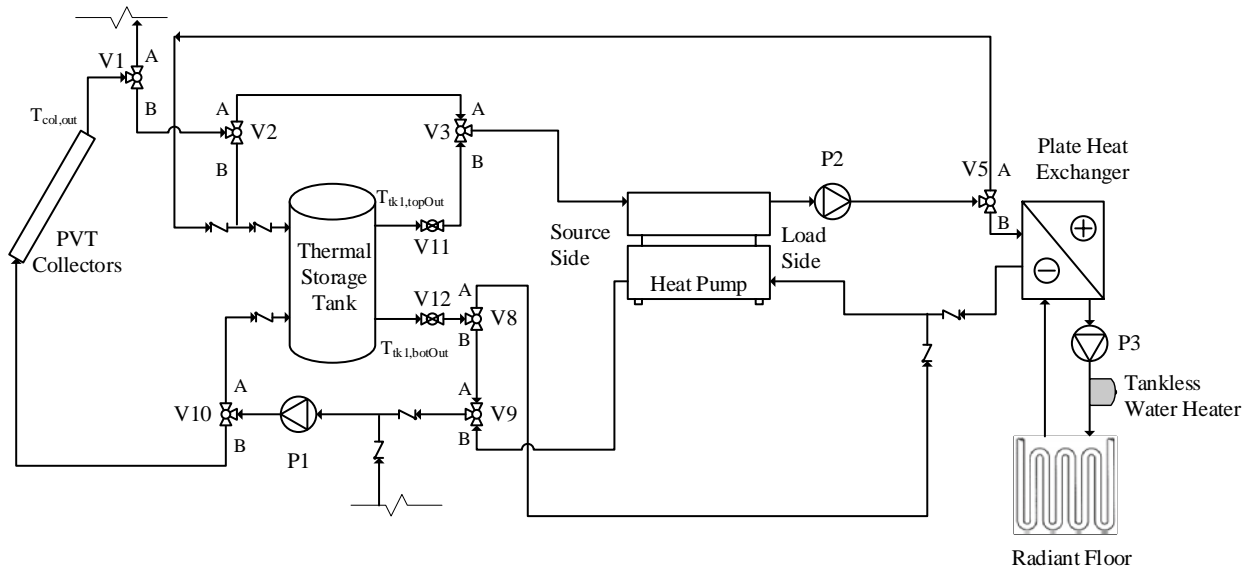


Figure 5-26: Schematic diagram of the SAHP system with simplified controls in Baltimore

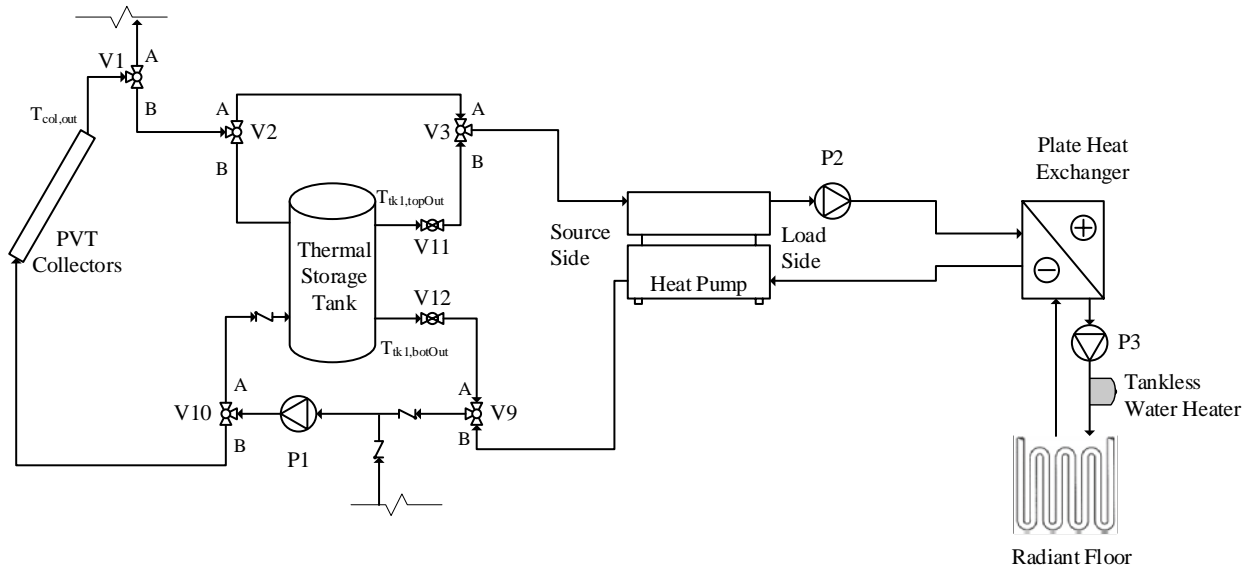


Figure 5-27: Schematic diagram of the SAHP system with simplified controls in Las Vegas

Based on the simplified system and controls, the simulation is run for both locations. The annual SPF of the simplified system is 2.58 and 3.63, respectively, in Baltimore and Las Vegas, which is less than 4% different from the original system (Table 5-2).

Table 5-2: Annual SPF of the system before and after the simplification

Controls	Annual SPF	
	Baltimore	Las Vegas
Original controls	2.69	3.70
Simplified controls	2.58	3.63

CHAPTER 6: INVESTIGATION OF SYSTEM PERFORMANCE IMPROVEMENT STRATEGIES

Three strategies that could potentially improve the performance of the SAHP system are explored in this chapter. These strategies include 1) replacing the water tank with an outdoor swimming pool for thermal storage, 2) replacing the water tank with a tank having phase change materials for latent thermal storage, and 3) replacing the liquid-to-liquid heat pump with a dual-source heat pump. The first two strategies intend to increase the thermal storage capacity, while the third strategy intends to use the favorable source for heat pump operation. For each of the three investigated strategies, the new components are described, and the system performance from TRNSYS simulation is discussed using SPF as the main criterion.

6.1 Strategy 1: Using an outdoor swimming pool for thermal storage

A 2 m³ tank filled with propylene glycol is used in the system presented in Chapter 3. The tank size is subject to space limitation, especially in residential buildings. In addition, the storage tank is not a small investment. Considering that some single-family houses have in-ground private swimming pools, it is worthwhile exploring the use of the pool for thermal storage. The pool can be covered in winter to store heat while keep open in summer to utilize water evaporation, convection, and radiation to the sky for cooling water storage. Figure 6-1 shows the schematic diagram of the system having a swimming pool. Only the schematic for space conditioning is shown because the schematic for DHW production is the same as the original system using a thermal storage tank.

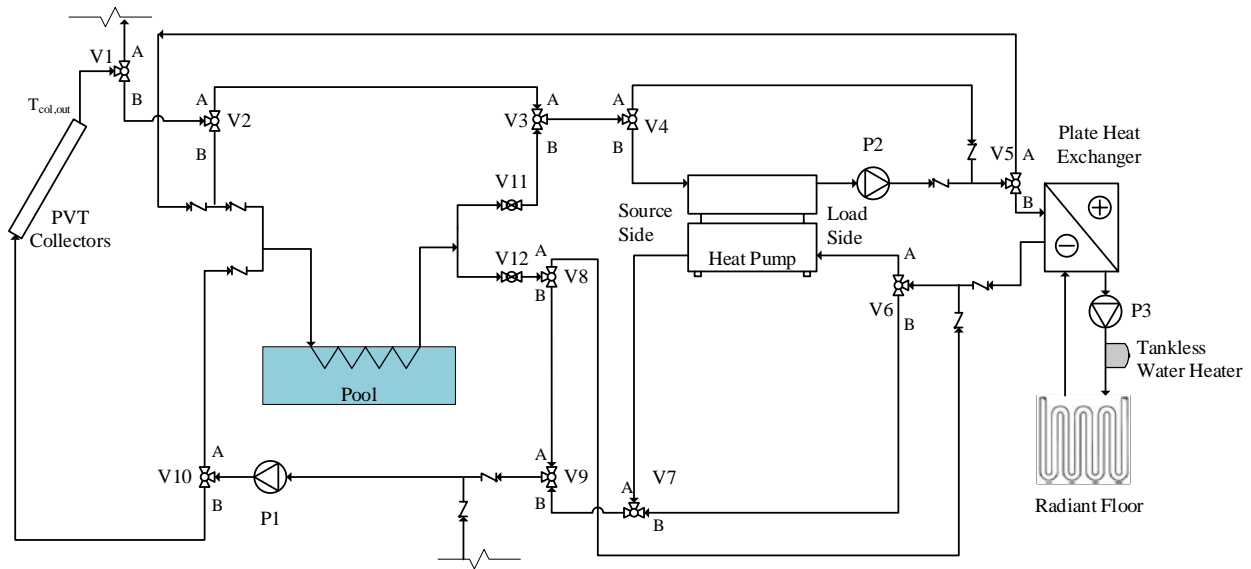


Figure 6-1: Schematic diagram of the SAHP system with a swimming pool

6.1.1 Swimming pool modeling

TRNSYS Type 344b is used to model the outdoor swimming pool. The model assumes that the pool water is ideally mixed, and the pool has one inlet and one outlet for water circulation. The pool can be fully covered, fully uncovered, and partially covered. As shown in Figure 6-2, the heat transfer items used to establish the heat balance for the control volume of pool water include heat loss due to water evaporation (Q_{evap}), heat loss to the surrounding due to convection (Q_{conv}), heat loss through the pool cover via conduction (Q_{cond}), solar absorption (Q_{sol}), long-wave thermal radiation to the sky (Q_{rad}), heat exchange due to water circulation (Q_{wc}), and heat change due to the fresh makeup water supply (Q_{fw}). Heat loss to the ground is not considered because of the challenge of modeling accuracy and the minor impact of heat transfer between the pool and the ground.

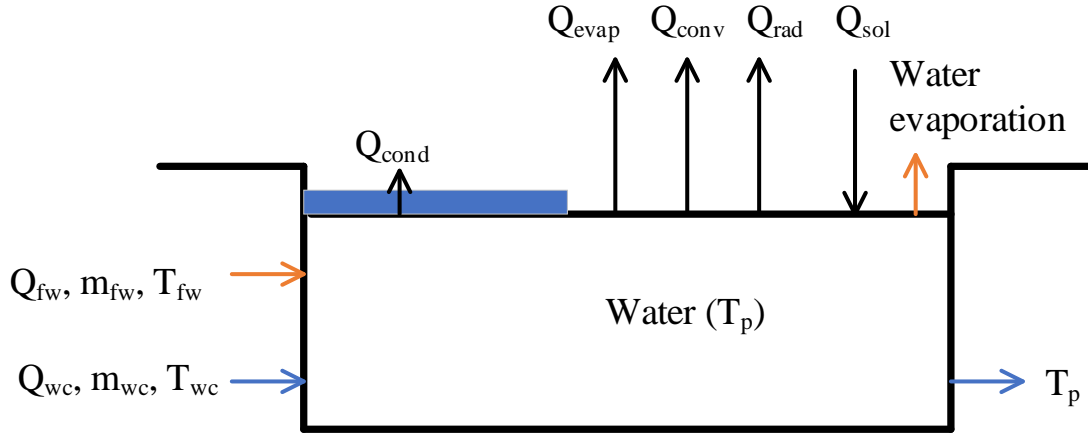


Figure 6-2: Energy balance of the swimming pool water

At every time step of the system simulation, the heat balance of the pool water leads to the following equation:

$$Q_{sol} + Q_{wc} + Q_{fw} - Q_{evap} - Q_{conv} - Q_{cond} - Q_{rad} = 0 \quad (6-1)$$

Of the items in Equation (6-1), the heat loss rate due to water evaporation (Q_{evap} , W) is calculated as:

$$Q_{evap} = A_p * (1 - f_{cover}) * (42.39 + 56.52 * V) * (P_{sat,T_p} - \varphi * P_{sat,T_a}) \quad (6-2)$$

where, A_p is the pool area (m^2), f_{cover} is the fraction of pool coverage, V is the wind speed near the pool surface (m/s), φ is the ambient air relative humidity, P_{sat,T_p} and P_{sat,T_a} refer to the saturated vapor pressure (Pa) at the pool temperature (T_p , °C) and the ambient air temperature (T_a , °C), respectively.

The convective heat loss (Q_{conv} , W) to the surrounding is calculated as:

$$Q_{conv} = A_p * (1 - f_{cover}) * (3.1 + 4.1 * V) * (T_p - T_a) \quad (6-3)$$

The conductive heat loss (Q_{cond} , W) from the pool water to the pool cover is calculated as:

$$Q_{cond} = A_p * f_{cover} * \frac{k_{cover}}{d_{cover}} * (T_p - T_{cover}) \quad (6-4)$$

where, k_{cover} , d_{cover} , and T_{cover} indicate the thermal conductivity (W/m-°C), thickness (m), and temperature (°C) of the pool cover.

The long-wave thermal radiation to the sky (Q_{rad} , W) is calculated as:

$$Q_{rad} = A_p * (1 - f_{cover}) * \epsilon_w * \sigma * [(T_p + 273.15)^4 - (T_{sky} + 273.15)^4] \quad (6-5)$$

where, T_{sky} is the effective sky temperature (°C) and ϵ_w is the emissivity of water (=0.9).

The calculation of T_{sky} has been discussed in Section 4.1.

The solar radiation is calculated as:

$$Q_{sol} = A_p * (1 - f_{cover}) * \alpha_w * G \quad (6-6)$$

where, G is the global horizontal solar radiation (W/m²) and α_w is the solar absorptivity of water (=0.9).

The heat exchange rates due to water circulation (Q_{wc} , W) and fresh water makeup (Q_{fr} , W) are calculated as:

$$Q_{wc} = m_{wc} * C_p * (T_{wc} - T_p) \quad (6-7)$$

$$Q_{fr} = m_{fr} * C_p * (T_{fr} - T_p) \quad (6-8)$$

where, C_p is the specific heat of the water in J/kg-°C, m_{wc} and m_{fr} are the mass flow rates (kg/s) of water circulating through the pool and fresh water makeup, T_{wc} and T_{fr} are the inlet temperature (°C) of circulating water and fresh water supply.

To calculate the pool cover temperature used in Equation (6-4), a heat balance equation needs to be established for the cover in a similar manner as that for the pool water. Certainly, some

heat transfer items, such as heat losses due to water evaporation and heat exchange due to water circulation, do not apply.

The in-ground pool used in the simulation model has a typical medium size of 4.6m X 9.1m (15 ft X 30 ft). Based on an average depth of 1.7m (5.5 ft), the pool volume is 70 m³. The pool is fully covered from October 1st to April 30th in Baltimore and from November 1st to March 31st in Las Vegas, whereas the pool is fully open for the rest of the year. Based on a commercial product (ThermGard), the pool cover has a composite, laminated material with the following properties: thickness (8 mm), thermal conductivity (0.036 W/m-K), emissivity (0.6), and solar absorptivity (0.6).

6.1.2 System simulation and results for Strategy 1

The system simulation model is set up by replacing the thermal storage tank in Figure 4-3 with the outdoor swimming pool as described in the previous section. Because the pool has water and Type 344b does not support the use of an immersed heat exchanger, an external heat exchanger is used to isolate the water loop for the pool and the rest of the system (Figure 6-3). The rest of TRNSYS model is identical to Figure 4-3 and is not shown in Figure 6-3 for clarity. To approximate the real system design and operation (Figure 6-3), a pump with zero-energy consumption is used in the loop between the heat exchanger and the pool. In addition, the minimum allowable fluid temperature (i.e., T_{sp2}) of the thermal storage is increased from -3°C for the tank to 3°C for the pool.

- Mode 6 is used only in Baltimore for four months, from November to February. If the conditions for running Mode 6 are met, it can be activated until the storage temperature reaches a predefined limit of 45°C.
- Mode 5 is used in both Baltimore and Las Vegas. This mode can be activated as long as its running conditions are met. No storage temperature limit is applied when running Mode 5.

Accordingly, the investigation on control improvement is made by performing sensitivity analysis on two aspects: 1) In Baltimore, the storage temperature limit is varied from 0°C to 45°C with a step of 5°C when the system runs in Mode 6; 2) In Las Vegas, the storage temperature limit is applied, and it is varied from 5°C to 20°C with a step of 5°C when the system runs in Mode 5. Note that running Mode 5 is normally favorable in cold climates, and therefore, the investigation of Mode 5 running is made for Las Vegas only. Figure 6-4 and Figure 6-5 show the results of sensitivity analysis.

In Baltimore, as Figure 6-4 shows, the SPF initially increases from 2.34 to 2.73 as the pool temperature limit is increased from 0°C to 20°C in Mode 6. Then, the SPF decreases from 2.73 to 2.71 when the pool temperature limit is increased from 20°C to 25°C, beyond which the SPF no longer changes. The above trend of SPF can be explained. With the increase of the pool temperature limit, the pool water can reach a gradually higher temperature at the beginning, which leads to 1) reduced backup electric heater usage because of the higher heat pump heating capacity, 2) improved efficiency when the heat pump is used for space heating, and 3) increased heat pump running time. The first two effects play a dominating role at the beginning and thus increase the SPF. However, when the pool temperature limit is increased from 20°C to 25°C, the benefits from the reduced usage of auxiliary electric heater and improved heat pump efficiency are exceeded by

the increased electricity consumption caused by the increase of heat pump runtime. Therefore, the SPF decreases. The SPF remains unchanged after the pool temperature limit is increased above 25°C because the pool temperature never reaches above 25°C. Since the case of pool temperature limit at 0°C is equivalent to the case of not using Mode 6, the sensitivity analysis also demonstrates the value of Mode 6 even if the pool is used as the thermal storage.

In Las Vegas, as Figure 6-5 shows, the SPF slightly increases from 4.32 to 4.33 as the pool temperature limit is increased from 5°C to 10°C in Mode 6 and then decreases from 4.33 to 4.23 when the pool temperature limit is further increased from 10°C to 20°C. Because the mode of running auxiliary electric heater is rarely used for space heating, the change of pool temperature (limit) affects the interaction between the circulation pump energy in Mode 5 and the heat pump energy when the heat pump is used for space heating. With a mild climate in Las Vegas, a higher pool temperature limit implies that Mode 5 is heavily used, leading to higher pump energy consumption. However, the increased pump energy consumption in Mode 5 may not be compensated with the reduction of heat pump energy use. Figure 6-5 clearly demonstrates the importance of setting an appropriate pool temperature limit in Mode 5 because the case of not having a limit has the lowest SPF in all investigated cases.

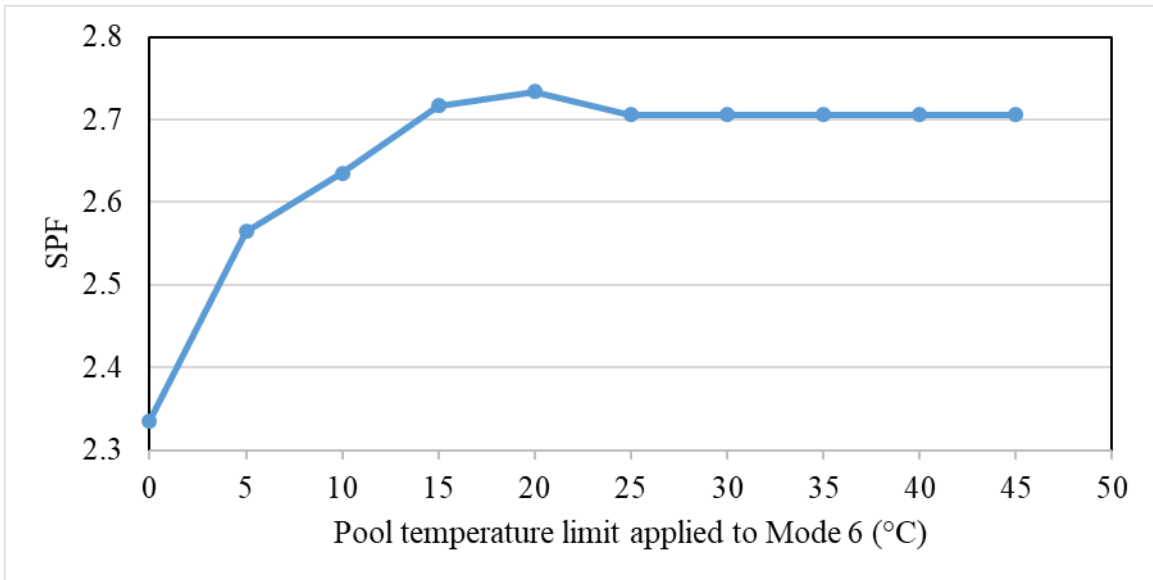


Figure 6-4: The change of annual SPF with the pool temperature limit applied to Mode 6 in Baltimore

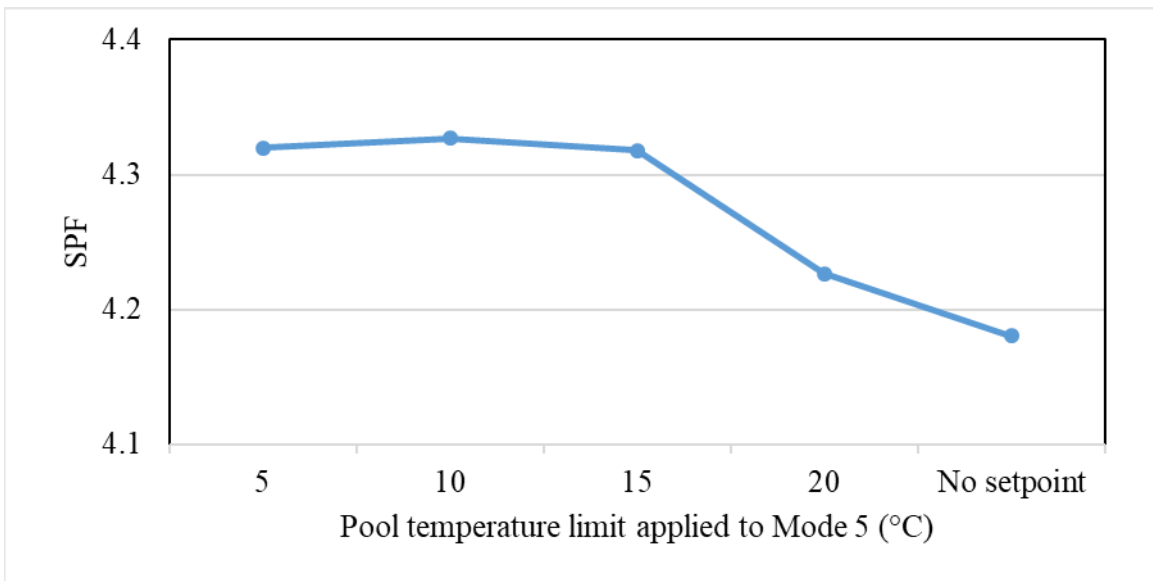


Figure 6-5: The change of annual SPF with the pool temperature limit applied to Mode 5 in Las Vegas

In summary, replacing the 2 m³ water tank with an outdoor swimming pool for thermal storage improves the system performance. The improvement is more significant in hot climates

than in cold climates. The pool temperature limit settings for Mode 5 in hot climates and Mode 6 in cold climates have a big impact on the system performance. With appropriate settings, the system with a typical in-ground pool has an annual SPF of 2.73 in Baltimore and 4.33 in Las Vegas, 1% and 17% higher than the original system design with a water tank.

6.2 Strategy 2: Using a tank with integrated phase-change-material (PCM) modules for thermal storage

The previous section has shown that the performance of solar-assisted heat pump systems, evaluated by the SPF, can be improved by replacing the 2 m³ tank with an outdoor swimming pool for thermal storage. Because many single-family houses do not have swimming pools, it is worthwhile exploring other approaches to increase the thermal storage capacity. In this section, the use of a tank with integrated PCM modules and its impact on the system performance is studied. PCMs are used to take advantage of the latent heat of the phase change between their solid and liquid states for thermal energy storage. The phase change process can store or release a large amount of thermal energy in the latent form with small temperature changes. High thermal conductivity, high heat of fusion, high density, and high specific heat are the desired thermal-physical properties of PCMs. Adding PCM to the thermal storage tank does not change the system configuration. Therefore, the original system diagram (Figure 3-1) is still valid for the SAHP system using a tank with integrated PCM modules for thermal storage.

6.2.1 PCM storage tank modeling

TRNSYS Type 840 is used to model a tank with integrated PCM modules, which can have the shape of cylinder and sphere. Type 840 also supports the modeling of a tank filled with PCM

slurries. Based on the technical manual of Type 840, it can model a tank with one built-in auxiliary heater and up to five pairs of ports. Each pair of ports can be either direct inlet and outlet fluid connections to the tank or the inlet and outlet of an immersed heat exchanger. Similar to the model for a conventional water tank (Type 158) as described in Section 4.3, the PCM storage tank is modeled with a number of nodes, which represents the same number of evenly divided horizontal layers. Each node's energy balance is established by considering the following mechanisms: heat flow through fluid movement due to inlet and outlet flow streams, the heat exchange between the tank fluid and the fluid in the immersed heat exchanger, the heat input from the internal auxiliary heater, thermal conduction between the neighboring nodes, heat loss to the ambient through the tank surfaces, and the heat exchange with the PCM modules. Type 840 also divides the integrated PCM module into a user-defined number of radial nodes. The energy balance for each radial node includes the heat transfer between the storage fluid and PCM modules (for the outmost node only), the heat conduction between neighboring PCM nodes, and the latent energy from the phase change process. The convective heat transfer in the liquid phase of the PCM is not considered in the model.

Type 840 uses the enthalpy approach to account for the change of thermal properties during the phase change process. The enthalpy approach assumes that enthalpy is a continuous and invertible function of temperature. Therefore, the thermal-physical properties of the PCM, including enthalpy, density, thermal conductivity, and, viscosity are provided as a function of temperature through a text file. This text file can include a maximum of 100 different temperatures and the corresponding thermal-physical properties. The text file is then read by Type 840 during simulation to derive the required properties.

In this work, the PCM storage tank has two pairs of ports for direct fluid inlets and outlets: one pair of ports is configured to have its inlet at the tank's top and the outlet at the bottom, whereas

the other pair of ports have the opposite configuration. The PCM storage tank does not have immersed heat exchangers and auxiliary heaters. The PCM modules are solid cylinders with a diameter of 150 mm. The PCM cylinder modules are filled with Sodium Acetate Trihydrate (SA) made by SGL Carbon. The selected PCM has a latent heat of 180 kJ/kg. Because SA has low thermal conductivity, Graphite is mixed with SA to increase the thermal conductivity of the PCM module. Table 6-1 summarizes the major parameters of the PCM storage tank. Except for the parameters related to the PCM, all tank parameters are the same as the thermal storage tank discussed in Chapter 4.

Table 6-1: PCM tank major parameters

Parameter	PCM Storage tank (Type 840)
Fluid in the tank	Water
Tank volume (m ³)	2.0
Tank height (m)	1.8
Number of tank nodes	6
Heat loss rate (W/K)	9.0
Height fraction of inlet 1	1
Height fraction of outlet 1	0
Height fraction of inlet 2	0
Height fraction of outlet 2	1
PCM material	SA + Graphite
PCM module shape	Cylinder
PCM inner diameter (mm)	0.0
PCM outer diameter (mm)	150.0
PCM number of radial nodes	3
Thickness of PCM container (mm)	0.5
Therm. Cond. of PCM container (W/m-K)	177

Table 6-1 cont: PCM tank major parameters

Parameter	PCM Storage tank (Type 840)
C_p of PCM container (J/kg-K)	875
Density of PCM container (kg/m ³)	2770

6.2.2 System simulation and results for Strategy 2

The system simulation model is set up by replacing the storage tank in Figure 4-3 with the PCM tank as described in the previous section. It is found that TRNSYS Type 840 does not support the use of glycol solution in the tank with integrated PCM modules. The fluid in the PCM tank can be water only. Therefore, the tank fluid is changed from the propylene glycol solution to water. Because of the change of tank fluid, the minimum allowable fluid temperature (i.e., T_{sp2}) of the thermal storage is increased from -3°C for the sensible storage tank to 3°C for the PCM tank. In addition, as Figure 6-6 shows, the PCM tank is separated from the rest of the system through external heat exchangers to avoid the mix of tank water and the glycol solution used in the heat pump and collector loops. Other than the above changes, the system operation modes and controls are the same as those described in Section 3.2 for the sensible storage tank.

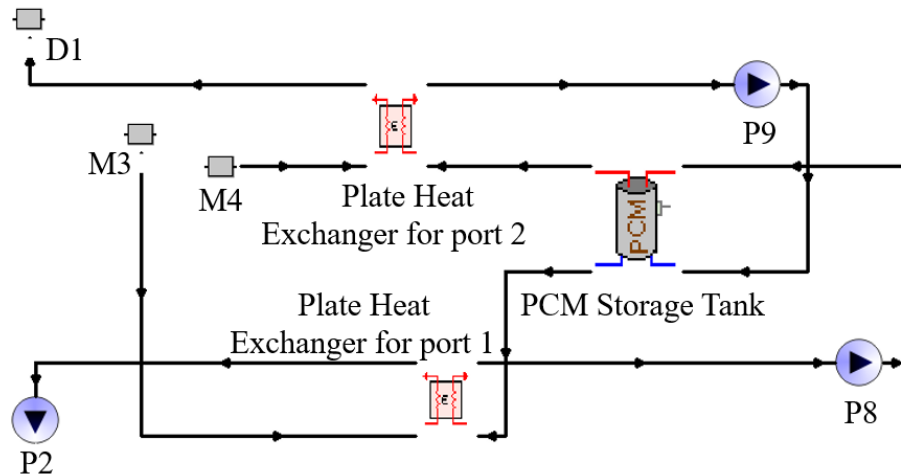


Figure 6-6: The modified section of the TRNSYS model for the PCM tank case

When modeling the system performance, there are two important considerations: the melting temperature and the percentage of PCM in the tank. The melting temperature refers to the temperature at which the PCM changes between its solid and liquid phases. The latent heat of the PCM module is available only when the tank temperature reaches the PCM's melting temperature. Therefore, the melting temperature of the PCM module is critical to determine the thermal storage capacity. Similarly, the percentage of tank volume occupied by PCM modules also determines the thermal storage capacity. In this subsection, the impact of PCM melting temperature and volume is investigated sequentially.

Most commercial PCMs are available in a range of melting temperatures. Therefore, it is reasonable to explore PCM modules with similar thermal properties and differing melting temperatures. While keeping the tank filled with 50% PCM modules, the melting temperature is varied from 5°C to 30°C with a step of 5°C. For each melting temperature, the system is run in Baltimore and Las Vegas, and the SPF is used to compare the system performance. Figure 6-7 and

Figure 6-8 show the SPF, including both monthly and annual values, corresponding to different melting temperatures in the two locations. These two figures indicate the following:

- During the heating season (November-April in Baltimore and December-February in Las Vegas), PCM modules with a lower melting temperature (in the range between 5°C and 15°C) tend to have a higher SPF. A low melting temperature implies that 1) the tank may be charged with PVT collectors longer; 2) the heat pump may run at high efficiency when it is used to charge the tank; and 3) the heat pump may run at low efficiency when it uses the tank as the source for space heating. Because the time in different operational modes varies, the optimal melting temperature varies with different months in the heating season.
- In the shoulder season (May & October in Baltimore and March & November for Las Vegas), PCM modules with a moderate melting temperature between 10°C and 20°C tend to have a high SPF.
- In the cooling season (June-September in Baltimore and April-October in Las Vegas), PCM modules with a higher melting temperature in the range between 20°C and 30°C tend to have a higher SPF. A high melting temperature implies that 1) the tank may be charged with PVT collectors longer for radiative cooling; and 2) the heat pump may run at low efficiency when it uses the tank as the sink for space cooling. Because the time in different operational modes varies, the optimal melting temperature varies with different months in the cooling season as well. It needs to be noted that the phase change may never occur in PCM modules with a very low melting temperature. Such a case can be observed in Figure 6-7 and Figure 6-8, which have almost the same SPF in July and August when the melting temperature is lower than 20°C.

- Both locations have the highest annual SPF when the PCM has a melting temperature of 10°C. The highest annual SPF is 2.52 in Baltimore, and it is 3.52 in Las Vegas. Both values are lower than the ones corresponding to the original SAHP system.

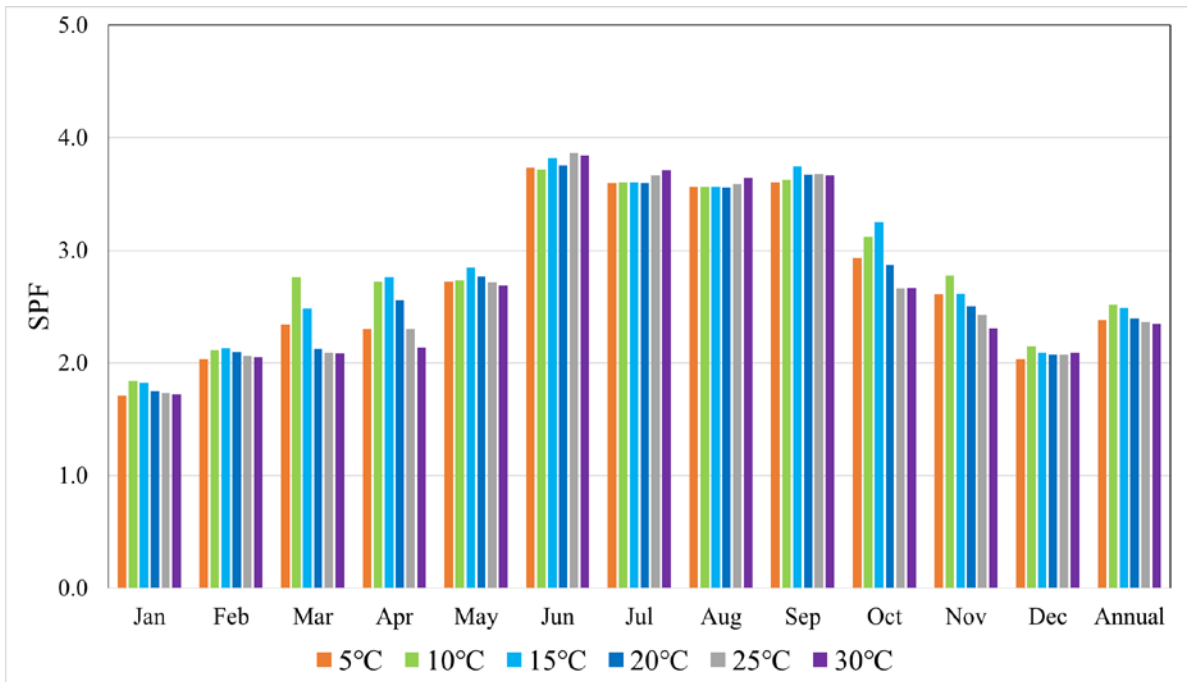


Figure 6-7: Comparison of the SPF for systems featured the use of PCM with different melting temperatures in Baltimore while keeping the PCM module at 50% of the tank volume

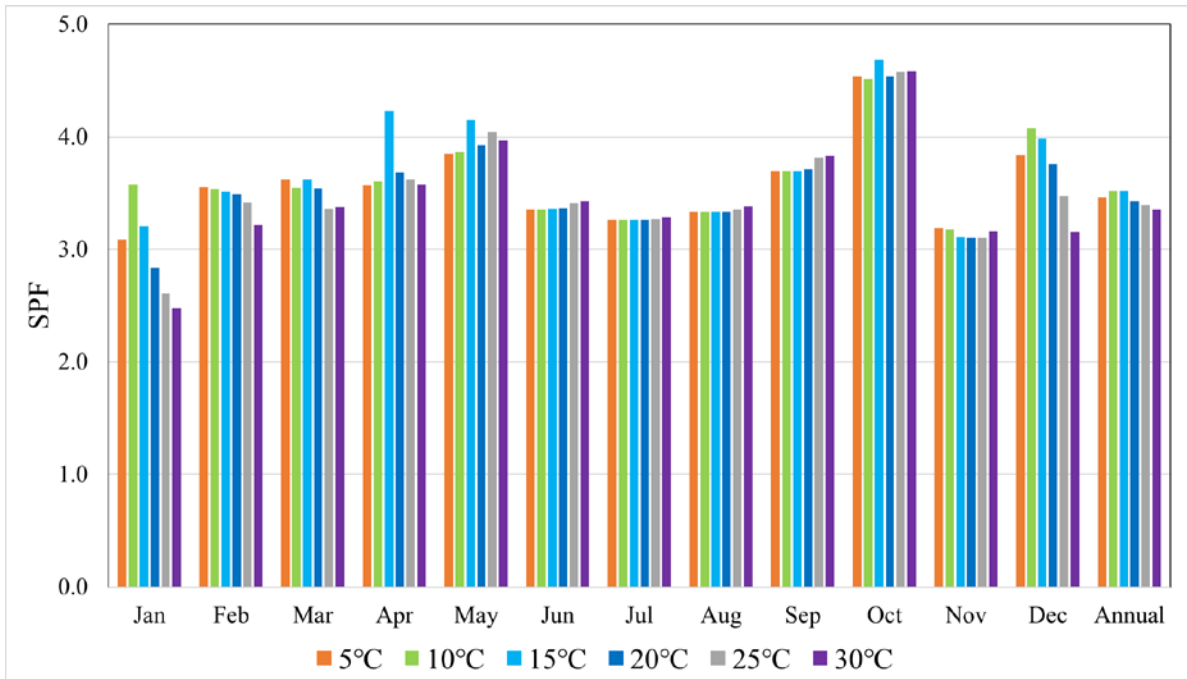


Figure 6-8: Comparison of the SPF for systems featured the use of PCM with different melting temperatures in Las Vegas while keeping the PCM module at 50% of the tank volume

The above analysis has assumed that the PCM modules occupy 50% of the tank volume. A natural extension is to investigate the impact of PCM volume on the system performance while keeping the PCM's melting temperature at 10°C. Figure 6-9 and Figure 6-10 show the system performance, evaluated by SPF, for different percentages (i.e., 0%, 25%, 50%, and 75%) of the tank storage volume filled with the PCM modules. The case of 0% represents that PCM modules are not used in the tank. The following can be observed:

- Using more PCM modules leads to higher SPF's for the entire heating season in Baltimore and for the coldest months (December and January) in Las Vegas. The reason is that in these months, the PCM's melting temperature (10°C) falls into the range of tank operating temperatures.

- Using more PCM modules generally leads to lower SPF_s for the cooling season (i.e., June to September in Baltimore and April to October in Las Vegas). This can be explained from the following aspects. First, in the cooling season, the tank operating temperature rarely goes to 10°C or below. Therefore, the latent heat of PCMs does not contribute to the system operation. Furthermore, the PCM has approximately 50% lower specific heat capacity than water. Hence, using PCM modules in the tank actually decreases the thermal storage capacity when only sensible heat is involved.
- If evaluated for the whole year, in Baltimore, the annual SPF increases with the percentage of tank volume used for the PCM modules. Relative to the case of not using PCM, the annual SPF is increased by 1%, 5%, and 6%, respectively, for the case of using 25%, 50%, and 75% of the tank volume for the PCM modules. In Las Vegas, the annual SPF_s have negligible differences for different cases.

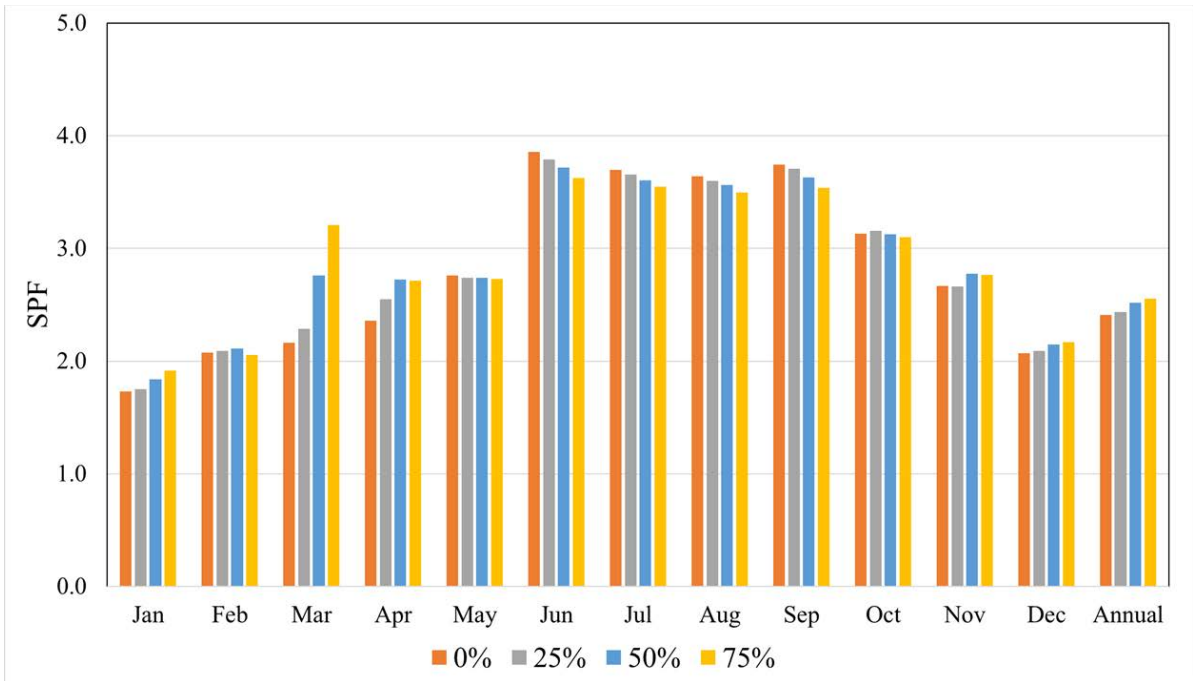


Figure 6-9: Comparison of the SPF for systems with different percentages of the tank volume used by the PCM module having a melting temperature of 10°C (Baltimore)

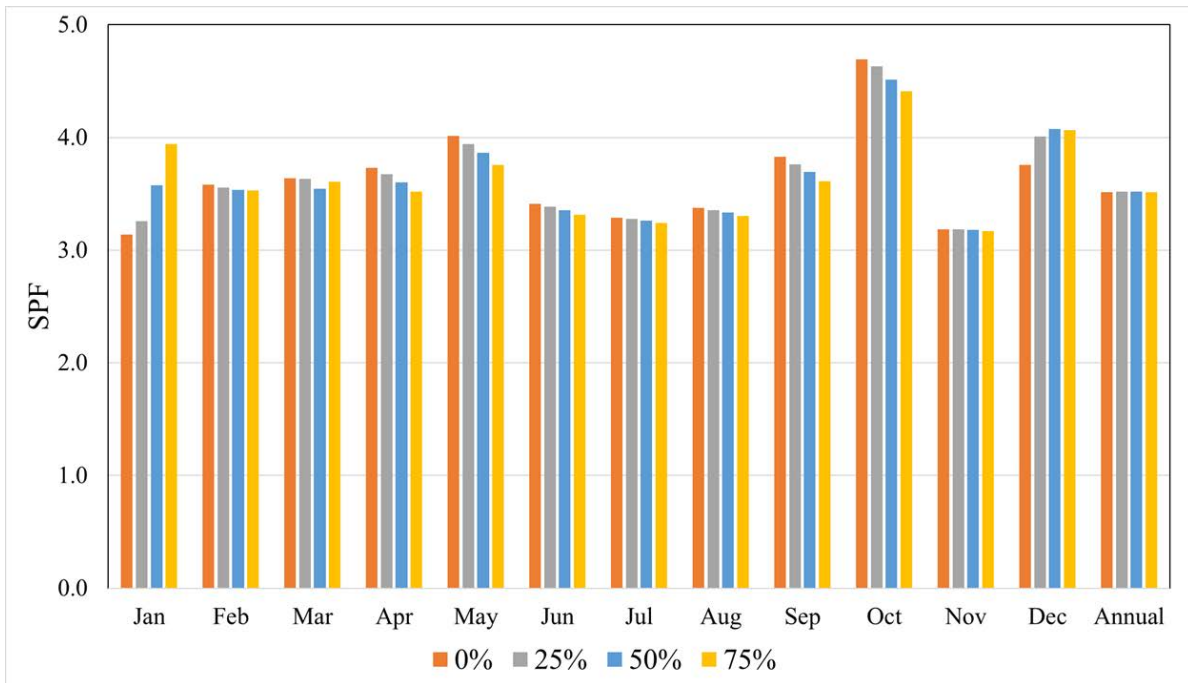


Figure 6-10: Comparison of the SPF for systems with different percentages of the tank volume used by the PCM modules having a melting temperature of 10°C (Las Vegas)

In summary, based on the proposed system design and controls, the simulation results show that integrating PCM modules in the tank may not increase the annual SPF. The PCM's melting temperature and the tank operating temperature profiles play important roles in determining the benefits of using PCMs. If the tank operating temperature profiles cross the melting temperature frequently, using PCMs will contribute to the improvement of system performance; otherwise, using PCMs will unlikely bring any benefits and even degrade the system performance if the PCM has a lower specific heat than the tank liquid.

6.3 Strategy 3: Dual-source heat pump

The original system design uses a liquid-to-liquid heat pump. Glycol solution is used to transfer energy between PVT collectors or the thermal storage tank and the heat pump. Because the thermal storage tank is charged by PVT collectors (either directly or indirectly through the heat pump), PVT collectors are regarded as the only source of the heat pump. However, based on the analysis in Chapter 5, the original system may have the following two issues caused by the use of a single source. First, in cold winter conditions, the tank temperature may fall below its low limit for heat pump operation, which triggers the frequent use of auxiliary electric heating. Second, sometimes when the tank is used as the source of the heat pump operation, the tank temperature is not favorable at all in comparison with the air temperature. For example, in summer, if the tank cannot be adequately cooled through nighttime radiative cooling, the tank may have a higher temperature than the ambient air. In this situation, it would be more favorable to use ambient air as the source of the heat pump operation. The above two problems can be addressed by adding another source to the heat pump's operation, leading to a dual-source heat pump system design.

Both ground and air are candidates for the additional energy sources of the heat pump. Air is selected in this work because of its considerably lower installation cost compared to geothermal systems. Therefore, the dual-source SAHP system features the use of both ambient air and glycol solution as the energy sources of the heat pump. These two sources are connected in parallel so that each can be used independently, as shown in Figure 6-11.

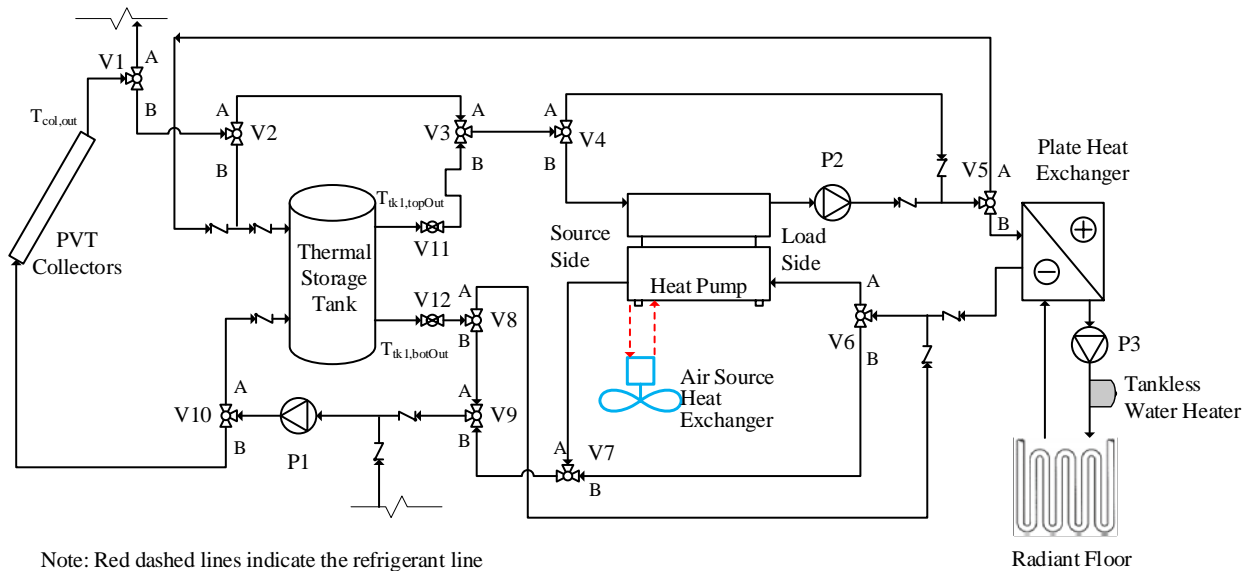


Figure 6-11: Schematic diagram of the PVT-dual-source HP system

6.3.1 Dual-source heat pump modeling

TRNSYS does not have a model dedicated for dual-source heat pumps. Therefore, a workaround solution is to simulate two separate heat pumps: one air-source heat pump and one solar-assisted liquid-source heat pump. These two heat pumps are connected in parallel and which one operates depends on the controls to be discussed later. TRNSYS Type 927 is used to model the liquid-source heat pump, with the same approach and parameters presented in Chapter 4. TRNSYS Type 941 is used for modeling single-stage air-to-liquid heat pumps. The modeling

approach is very similar to that for Type 927. The heat pump's performance is based on two external data files containing catalog data for normalized capacity and normalized power consumption at different operating conditions (i.e., entering air temperature on the source side and entering liquid temperature at the load side). One data file is for heating, and the other data file is for cooling. In this work, the data files are developed based on Carrier's reversible air-to-water heat pump (Model 30AWH012-3Ph). The normalized data files are attached in Appendix B. Table 6-2 lists the parameters of the air-to-liquid heat pump used in TRNSYS. Figure 6-12 shows the modifications made to the TRNSYS figure of the original multifunctional SAHP system (Figure 4-3). The red lines are the modifications related to DHW production using heat pump desuperheater, and the black lines represent the modifications regarding space heating and cooling.

Table 6-2: Air-to-liquid heat pump parameters

Parameter	Air-to-liquid HP (Type 941)
Liquid in the load side	propylene glycol
Liquid flowrate (GPM)	10
Air flowrate (CFM)	1660
Rated cooling capacity (kW)	10.2
Rated EER for cooling (Btu/h/W)	10.3
Rated heating capacity (kW)	12.0
Rated COP for heating (-)	4.3
Capacity of auxiliary heater (kW)	4
Compressor cutout temperature (°C)	-20
Auxiliary heater lockout temperature (°C)	-10

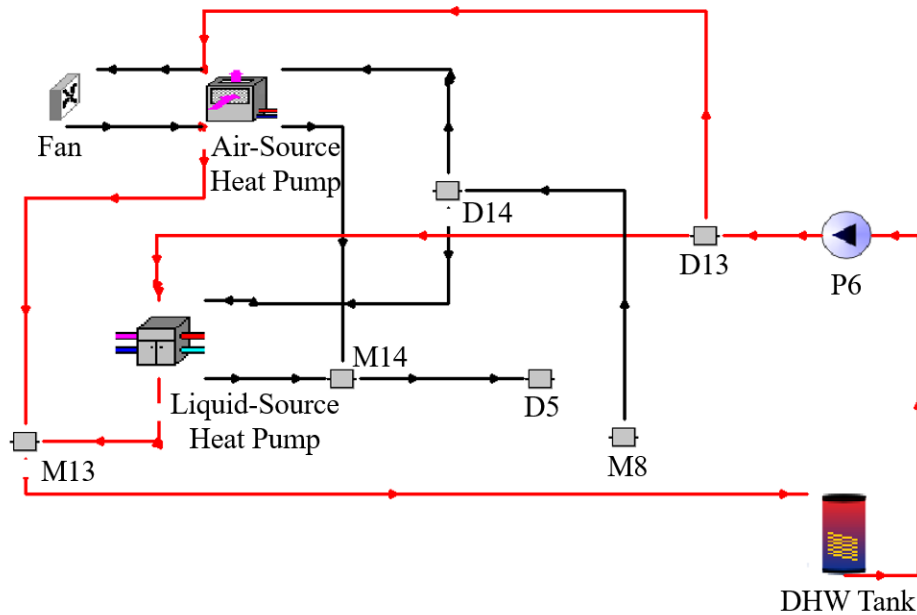


Figure 6-12: The modified section of the TRNSYS model for the dual-source heat pump case

In Table 6-2, the rated conditions in cooling have the evaporator liquid entering/leaving temperature at 12°C/7°C and the outside air temperature at 35°C. The rated conditions in heating have the condenser liquid entering/leaving temperature at 30°C/35°C and the outside air temperature at 7°C (Carrier n.d.). The air-to-water heat pump has a desuperheater that uses the superheated gas leaving from the compressor for hot water generation. The desuperheater has the same parameter settings as used for Type 927 (see Chapter 4).

A natural question of operating the dual-source SAHP system is which source is used at what conditions. In this work, the ambient air temperature (T_{air}), the PVT outlet temperature ($T_{col,out}$), and the tank top temperature ($T_{tk1,top}$) are compared to determine the more favorable source of the heat pump. As a result, the following modes are added to the control sequence of the system operation:

- Mode 15: Air-source heat pump for space heating. In this mode, the outdoor fan circulates air to the outdoor coil (i.e., evaporator) of the heat pump, while Pump P2 circulates the glycol solution between the condenser and the plate heat exchanger on the demand side.
- Mode 16: Air-source heat pump for space cooling. In this mode, the outdoor fan circulates air to the outdoor coil (i.e., condenser) of the heat pump, while Pump P2 circulates the glycol solution between the evaporator and the plate heat exchanger on the demand side.

Mode 15 operates when the following conditions are all satisfied: 1) The space calls for heating; 2) The ambient air temperature (T_{air}) is higher than the liquid-source temperature (the larger value of $T_{col,out}$ and $T_{tk1,top}$) by a predefined offset value (T_{offset}) or the liquid-source temperature is lower than the low bound for operating the liquid-source heat pump; and 3) The ambient air temperature is above the compressor cutout temperature. Because the air-to-water heat pump has an integrated auxiliary heater that is activated when T_{air} is lower than the auxiliary heater lockout temperature, Mode 15 actually consists of two sub-modes: Mode 15-1 having the auxiliary heater off and Mode 15-2 having the auxiliary heater on.

Mode 16 operates when the following conditions are all satisfied: 1) The space calls for cooling; and 2) The ambient air temperature (T_{air}) is lower than the liquid-source temperature (the smaller value of $T_{col,out}$ and $T_{tk1,top}$) by a predefined offset value (T_{offset}).

The temperature offset value (T_{offset}) plays an important role in determining whether the ambient air or the glycol solution is the preferred source of the heat pump operation. An offset value of zero implies selecting the source with the higher temperature for heating and the lower temperature for cooling. However, the above simple setting may not necessarily result in better

system performance because the liquid-to-liquid heat pump and the air-to-liquid heat pump have different rated efficiency and may have different operational efficiency even at the same source temperature conditions. Therefore, the temperature offset, which can take a non-zero value, is considered in the study. The air source can be used for heating if the ambient air is higher than the water-source temperature plus the offset value, and the air source can be used for cooling if the ambient air is lower than the water-source temperature minus the offset value.

6.3.2 System simulation results for Strategy 3

The impact of the temperature offset on system performance is investigated by varying the offset value from -3°C to 6°C . Figure 6-13 and Figure 6-14 show the change of annual SPF with the temperature offset for Baltimore and Las Vegas, respectively.

Both figures show that the annual SPF has small changes (less than 1%) across the considered temperature offset values. This indicates a “fuzzy” range instead of an exact point for switching the dual-source heat pump operation between the air source and the (solar) liquid source. Moreover, all investigated cases of the dual-source heat pump system have higher annual SPF than the original liquid-source only SAHP system (SPF = 2.69 for Baltimore and SPF = 3.70 for Las Vegas).

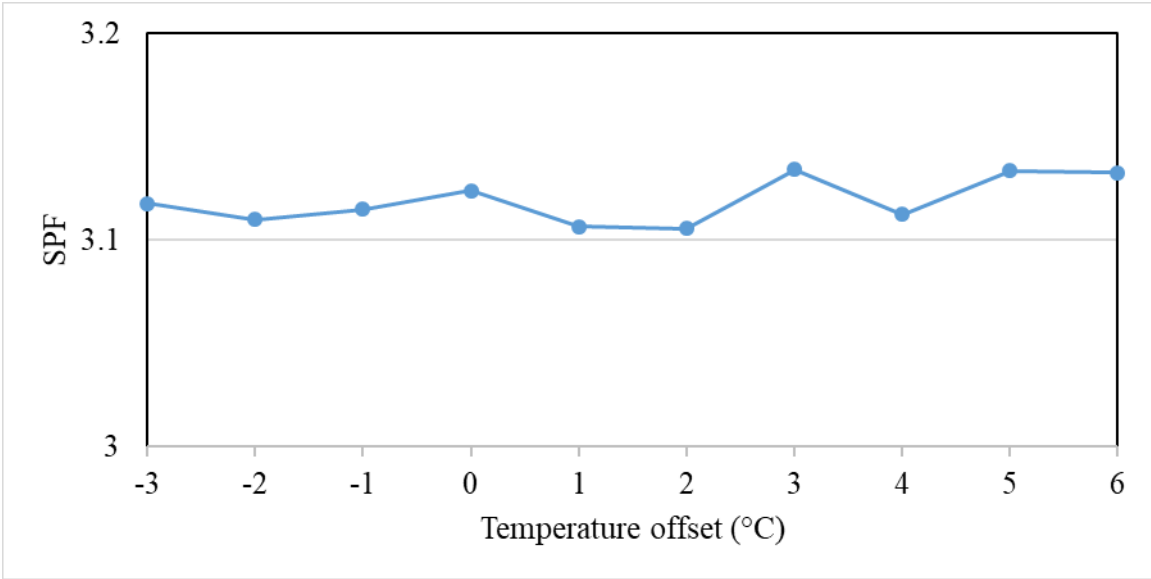


Figure 6-13: The impact of temperature offset on annual SPF in Baltimore

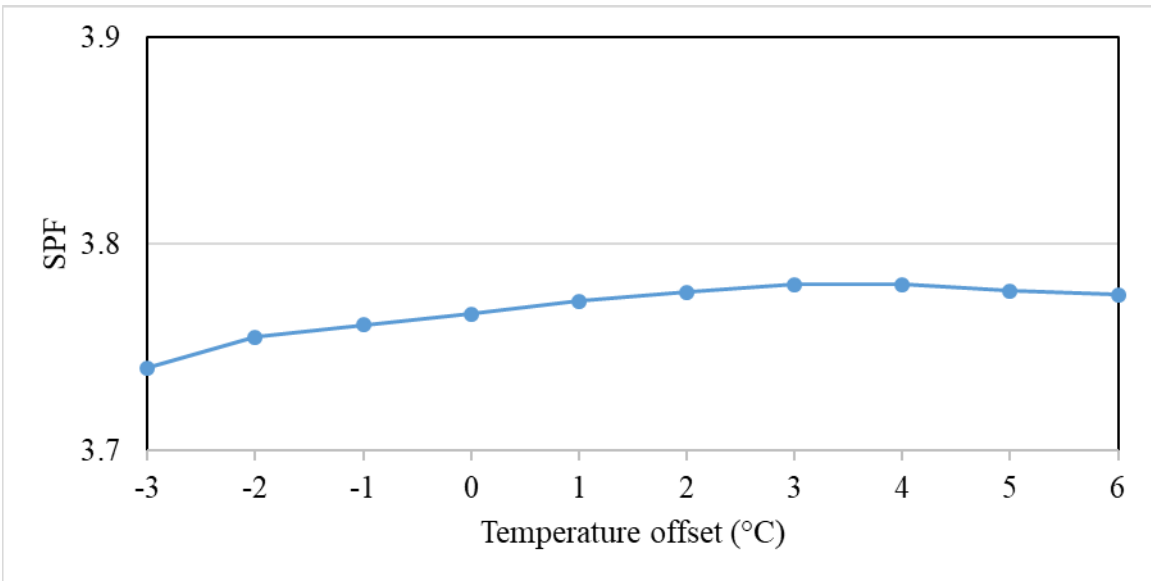


Figure 6-14: The impact of temperature offset on annual SPF in Las Vegas

To better understand the system operation using the dual-source heat pump, the time of the system running in different modes is illustrated in Figure 6-15 and Figure 6-16 for the two

locations. The two figures are based on the case of having 3°C for the temperature offset. Figure 6-15 shows that Mode 13 that uses an instantaneous water heater for space heating is no longer needed in Baltimore. Thus, the instantaneous water heater can be removed from the dual-source heat pump system.

Based on the numbers in Figure 6-15 and Figure 6-16, the time used in operational modes for space heating and space cooling is summarized across the whole year while the two sources are distinguished. Table 6-3 and Table 6-4 show the results, together with those from the original SAHP discussed in Chapter 5. These two tables indicate the following:

- In Baltimore, for the dual-source SAHP system, the (solar) liquid source (M2, M3, and M4) is used in 73% of the system's total operation time for space heating, and the air source (M15-1 and M15-2) is used in the rest 27% operation time. In contrast, for the original liquid-source only SAHP system, the (solar) liquid source is used in 74% of the system's total operation time for space heating, while M13 (instantaneous water heating) is used in the remaining 26% operation time. The air-source heat pump actually replaces the instantaneous water heater. Because the heat pump has a COP higher than 1, the dual-source heat pump system has a higher SPF. The same observation can be made for Las Vegas, but the role of the air-source heat pump is significantly reduced because of the mild climate.
- In Baltimore, the system's total operation time for space cooling is almost evenly split between the (solar) liquid source (M8, M9, and M10) and the air source (M16). In Las Vegas, the liquid source and the air source are used respectively in 44% and 56% of the system's total operation time for cooling.

Table 6-3: Comparison of the system running time in different modes and with different sources for space heating

Operating Mode		Annual mode time (hr)			
		Baltimore		Las Vegas	
		Liquid-source only SAHP system	Dual-source SAHP system	Liquid-source only SAHP system	Dual-source SAHP system
Solar source	M2 (TSG-SH)	79 (10%)	79 (10%)	25 (11%)	25 (11%)
	M3 (PVT-HP-SH)	54 (7%)	45 (6%)	7 (3%)	5 (2%)
	M4 (TSG-HP-SH)	442 (57%)	436 (57%)	191 (84%)	190 (84%)
	M13 (Backup SH)	201 (26%)	-	4 (2%)	-
Air source	M15-1 (Air-HP-SH w/o aux)	-	166 (22%)	-	7 (3%)
	M15-2 (Air-HP-SH w/ aux)	-	36 (5%)	-	-

Table 6-4: Comparison of the system running time in different modes and with different sources for space cooling

Operating Mode		Annual mode time (hr)			
		Baltimore		Las Vegas	
		Liquid-source only SAHP system	Dual-source SAHP system	Liquid-source only SAHP system	Dual-source SAHP system
Solar source	M8 (TSG-SC)	27 (8%)	31 (9%)	27 (3%)	27 (3%)
	M9 (PVT-HP-SC)	66 (19%)	4 (1%)	309 (36%)	21 (3%)
	M10 (TSG-HP-SC)	257 (73%)	132 (40%)	529 (61%)	320 (39%)
Air source	M16 (Air-HP-SC)	-	167 (50%)	-	463 (56%)

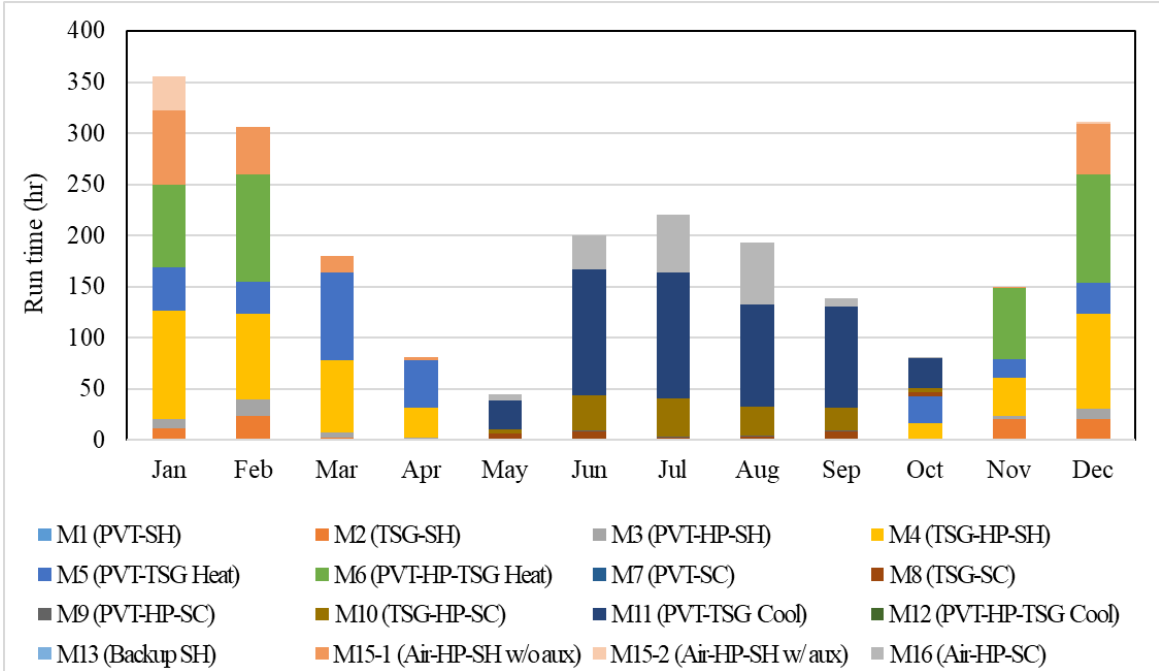


Figure 6-15: Baltimore monthly mode time activation

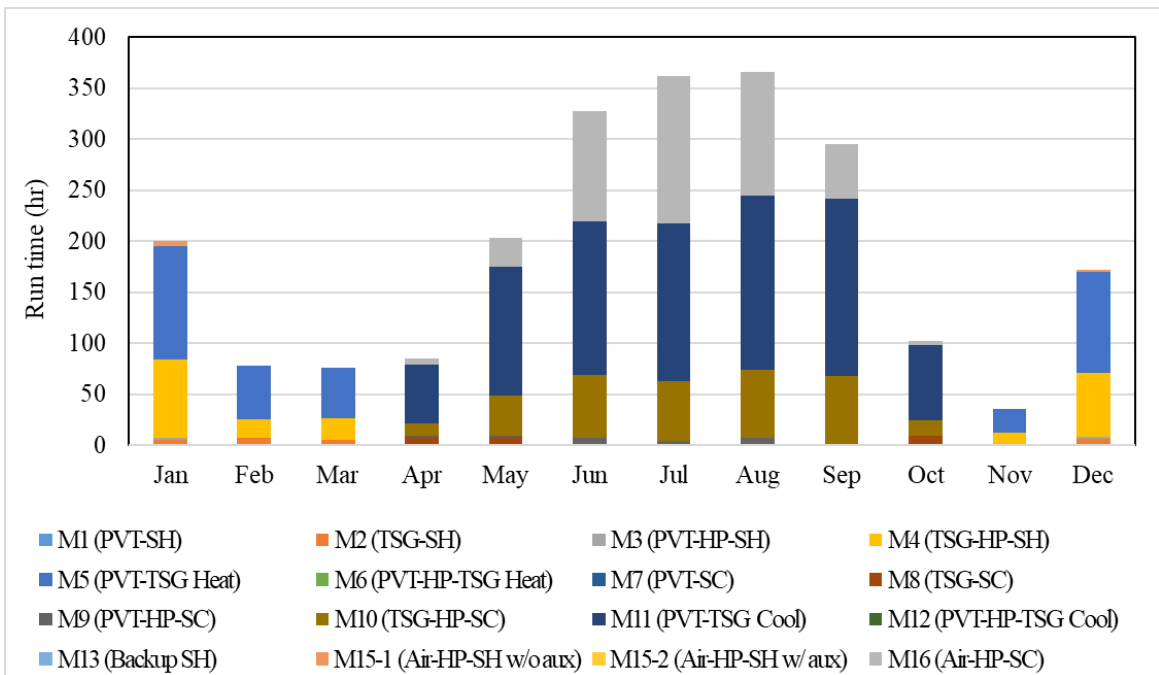


Figure 6-16: Las Vegas monthly mode time activation

CHAPTER 7: SYSTEM ECONOMIC ANALYSIS

In this chapter, a high-level economic analysis is performed to compare the multifunctional SAHP system and the reference conventional air-source heat pump system. For both systems, the capital costs are estimated first. Then, the simple payback period of the additional investment of the proposed SAHP system is calculated.

7.1 Capital cost estimation

As presented in Chapters 3 and 4, major components of the proposed SAHP system include unglazed PVT collectors, an inverter, a liquid-to-liquid heat pump, a thermal storage tank for space conditioning, a DHW tank, two instantaneous water heaters (one for space heating and one for DHW), a plate heat exchanger, and four circulating pumps. Major components of the reference conventional air-source heat pump system include a split air-source heat pump, an auxiliary electric heater of the heat pump for space heating, and an electric water heater for DHW production.

The prices of most components are obtained by researching the U.S. market. However, for PVT collectors and the thermal storage tank, a reliable source of their prices in the U.S. market could not be found. Therefore, Report A1 of IEA SHC Task 60 (Ramschak 2020), which discusses the installed PVT systems in European countries, has been used as the resource for estimating the cost of PVT collectors and the thermal storage tank. Table 7-1 and Table 7-2 list the estimated costs of the major components used in the two systems. Note that the two tables cover major pieces of equipment only while pipes, ducts, valves, and other accessories are not included. In addition,

all estimated costs are for equipment procurement but not including installation because of the lack of resources.

Table 7-1: Estimated equipment costs of the proposed SAHP system

Equipment	Model	Price per unit	Number of units	Total price
Liquid-to-Liquid heat pump (3.3 ton)	WaterFurnace Series 5 NSW040G12RCSS0AA	\$6000	1	\$6000
Circulation pump	Taco 0013 Cast Iron Circulator, 1/6 HP 0013-F3	\$360	3	\$1080
Desuperheater pump	Taco 007 Cast Iron Circulator, 1/25 HP 007-F5	\$100	1	\$100
PVT (30 m ²)	Consolar SOLINK (2 m ²)	\$850	15	\$12750
Inverter	SMA Sunny Boy 5.0-US-41 Inverter	\$1475	1	\$1475
Auxiliary tankless water heater for space heating	Rheem RTEX-36	\$560	1	\$560
Heat exchanger	Bell & Gossett BPX Brazed Plate Heat Exchanger BP400-10LP	\$170	1	\$170
Auxiliary tankless water heater for DHW	Rheem RTEX-04	\$170	1	\$170
DHW tank	AO Smith 80 Gallon - 4,500 Watt ProMax Residential Electric Direct Solar Booster Water Heater SUN-80	\$1050	1	\$1050
Thermal storage tank (2 m ³)	Average from IEA SHC Task 60 (\$2054 per m ³)	\$4108	1	\$4108

Table 7-2: Estimated equipment costs of reference conventional air-source heat pump system

Equipment	Model	Price per unit	Number of units	Total price
Air-source heat pump (3 ton)	Carrier Model 25HCE436	\$3600	1	\$3600
DHW tank with electric heater	AO Smith 80 Gallon ProLine Electronic Thermostat High Capacity Residential Electric Water Heater EGR-80	\$1675	1	\$1675
Electric air heater	Fantech 8" Makeup Air Heater (6 kW) MUAH8/6	\$740	1	\$740

Based on the information in Table 7-1 and Table 7-2, the system cost is calculated to be \$27,463 for the proposed SAHP system ($C_{PS,tot}$) and \$6,015 for the reference system ($C_{RS,tot}$). A large portion of the cost difference attributes to the use of PVT collectors and the thermal storage tank in the SAHP system.

7.2 Simple payback period

The simple payback period (SPB) refers to the number of years required to recover the additional investment of the SAHP system with the operating cost savings. SPB is calculated using Equations (7-1)-(7-4).

$$SPB = \frac{C_{PS,tot} - C_{RS,tot}}{J_{tot}} \quad (7-1)$$

$$J_{tot} = C_{op,RS} - C_{op,PS} \quad (7-2)$$

$$C_{op,RS} = E_{RS} \times Pr_{el} \quad (7-3)$$

$$C_{op,PS} = (E_{PS} - E_{PVT,el}) \times Pr_{el} \quad (7-4)$$

where, $C_{PS,tot}$ and $C_{RS,tot}$ indicate the cost of the proposed SAHP system and the reference system, respectively; $C_{op,PS}$, and $C_{op,RS}$ are the operating energy costs of the SAHP system and the reference system, and J_{tot} is the difference between them; E_{PS} and E_{RS} specify the annual electricity consumption of the SAHP system and reference system; $E_{PVT,el}$ is the annual electricity generation from the PVT collectors, and Pr_{el} denotes the electricity price.

In Equation (7-3) and Equation (7-4), the annual electricity consumption of the reference system (E_{RS}), the annual electricity consumption of the SAHP system (E_{PS}), and the annual electricity generation from the PVT collectors ($E_{PVT,el}$) are all from the TRNSYS simulations. The results are reported in Table 7-3. In this table, the electricity consumption is for the whole building, including the system, lighting, appliance, and plug loads.

Equation (7-3) calculates the operating energy cost of the reference system ($C_{op,RS}$) by multiplying the annual electricity consumption by the electricity price (Pr_{el}). Equation (7-4) calculates the operating energy cost of the SAHP system ($C_{op,PS}$) by multiplying the difference between the annual electricity consumption and generation by the electricity price. The approach is valid if extra onsite electricity generation is sold back to the grid at the retail rate (e.g., net metering), which is currently available in many locations, including Baltimore and Las Vegas. The electricity price is from the state average value from IEA (2019), which is 12.00 cents/kWh in Baltimore and 13.12 cents/kWh in Las Vegas, respectively.

Table 7-3: Annual electricity consumption and production of the single-family house simulated in this work in Baltimore and Las Vegas

Location	Electricity consumption/production (in 1000 kWh)		
	Reference system electricity consumption (E_{RS})	Proposed system electricity consumption (E_{PS})	Proposed system electricity production ($E_{PVT,el}$)
Baltimore	17.8	12.6	6.89
Las Vegas	16.9	10.9	9.31

Applicable solar tax credits and incentives can be taken into account when determining the investment costs and calculating the simple payback period. For example, currently, there is a federal solar investment tax credit (ITC) at 26% of the installed cost of solar systems (DOE, n.d.). This tax credit is equivalent to the same amount of investment cost reduction. Therefore, the simple payback period is calculated for two scenarios: one with the federal solar ITC and another without. The results are shown in Table 7-4. This table shows the following:

- Without any credits and incentives, the SPB is 13.5 years in Baltimore and 11.6 years in Las Vegas. The payback period of more than 10 years is a realistic problem for the market acceptance of the proposed SAHP system.
- After considering the federal solar ITC, the SPB is reduced to 9.0 years and 7.7 years in Baltimore and Las Vegas, respectively. If state- or utility-level incentives exist, the SPB can be reduced further. This means that incentives and credits are important to motivate the use of SAHP systems.

Table 7-4: Simple payback periods of the solar-assisted multifunctional heat pump system against the conventional air-source heat pump system

Location	Simple payback period (years)	
	without federal ITC	with federal ITC
Baltimore	13.5	9.0
Las Vegas	11.6	7.7

CHAPTER 8: SUMMARY, CONTRIBUTIONS, AND FUTURE WORK

8.1 Summary

This research has proposed and evaluated a novel hybrid PVT-based multifunctional SAHP system capable of space heating, space cooling, DHW, and onsite electricity generation. The main components of the multifunctional system include unglazed PVT collectors, a liquid-to-liquid heat pump, a thermal storage tank, a DHW tank, and two instantaneous electric water heaters (for space heating and DHW production). The PVT collectors can be used directly or as the source of the heat pump or used to charge the thermal storage tank and the DHW tank. The system has fourteen operating modes. The sequence of operation is based on the space thermostat signals, the collector temperature, the thermal storage tank water temperature, and the DHW tank temperature. TRNSYS software is used to model the system and evaluate its performance with a number of metrics such as seasonal performance factor, solar fraction, and self-consumption. To facilitate performance evaluation, a 200 m² single-family house is modeled in two locations with different climates: Baltimore, MD in a cold climate and Las Vegas, NV in a warm and dry climate. The components are sized accordingly based on the load calculation and sensitivity analysis. The performance of the multifunctional SAHP is compared with a reference system that has a split air-source heat pump system for space heating and cooling and an electric water heater for DHW production. Based on the TRNSYS simulations, efforts have been taken to improve the multifunctional SAHP system by exploring the use of an outdoor swimming pool and PCMs for thermal storage and replacing the liquid-source only heat pump with a dual-source heat pump. Major research findings from this work are summarized below:

- Statistical analysis of the proposed system operational modes shows that Mode 4 (Tank-HP for space heating) and Mode 10 (Tank-HP for space cooling) are the dominant space heating and space cooling modes. Direct PVT-Tank heating and cooling modes (Mode 5 and Mode 11) are essential for the system's operation in Baltimore and Las Vegas locations. In addition, using the heat pump to charge the tank for heating (Mode 6) is shown to be necessary to keep the thermal storage tank from running out of extractable thermal energy and avoid the excessive use of a backup electric heater to provide space heating in Baltimore. DHW production is achieved utilizing PVT collectors (Mode 14) and the HP desuperheater. Mode 14 is predominantly used in summer, while the heat pump desuperheater is the main DHW production source in winter.
- The performance metric analysis presents that the annual solar energy utilization ratio is 27% and 20%, respectively, in Baltimore and Las Vegas. The case studies in Baltimore and Las Vegas have solar thermal fractions of 9% and 34%, correspondingly. Annual system solar electrical fractions are 118% for Baltimore and 228% for Las Vegas cases, while 53% and 83% are reported for the annual site (system and building) solar electrical fractions for these locations, correspondingly. Also, annual system and site self-consumption are 27% and 45% in Baltimore and 19% and 35% in Las Vegas.
- The proposed system is much more efficient than the reference system. The fractional energy savings of the proposed system compared to the reference system are 84%, 11%, and 48% for the DHW portion, space conditioning portion, and the total consumed energy in Baltimore. The savings mentioned above are 88%, 28%, and 61% in Las Vegas.
- By eliminating rarely used modes, the controls can be simplified to reduce the system complexity while having little impact on the system performance. The annual SPF's of the

system with the simplified controls are reduced by less than 4% relative to the original system with a fourteen-mode control strategy.

- Replacing the water tank with an outdoor swimming pool for thermal storage improves system performance, especially in cooling-dominated locations. Using the swimming pool in Las Vegas increases the annual SPF 17% higher than the original system design with a water tank. However, increasing the capacity of the thermal storage tank by using a tank having phase change materials may not increase the annual SPF.
- Replacing the liquid-to-liquid heat pump (solar-source) with a dual-source heat pump (solar-source & air-source) enhances system performance, particularly in heating-dominated locations. An annual SPF increase of 17% relative to the original system design that uses a single source liquid-to-liquid heat pump is observed in Baltimore.
- The proposed system would have the best economic feasibility in hot and arid locations with high electricity prices. The simple payback period of the proposed system is 13.5 years without an incentive in Baltimore, while SPB is reduced to 9.0 years with the federal solar tax credit incentive. Also, SPBs are 11.6 and 7.7 years without and with the federal incentive in Las Vegas, respectively.

8.2 Contributions

The PVT-based SAHP system is distinctive from previous studies because of its multifunctionalities, including onsite electricity generation, space heating, space cooling, and DHW heating. The system has a number of unique features. First, the PVT collectors are a multi-purpose component of the system. They generate electricity and collect the heat energy during the daytime and can work as radiative cooling panels for space cooling. The use of PVT collectors

together with the heat pump for space cooling has never been studied in literature to the best of our knowledge. Second, the system has energy cascading features such as using the heat collected from PVT collectors for space heating and DHW and using the desuperheater for DHW production. Third, the mode of using the heat pump to actively charge the thermal storage tank (Mode 6) is a unique feature. The value of this mode in cold climates has been verified with simulations in this work.

This work has provided a comprehensive study of possible operational modes and the sequence of their controls. Simulations are used to determine the time of system operation in different modes. The results show that some modes (e.g., using PVT collectors or the thermal storage tank directly for space heating and cooling) are rarely used and can thus be omitted in future system design. The simplification of system design and operation has a minor impact on system performance. This research investigates three performance improvement strategies that are essentially three novel SAHP systems: using an outdoor swimming pool as the thermal storage, using a PCM-integrated storage tank to enhance the heat capacity, and using a dual-source heat pump to replace the liquid-source only heat pump. The performance of these novel multifunctional SAHP systems has rarely been studied in the literature. Many findings from this work, such as the impact of melting temperature and PCM volume percentage of the tank on energy performance, the impact of different conditions for switching between the dual sources, are important to guide future system improvement.

8.3 Future work

The work presented in this dissertation could be extended further in the future along with the following directions:

- Building performance simulation is the approach used in this work to evaluate the multifunctional SAHP system. Although TRNSYS is a reputable program and all components have been validated to different extents by the model developers and users, there is a need to verify the findings from the simulations with experimental studies and field tests. In this regard, a hardware-in-the-loop experimental facility developed by van Arnold (2020) has been built up at the EPIC building, UNC Charlotte. Once completed, the facility can support all operational modes included in this work and thus can be used to verify the simulation work.
- The parameter settings used in the system controls are primarily based on engineering judgment and literature. Optimization could be pursued to determine the optimal settings. In particular, advanced control methods such as model predictive controls based on the forecasted loads and weather conditions are worth considering to determine when to charge and discharge the storage tank.
- The work in this dissertation has a focus on the thermal energy generation and use. No attention has been given to the balance of onsite electricity generation and consumption. In the future, rather than relying on the power grid to balance the PV electricity generation and the building electric load, thermal storage can be leveraged to provide flexibility of the household net residual load and improve the self-sufficiency of PV power generation. Electric load shifting and peak shaving can also be explored by leveraging the thermal storage.
- This work has considered two locations with different climates. It would be useful to perform the energy and economic analysis in more locations with different climates and utility rates.

- Radiant floor heating and cooling is an appropriate design in the context of SAHP systems because of its use of low-temperature heating and high-temperature cooling. However, unlike conventional air-based HVAC systems, radiant floor cooling does not have the functionality of space dehumidification. Though the lack of space dehumidification is not a problem for dry climates, specialized space dehumidification needs to be considered in humid climates.

REFERENCES

- AHRI Standard. 2017. "210/240 (2017)“Performance Rating of Unitary Air Conditioning and Air-Source Heat Pump Equipment,”.” Air-Conditioning, Heating, & Refrigeration Institute, Arlington, VA 22201, USA.
- Asaee, S. Rasoul, V. Ismet Ugursal, and Ian Beausoleil-Morrison. 2017. “Techno-Economic Assessment of Solar Assisted Heat Pump System Retrofit in the Canadian Housing Stock.” *Applied Energy* 190: 439–52. <https://doi.org/10.1016/j.apenergy.2016.12.053>.
- ASHRAE. 2017. *ASHRAE Handbook: Fundamentals: SI Edition*. Atlanta, GA: ASHRAE, 2017, ©2017.
- Aydin, Devrim, Zafer Utlu, and Olcay Kincay. 2015. “Thermal Performance Analysis of a Solar Energy Sourced Latent Heat Storage.” *Renewable and Sustainable Energy Reviews* 50: 1213–25. <https://doi.org/10.1016/j.rser.2015.04.195>.
- Babiak, Jan, Petrás Dusan, and Bjarne W. Olesen. 2007. *Low Temperature Heating and High Temperature Cooling*. Bruselas: Rehva.
- Bai, Y., T. T. Chow, C. Ménézo, and P. Dupeyrat. 2012. “Analysis of a Hybrid PV/Thermal Solar-Assisted Heat Pump System for Sports Center Water Heating Application.” *International Journal of Photoenergy* 2012: 1–13. <https://doi.org/10.1155/2012/265838>.
- Bakirci, Kadir, and Bedri Yuksel. 2011. “Experimental Thermal Performance of a Solar Source Heat-Pump System for Residential Heating in Cold Climate Region.” *Applied Thermal Engineering* 31 (8-9): 1508–18. <https://doi.org/10.1016/j.applthermaleng.2011.01.039>.
- Bakker, M., H.A. Zondag, M.J. Elswijk, K.J. Strootman, and M.J.M. Jong. 2005. “Performance and Costs of a Roof-Sized PV/Thermal Array Combined with a Ground Coupled Heat Pump.” *Solar Energy* 78 (2): 331–39. <https://doi.org/10.1016/j.solener.2004.09.019>.
- Banister, Carsen J., and Michael R. Collins. 2015. “Development and Performance of a Dual Tank Solar-Assisted Heat Pump System.” *Applied Energy* 149: 125–32. <https://doi.org/10.1016/j.apenergy.2015.03.130>.
- Bellos, Evangelos, and Christos Tzivanidis. 2017. “Energetic and Financial Sustainability of Solar Assisted Heat Pump Heating Systems in Europe.” *Sustainable Cities and Society* 33: 70–84. <https://doi.org/10.1016/j.scs.2017.05.020>.
- Bellos, Evangelos, Christos Tzivanidis, Konstantinos Moschos, and Kimon A. Antonopoulos. 2016. “Energetic and Financial Evaluation of Solar Assisted Heat Pump Space Heating Systems.” *Energy Conversion and Management* 120: 306–19. <https://doi.org/10.1016/j.enconman.2016.05.004>.

- Bertram, Erik, Jens Glembin, and Gunter Rockendorf. 2012. "Unglazed PVT Collectors as Additional Heat Source in Heat Pump Systems with Borehole Heat Exchanger." *Energy Procedia* 30: 414–23. <https://doi.org/10.1016/j.egypro.2012.11.049>.
- Bertram, Erik. 2014. "Solar Assisted Heat Pump Systems with Ground Heat Exchanger – Simulation Studies." *Energy Procedia* 48: 505–14. <https://doi.org/10.1016/j.egypro.2014.02.060>.
- Besagni, Giorgio, Lorenzo Croci, Riccardo Nesa, and Luca Molinaroli. 2019. "Field Study of a Novel Solar-Assisted Dual-Source Multifunctional Heat Pump." *Renewable Energy* 132: 1185–1215. <https://doi.org/10.1016/j.renene.2018.08.076>.
- Bourdakis, Eleftherios, Thibault Q. Péan, Luca Gennari, and Bjarne W. Olesen. 2016. "Daytime Space Cooling with Phase Change Material Ceiling Panels Discharged Using Rooftop Photovoltaic/Thermal Panels and Night-Time Ventilation." *Science and Technology for the Built Environment* 22 (7): 902–10. <https://doi.org/10.1080/23744731.2016.1181511>.
- Busato, Filippo, Renato Lazzarin, and Marco Noro. 2015. "Ground or Solar Source Heat Pump Systems for Space Heating: Which Is Better? Energetic Assessment Based on a Case History." *Energy and Buildings* 102: 347–56. <https://doi.org/10.1016/j.enbuild.2015.05.053>.
- Cai, Jingyong, Jie Ji, Yunyun Wang, and Wenzhu Huang. 2016. "Numerical Simulation and Experimental Validation of Indirect Expansion Solar-Assisted Multi-Functional Heat Pump." *Renewable Energy* 93: 280–90. <https://doi.org/10.1016/j.renene.2016.02.082>.
- Cai, Jingyong, Jie Ji, Yunyun Wang, and Wenzhu Huang. 2017. "Operation Characteristics of a Novel Dual Source Multi-Functional Heat Pump System under Various Working Modes." *Applied Energy* 194: 236–46. <https://doi.org/10.1016/j.apenergy.2016.10.075>.
- Cao, Chihong, Huixing Li, Guohui Feng, Ran Zhang, and Kailiang Huang. 2016. "Research on PV/T – Air Source Heat Pump Integrated Heating System in Severe Cold Region." *Procedia Engineering* 146: 410–14. <https://doi.org/10.1016/j.proeng.2016.06.422>.
- Carbonell, D., D. Philippen, M. Granzotto, and M.Y. Haller. 2016. "Simulation of a Solar-Ice System for Heating Applications. System Validation with One-Year of Monitoring Data." *Energy and Buildings* 127: 846–58. <https://doi.org/10.1016/j.enbuild.2016.06.058>.
- Carbonell, D., D. Philippen, M.Y. Haller, and E. Frank. 2015. "Modeling of an Ice Storage Based on a De-Icing Concept for Solar Heating Applications." *Solar Energy* 121: 2–16. <https://doi.org/10.1016/j.solener.2015.06.051>.
- Carbonell, D., D. Philippen, M.Y. Haller, and S. Brunold. 2016. "Modeling of an Ice Storage Buried in the Ground for Solar Heating Applications. Validations with One Year of

- Monitored Data from a Pilot Plant.” *Solar Energy* 125: 398–414.
<https://doi.org/10.1016/j.solener.2015.12.009>.
- Carbonell, D., M.Y. Haller, and E. Frank. 2014. “Potential Benefit of Combining Heat Pumps with Solar Thermal for Heating and Domestic Hot Water Preparation.” *Energy Procedia* 57: 2656–65. <https://doi.org/10.1016/j.egypro.2014.10.277>.
- Carbonell, Daniel, Michel Y. Haller, Daniel Philippen, and Elimar Frank. 2014. “Simulations of Combined Solar Thermal and Heat Pump Systems for Domestic Hot Water and Space Heating.” *Energy Procedia* 48: 524–34. <https://doi.org/10.1016/j.egypro.2014.02.062>.
- Carrier. n.d. “30AWH - AquaSnap® - Reversible Air-to Water Heat Pump: Carrier Heating, Ventilation and Air Conditioning.” Carrier. Accessed July 6, 2021.
<https://www.carrier.com/commercial/en/eu/products/heating-air-conditioning/air-to-water-heat-pumps/30awh/>.
- Cağlar, Ahmet, and Cemil Yamalı. 2012. “Performance Analysis of a Solar-Assisted Heat Pump with an Evacuated Tubular Collector for Domestic Heating.” *Energy and Buildings* 54: 22–28. <https://doi.org/10.1016/j.enbuild.2012.08.003>.
- Chargui, Ridha, and Sami Awani. 2017. “Determining of the Optimal Design of a Closed Loop Solar Dual Source Heat Pump System Coupled with a Residential Building Application.” *Energy Conversion and Management* 147: 40–54.
<https://doi.org/10.1016/j.enconman.2017.05.025>.
- Chen, J.F., Y.J. Dai, and R.Z. Wang. 2016. “Experimental and Theoretical Study on a Solar Assisted CO₂ Heat Pump for Space Heating.” *Renewable Energy* 89: 295–304.
<https://doi.org/10.1016/j.renene.2015.12.039>.
- Chow, T.T., Y. Bai, K.F. Fong, and Z. Lin. 2012. “Analysis of a Solar Assisted Heat Pump System for Indoor Swimming Pool Water and Space Heating.” *Applied Energy* 100: 309–17. <https://doi.org/10.1016/j.apenergy.2012.05.058>.
- Chu, Jenny, Wilkie Choi, Cynthia A. Cruickshank, and Stephen J. Harrison. 2014. “Modeling of an Indirect Solar Assisted Heat Pump System for a High Performance Residential House.” *Journal of Solar Energy Engineering* 136 (4). <https://doi.org/10.1115/1.4027486>.
- Crawley, Drury B., Jon W. Hand, Michaël Kummert, and Brent T. Griffith. 2008. “Contrasting the Capabilities of Building Energy Performance Simulation Programs.” *Building and Environment* 43 (4): 661–73. <https://doi.org/10.1016/j.buildenv.2006.10.027>.
- Cremers, Jan, Irina Mitina, Nansi Palla, Fritz Klotz, Xavier Jobard, and Ursula Eicker. 2015. “Experimental Analyses of Different PVT Collector Designs for Heating and Cooling Applications in Buildings.” *Energy Procedia* 78: 1889–94.
<https://doi.org/10.1016/j.egypro.2015.11.356>.

- Dannemand, Mark, Bengt Perers, and Simon Furbo. 2019. "Performance of a Demonstration Solar PVT Assisted Heat Pump System with Cold Buffer Storage and Domestic Hot Water Storage Tanks." *Energy and Buildings* 188-189: 46–57.
<https://doi.org/10.1016/j.enbuild.2018.12.042>.
- Del Amo, A., A. Martínez-Gracia, T. Pintanel, A.A. Bayod-Rújula, and S. Torné. 2020. "Analysis and Optimization of a Heat Pump System Coupled to an Installation of PVT Panels and a Seasonal Storage Tank on an Educational Building." *Energy and Buildings* 226: 110373. <https://doi.org/10.1016/j.enbuild.2020.110373>.
- Deng, S., Y.J. Dai, and R.Z. Wang. 2013. "Performance Optimization and Analysis of Solar Combi-System with Carbon Dioxide Heat Pump." *Solar Energy* 98: 212–25.
<https://doi.org/10.1016/j.solener.2013.10.001>.
- DOE. n.d. "Homeowner's Guide to the Federal Tax Credit for Solar Photovoltaics." Energy.gov. Accessed July 6, 2021. <https://www.energy.gov/eere/solar/homeowners-guide-federal-tax-credit-solar-photovoltaics>.
- Dott, Ralf, Andreas Genkinger, and Thomas Afjei. 2012. "System Evaluation of Combined Solar & Heat Pump Systems." *Energy Procedia* 30: 562–70.
<https://doi.org/10.1016/j.egypro.2012.11.066>.
- Duffie, John A., and William A. Beckman. 2006. *Solar Engineering of Thermal Processes*. Hoboken: J. Wiley.
- EIA. 2018. "Residential Energy Consumption Survey (RECS) - 2015 Data - U.S. Energy Information Administration (EIA)."
- EIA. 2019. "U.S. Energy Information Administration - EIA - Independent Statistics and Analysis. Electric Sales, Revenue, and Average Price"
- EIA. 2021. "Total Energy Monthly Data - U.S. Energy Information Administration (EIA)."
- Eicher, Sara, Catherine Hildbrand, Annelore Kleijer, Jacques Bony, Mircea Bunea, and Stéphane Citherlet. 2014. "Life Cycle Impact Assessment of a Solar Assisted Heat Pump for Domestic Hot Water Production and Space Heating." *Energy Procedia* 48: 813–18.
<https://doi.org/10.1016/j.egypro.2014.02.094>.
- Eicher, Sara, Catherine Hildbrand, Jacques Bony, Mircea Bunea, Jean-Christophe Hadorn, and Stéphane Citherlet. 2012. "Solar Assisted Heat Pump for Domestic Hot Water Production." *Energy Procedia* 30: 571–79. <https://doi.org/10.1016/j.egypro.2012.11.067>.
- Eicker, Ursula, and Antoine Dalibard. 2011. "Photovoltaic–Thermal Collectors for Night Radiative Cooling of Buildings." *Solar Energy* 85 (7): 1322–35.
<https://doi.org/10.1016/j.solener.2011.03.015>.

- Emmi, Giuseppe, Angelo Zarrella, and Michele De Carli. 2017. "A Heat Pump Coupled with Photovoltaic Thermal Hybrid Solar Collectors: A Case Study of a Multi-Source Energy System." *Energy Conversion and Management* 151: 386–99. <https://doi.org/10.1016/j.enconman.2017.08.077>.
- Emmi, Giuseppe, Angelo Zarrella, Michele De Carli, and Antonio Galgaro. 2015. "An Analysis of Solar Assisted Ground Source Heat Pumps in Cold Climates." *Energy Conversion and Management* 106: 660–75. <https://doi.org/10.1016/j.enconman.2015.10.016>.
- Endef. 2020. "Projects." 2020. Endef. May 7, 2020. <https://endef.com/en/projects/>.
- Entchev, E., L. Yang, M. Ghorab, and E.J. Lee. 2014. "Performance Analysis of a Hybrid Renewable Microgeneration System in Load Sharing Applications." *Applied Thermal Engineering* 71 (2): 697–704. <https://doi.org/10.1016/j.applthermaleng.2013.10.057>.
- Evangelisti, Luca, Claudia Guattari, and Francesco Asdrubali. 2019. "On the Sky Temperature Models and Their Influence on Buildings Energy Performance: A Critical Review." *Energy and Buildings* 183: 607–25. <https://doi.org/10.1016/j.enbuild.2018.11.037>.
- Fine, J.P., J. Friedman, and S.B. Dworkin. 2017. "Detailed Modeling of a Novel Photovoltaic Thermal Cascade Heat Pump Domestic Water Heating System." *Renewable Energy* 101: 500–513. <https://doi.org/10.1016/j.renene.2016.08.063>.
- Fiorentini, Massimo, Paul Cooper, and Zhenjun Ma. 2015. "Development and Optimization of an Innovative HVAC System with Integrated PVT and PCM Thermal Storage for a Net-Zero Energy Retrofitted House." *Energy and Buildings* 94: 21–32. <https://doi.org/10.1016/j.enbuild.2015.02.018>.
- Fraga, Carolina, Pierre Hollmuller, Floriane Mermoud, and Bernard Lachal. 2017. "Solar Assisted Heat Pump System for Multifamily Buildings: Towards a Seasonal Performance Factor of 5? Numerical Sensitivity Analysis Based on a Monitored Case Study." *Solar Energy* 146: 543–64. <https://doi.org/10.1016/j.solener.2017.02.008>.
- Furbo, Simon. 2004. "Hot water tanks for solar heating systems."
- Girard, Aymeric, Eulalia Jadraque Gago, Tariq Muneer, and Gustavo Caceres. 2015. "Higher Ground Source Heat Pump COP in a Residential Building through the Use of Solar Thermal Collectors." *Renewable Energy* 80: 26–39. <https://doi.org/10.1016/j.renene.2015.01.063>.
- Grossule, Fabio. 2015. "The use of phase changing materials for cooling of buildings combined with night sky radiant cooling." Masters Thesis, Technical University of Denmark.

- Gürlich, Daniel, Antoine Dalibard, and Ursula Eicker. 2017. "Photovoltaic-Thermal Hybrid Collector Performance for Direct Trigeneration in a European Building Retrofit Case Study." *Energy and Buildings* 152: 701–17. <https://doi.org/10.1016/j.enbuild.2017.07.081>.
- Hadorn, Jean-Christophe. 2015. *Solar and Heat Pump Systems for Residential Buildings*. Berlin: Ernst & Sohn.
- Hailu, Getu, Peter Dash, and Alan S. Fung. 2015. "Performance Evaluation of an Air Source Heat Pump Coupled with a Building-Integrated Photovoltaic/Thermal (BIPV/T) System under Cold Climatic Conditions." *Energy Procedia* 78: 1913–18. <https://doi.org/10.1016/j.egypro.2015.11.370>.
- Haller, Michel Y., Robert Haberl, Igor Mojic, and Elimar Frank. 2014. "Hydraulic Integration and Control of Heat Pump and Combi-Storage: Same Components, Big Differences." *Energy Procedia* 48: 571–80. <https://doi.org/10.1016/j.egypro.2014.02.067>.
- Haller, Michel, and Elimar Frank. 2011. "On the Potential of Using Heat From Solar Thermal Collectors for Heat Pump Evaporators." *Proceedings of the ISES Solar World Congress 2011*. <https://doi.org/10.18086/swc.2011.26.06>.
- IEA. SHC. Task 60. n.d. "Task 60 || Application of PVT Collectors." IEA SHC. Accessed July 6, 2021. <https://task60.iea-shc.org/>.
- IECC. 2006, International Code Council. n.d. "2006 INTERNATIONAL ENERGY CONSERVATION CODE (IECC): ICC DIGITAL CODES." Accessed July 6, 2021. <https://codes.iccsafe.org/content/IECC2006>.
- Jonas, Danny, and Georg Frey. 2018. "Model-Based Analysis of the Performance and the Environmental Impact of Solar Thermal and Heat Pump Systems." *2018 9th International Renewable Energy Congress (IREC)*. <https://doi.org/10.1109/irec.2018.8362569>.
- Jonas, Danny, Danjana Theis, Felix Felgner, and Georg Frey. 2017. "A TRNSYS-Based Simulation Framework for the Analysis of Solar Thermal and Heat Pump Systems." *Applied Solar Energy* 53 (2): 126–37. <https://doi.org/10.3103/s0003701x17020074>.
- Jonas, Danny, Georg Frey, and Danjana Theis. 2017. "Simulation and Performance Analysis of Combined Parallel Solar Thermal and Ground or Air Source Heat Pump Systems." *Solar Energy* 150: 500–511. <https://doi.org/10.1016/j.solener.2017.04.070>.
- Kamel, Raghad S., Alan S. Fung, and Peter R.H. Dash. 2015. "Solar Systems and Their Integration with Heat Pumps: A Review." *Energy and Buildings* 87: 395–412. <https://doi.org/10.1016/j.enbuild.2014.11.030>.
- Kang, Eun-Chul, Euy-Joon Lee, Mohamed Ghorab, Libing Yang, Evgeniy Entchev, Kwang-Seob Lee, and Nam-Jin Lyu. 2016. "Investigation of Energy and Environmental Potentials

- of a Renewable Trigeneration System in a Residential Application.” *Energies* 9 (9): 760. <https://doi.org/10.3390/en9090760>.
- Kim, Taehoon, Byung-II Choi, Yong-Shik Han, and Kyu Hyung Do. 2018. “A Comparative Investigation of Solar-Assisted Heat Pumps with Solar Thermal Collectors for a Hot Water Supply System.” *Energy Conversion and Management* 172: 472–84. <https://doi.org/10.1016/j.enconman.2018.07.035>.
- Klein, S., W.A. Beckman, J.A. Duffie and J.W. Mitchell. 2018. *Trnsys*.
- Lerch, W., A. Heinz, and R. Heimrath. 2015. “Direct Use of Solar Energy as Heat Source for a Heat Pump in Comparison to a Conventional Parallel Solar Air Heat Pump System.” *Energy and Buildings* 100: 34–42. <https://doi.org/10.1016/j.enbuild.2015.03.006>.
- Lerch, Werner, Andreas Heinz, and Richard Heimrath. 2014. “Evaluation of Combined Solar Thermal Heat Pump Systems Using Dynamic System Simulations.” *Energy Procedia* 48: 598–607. <https://doi.org/10.1016/j.egypro.2014.02.070>.
- Li, Hong, Liangliang Sun, and Yonggui Zhang. 2014. “Performance Investigation of a Combined Solar Thermal Heat Pump Heating System.” *Applied Thermal Engineering* 71 (1): 460–68. <https://doi.org/10.1016/j.applthermaleng.2014.07.012>.
- Li, Huai, Wei Xu, Zhen Yu, Jianlin Wu, and Zhenyu Yu. 2018. “Discussion of a Combined Solar Thermal and Ground Source Heat Pump System Operation Strategy for Office Heating.” *Energy and Buildings* 162: 42–53. <https://doi.org/10.1016/j.enbuild.2017.12.021>.
- Li, Siwei, Jaewan Joe, Jianjun Hu, and Panagiota Karava. 2015. “System Identification and Model-Predictive Control of Office Buildings with Integrated Photovoltaic-Thermal Collectors, Radiant Floor Heating and Active Thermal Storage.” *Solar Energy* 113: 139–57. <https://doi.org/10.1016/j.solener.2014.11.024>.
- Liang, Cai-hua, Xiao-song Zhang, Xiu-wei Li, and Xia Zhu. 2011. “Study on the Performance of a Solar Assisted Air Source Heat Pump System for Building Heating.” *Energy and Buildings* 43 (9): 2188–96. <https://doi.org/10.1016/j.enbuild.2011.04.028>.
- Lin, Wenye, Zhenjun Ma, M. Imroz Sohel, and Paul Cooper. 2014. “Development and Evaluation of a Ceiling Ventilation System Enhanced by Solar Photovoltaic Thermal Collectors and Phase Change Materials.” *Energy Conversion and Management* 88: 218–30. <https://doi.org/10.1016/j.enconman.2014.08.019>.
- Liu, Yin, Jing Ma, Guanghui Zhou, Chao Zhang, and Wenlei Wan. 2016. “Performance of a Solar Air Composite Heat Source Heat Pump System.” *Renewable Energy* 87: 1053–58. <https://doi.org/10.1016/j.renene.2015.09.001>.

- Lv, Xiaolong, Gang Yan, and Jianlin Yu. 2015. "Solar-Assisted Auto-Cascade Heat Pump Cycle with Zeotropic Mixture R32/R290 for Small Water Heaters." *Renewable Energy* 76: 167–72. <https://doi.org/10.1016/j.renene.2014.11.012>.
- Lämmle, Manuel, María Herrando, and Glen Ryan. 2020. "Basic Concepts of PVT Collector Technologies, Applications and Markets." <https://doi.org/10.18777/ieashc-task60-2020-0002>.
- Martin, Marlo, and Paul Berdahl. 1984. "Characteristics of Infrared Sky Radiation in the United States." *Solar Energy* 33 (3-4): 321–36. [https://doi.org/10.1016/0038-092x\(84\)90162-2](https://doi.org/10.1016/0038-092x(84)90162-2).
- Mirsadeghi, M., D. Cóstola, B. Blocken, and J.L.M. Hensen. 2013. "Review of External Convective Heat Transfer Coefficient Models in Building Energy Simulation Programs: Implementation and Uncertainty." *Applied Thermal Engineering* 56 (1-2): 134–51. <https://doi.org/10.1016/j.applthermaleng.2013.03.003>.
- Mohanraj, M., Ye. Belyayev, S. Jayaraj, and A. Kaltayev. 2018. "Research and Developments on Solar Assisted Compression Heat Pump Systems – A Comprehensive Review (Part-B: Applications)." *Renewable and Sustainable Energy Reviews* 83: 124–55. <https://doi.org/10.1016/j.rser.2017.08.086>.
- Mojic, Igor, Michel Y. Haller, Bernard Thissen, and Elimar Frank. 2014. "Heat Pump System with Uncovered and Free Ventilated Covered Collectors in Combination with a Small Ice Storage." *Energy Procedia* 48: 608–17. <https://doi.org/10.1016/j.egypro.2014.02.071>.
- Ochs, Fabian, Georgios Dermentzis, and Wolfgang Feist. 2014. "Minimization of the Residual Energy Demand of Multi-Storey Passive Houses – Energetic and Economic Analysis of Solar Thermal and PV in Combination with a Heat Pump." *Energy Procedia* 48: 1124–33. <https://doi.org/10.1016/j.egypro.2014.02.127>.
- Palla, Nansi, Reiner Braun, Xavier Jobard, Irina Mitina, Jan Cremers, and Ursula Eicker. 2014. "Development of Multivalent PV-Thermal Collectors for Cooling, Heating and Generation of Electricity." In *International Plea Conference*, vol. 30, no. 2014, pp. 16-18.
- Panaras, G., E. Mathioulakis, and V. Belessiotis. 2013. "Investigation of the Performance of a Combined Solar Thermal Heat Pump Hot Water System." *Solar Energy* 93: 169–82. <https://doi.org/10.1016/j.solener.2013.03.027>.
- Peau, Thibault Quentin, Luca Gennari, Ongun Berk Kazanci, Eleftherios Bourdakos, and Bjarne W. Olesen. 2016. "Influence of the environmental parameters on nocturnal radiative cooling capacity of solar collectors." In *Proceedings of the 12th REHVA World Congress*, vol. 3.
- Plytaria, Maria T., Christos Tzivanidis, Evangelos Bellos, and Kimon A. Antonopoulos. 2018. "Energetic Investigation of Solar Assisted Heat Pump Underfloor Heating Systems with

- and without Phase Change Materials.” *Energy Conversion and Management* 173: 626–39. <https://doi.org/10.1016/j.enconman.2018.08.010>.
- Plytaria, Maria T., Evangelos Bellos, Christos Tzivanidis, and Kimon A. Antonopoulos. 2019. “Financial and Energetic Evaluation of Solar-Assisted Heat Pump Underfloor Heating Systems with Phase Change Materials.” *Applied Thermal Engineering* 149: 548–64. <https://doi.org/10.1016/j.applthermaleng.2018.12.075>.
- Poppi, Stefano, Chris Bales, Andreas Heinz, Franz Hengel, David Chèze, Igor Mojic, and Catia Cialani. 2016. “Analysis of System Improvements in Solar Thermal and Air Source Heat Pump Combisystems.” *Applied Energy* 173: 606–23. <https://doi.org/10.1016/j.apenergy.2016.04.048>.
- Poppi, Stefano, Chris Bales, Michel Y. Haller, and Andreas Heinz. 2016. “Influence of Boundary Conditions and Component Size on Electricity Demand in Solar Thermal and Heat Pump Combisystems.” *Applied Energy* 162: 1062–73. <https://doi.org/10.1016/j.apenergy.2015.10.190>.
- Qu, Minglu, Jianbo Chen, Linjie Nie, Fengshu Li, Qian Yu, and Tan Wang. 2016. “Experimental Study on the Operating Characteristics of a Novel Photovoltaic/Thermal Integrated Dual-Source Heat Pump Water Heating System.” *Applied Thermal Engineering* 94: 819–26. <https://doi.org/10.1016/j.applthermaleng.2015.10.126>.
- Qu, Shilin, Fei Ma, Ru Ji, Dongxu Wang, and Lixiang Yang. 2015. “System Design and Energy Performance of a Solar Heat Pump Heating System with Dual-Tank Latent Heat Storage.” *Energy and Buildings* 105: 294–301. <https://doi.org/10.1016/j.enbuild.2015.07.040>.
- Rad, Farzin M., Alan S. Fung, and Wey H. Leong. 2013. “Feasibility of Combined Solar Thermal and Ground Source Heat Pump Systems in Cold Climate, Canada.” *Energy and Buildings* 61: 224–32. <https://doi.org/10.1016/j.enbuild.2013.02.036>.
- Ramschak, Thomas. 2020. “Existing PVT systems and solutions.” SHC Task 60/Report A1.
- Razavi, Seyed Housman, Rouhollah Ahmadi, and Alireza Zahedi. 2018. “Modeling, Simulation and Dynamic Control of Solar Assisted Ground Source Heat Pump to Provide Heating Load and DHW.” *Applied Thermal Engineering* 129: 127–44. <https://doi.org/10.1016/j.applthermaleng.2017.10.003>.
- Ruschenburg, Jörn, and Sebastian Herkel. 2013. “A Review of Market-Available Solar Thermal Heat Pump Systems.” <https://doi.org/10.18777/ieashc-task44-2013-0001>.
- Sakellariou, Evangelos I., Andrew J. Wright, Petros Axaopoulos, and Muyiwa A. Oyinlola. 2019. “PVT Based Solar Assisted Ground Source Heat Pump System: Modelling Approach and Sensitivity Analyses.” *Solar Energy* 193: 37–50. <https://doi.org/10.1016/j.solener.2019.09.044>.

- Shan, M., T. Yu, and X. Yang. 2016. "Assessment of an Integrated Active Solar and Air-Source Heat Pump Water Heating System Operated within a Passive House in a Cold Climate Zone." *Renewable Energy* 87: 1059–66. <https://doi.org/10.1016/j.renene.2015.09.024>.
- Sharples, S., and P.S. Charlesworth. 1998. "Full-Scale Measurements of Wind-Induced Convective Heat Transfer from a Roof-Mounted Flat Plate Solar Collector." *Solar Energy* 62 (2): 69–77. [https://doi.org/10.1016/s0038-092x\(97\)00119-9](https://doi.org/10.1016/s0038-092x(97)00119-9).
- SIA. 2006. "SIA 2024 / 2006 Standard Conditions of Use for Energy and Building Technology." SIA.
- Simonetti, Riccardo, Luca Molinaroli, and Giampaolo Manzolini. 2019. "Experimental and Analytical Study of an Innovative Integrated Dual-Source Evaporator for Solar-Assisted Heat Pumps." *Solar Energy* 194: 939–51. <https://doi.org/10.1016/j.solener.2019.10.070>.
- Simonetti, Riccardo, Luca Moretti, Luca Molinaroli, and Giampaolo Manzolini. 2020. "Energetic and Economic Optimization of the Yearly Performance of Three Different Solar Assisted Heat Pump Systems Using a Mixed Integer Linear Programming Algorithm." *Energy Conversion and Management* 206: 112446. <https://doi.org/10.1016/j.enconman.2019.112446>.
- Sommerfeldt, Nelson, and Hatf Madani. 2019. "In-Depth Techno-Economic Analysis of PV/Thermal plus Ground Source Heat Pump Systems for Multi-Family Houses in a Heating Dominated Climate." *Solar Energy* 190: 44–62. <https://doi.org/10.1016/j.solener.2019.07.080>.
- Sterling, S.J., and M.R. Collins. 2012. "Feasibility Analysis of an Indirect Heat Pump Assisted Solar Domestic Hot Water System." *Applied Energy* 93: 11–17. <https://doi.org/10.1016/j.apenergy.2011.05.050>.
- Sunoyster. n.d. "SunOyster Components." Accessed July 6, 2021. <https://www.sunoyster.com/sunoyster-16/>.
- Tamasauskas, Justin, Michel Poirier, Radu Zmeureanu, and Roberto Sunyé. 2012. "Modeling and Optimization of a Solar Assisted Heat Pump Using Ice Slurry as a Latent Storage Material." *Solar Energy* 86 (11): 3316–25. <https://doi.org/10.1016/j.solener.2012.08.021>.
- Test, F. L., R. C. Lessmann, and A. Johary. 1981. "Heat Transfer During Wind Flow over Rectangular Bodies in the Natural Environment." *Journal of Heat Transfer* 103 (2): 262–67. <https://doi.org/10.1115/1.3244451>.
- Tsalikis, Georgios, and Georgios Martinopoulos. 2015. "Solar Energy Systems Potential for Nearly Net Zero Energy Residential Buildings." *Solar Energy* 115: 743–56. <https://doi.org/10.1016/j.solener.2015.03.037>.

- Tzivanidis, Christos, Evangelos Bellos, Georgios Mitsopoulos, Kimon A. Antonopoulos, and Asimakis Delis. 2016. "Energetic and Financial Evaluation of a Solar Assisted Heat Pump Heating System with Other Usual Heating Systems in Athens." *Applied Thermal Engineering* 106: 87–97. <https://doi.org/10.1016/j.applthermaleng.2016.06.004>.
- Vaishak, S., and Purnanand V. Bhale. 2019. "Photovoltaic/Thermal-Solar Assisted Heat Pump System: Current Status and Future Prospects." *Solar Energy* 189: 268–84. <https://doi.org/10.1016/j.solener.2019.07.051>.
- Vall, Sergi, and Albert Castell. 2017. "Radiative Cooling as Low-Grade Energy Source: A Literature Review." *Renewable and Sustainable Energy Reviews* 77: 803–20. <https://doi.org/10.1016/j.rser.2017.04.010>.
- Vallati, A., P. Ocloń, C. Colucci, L. Mauri, R. de Lieto Vollaro, and J. Taler. 2019. "Energy Analysis of a Thermal System Composed by a Heat Pump Coupled with a PVT Solar Collector." *Energy* 174: 91–96. <https://doi.org/10.1016/j.energy.2019.02.152>.
- van Arnold, George Benzion. 2020. "Design and Development of an Experimental Apparatus for Hardware-in-Loop Testing of Solar-Assisted Heat Pump Systems." Order No. 28086150, The University of North Carolina at Charlotte.
- Vega, Javier, and Cristian Cuevas. 2018. "Simulation Study of a Combined Solar and Heat Pump System for Heating and Domestic Hot Water in a Medium Rise Residential Building at Concepción in Chile." *Applied Thermal Engineering* 141: 565–78. <https://doi.org/10.1016/j.applthermaleng.2018.06.011>.
- Wang, Gang, Zhenhua Quan, Yaohua Zhao, Chenming Sun, Yuechao Deng, and Jiannan Tong. 2015. "Experimental Study on a Novel PV/T Air Dual-Heat-Source Composite Heat Pump Hot Water System." *Energy and Buildings* 108: 175–84. <https://doi.org/10.1016/j.enbuild.2015.08.016>.
- Wang, Qin, Yu-qian Liu, Guo-feng Liang, Jia-rong Li, Shu-fei Sun, and Guang-ming Chen. 2011. "Development and Experimental Validation of a Novel Indirect-Expansion Solar-Assisted Multifunctional Heat Pump." *Energy and Buildings* 43 (2-3): 300–304. <https://doi.org/10.1016/j.enbuild.2010.09.013>.
- Winteler, Christian, Ralf Dott, Thomas Afjei, and Bernd Hafner. 2014. "Seasonal Performance of a Combined Solar, Heat Pump and Latent Heat Storage System." *Energy Procedia* 48: 689–700. <https://doi.org/10.1016/j.egypro.2014.02.080>.
- Yang, Weibo, Lulu Sun, and Yongping Chen. 2015. "Experimental Investigations of the Performance of a Solar-Ground Source Heat Pump System Operated in Heating Modes." *Energy and Buildings* 89: 97–111. <https://doi.org/10.1016/j.enbuild.2014.12.027>.

- Youssef, W., Y.T. Ge, and S.A. Tassou. 2017. “Effects of Latent Heat Storage and Controls on Stability and Performance of a Solar Assisted Heat Pump System for Domestic Hot Water Production.” *Solar Energy* 150: 394–407. <https://doi.org/10.1016/j.solener.2017.04.065>.
- Zenhäusern, Daniel, Evelyn Bamberger, Alexis Baggenstos, and Andreas Häberle. 2017. “PVT Wrap-Up: Energy Systems with Photovoltaic Thermal Solar Collectors.” *Proceedings of SWC2017/SHC2017*. <https://doi.org/10.18086/swc.2017.18.12>.
- Zenhäusern, Daniel. 2020. “Key Performance Indicators for PVT Systems.” <https://doi.org/10.18777/ieashc-task60-2020-0007>.
- Zhao, M., Z.L. Gu, W.B. Kang, X. Liu, L.Y. Zhang, L.W. Jin, and Q.L. Zhang. 2017. “Experimental Investigation and Feasibility Analysis on a Capillary Radiant Heating System Based on Solar and Air Source Heat Pump Dual Heat Source.” *Applied Energy* 185: 2094–2105. <https://doi.org/10.1016/j.apenergy.2016.02.043>.

Appendix A: Reviewed studies of SAHP systems

In Table A-1-Table A-3, WWHP and AWHP stand for liquid-to-liquid heat pump and air-to-liquid heat pump, respectively. Also, integration between solar component and heat pump are either series (S), parallel (P), or parallel/series (P/S).

Table A-1: Reviewed studies of SAHP systems for domestic hot water heating

Reference	Integration between solar component and heat pump	System configuration	Approach
Bai, et al.(2012)	S	PVT-WWHP	Sim (TRNSYS)
Banister, Collins (2015)	P/S	STC-WWHP	Exp & Sim (TRNSYS)
Dannemand, Perers, & Furbo (2019)	P/S	PVT-WWHP	Exp
Eicher, et al. (2012)	S	STC-WWHP	Exp & Sim (TRNSYS)
Fine, Friedman, & Dworkin (2017)	S	PVT-WWHP	Sim
Kim, et al. (2018)	S, P, P/S	STC-WWHP & STC-AWHP	Exp & Sim
Lv, Yan, & Yu (2015)	S	STC- Dual (A+W)WHP	Sim
Panaras, Mathioulakis, & Belessiotis (2013)	P	STC-AWHP	Exp & Sim (Matlab)
Qu, et al. (2016)	S	PVT-Dual (A+W)WHP	Exp
Sterling & Collins (2012)	P/S	STC-WWHP	Sim (TRNSYS)
Wang, et al. (2015)	S	PVT-Dual (A+W)WHP	Exp
Youssef, Ge, & Tassou (2017)	P/S	STC-WWHP	Exp

Table A-2: Reviewed studies of SAHP systems for space heating

Reference	Integration between solar component and Heat Pump	System configuration	Approach
Aydin, Utlu, & Kincay (2015)	P/S	STC-WWHP	Exp & Sim
Bakirci, Kadir, & Yuksel (2011)	S	STC-WWHP	Exp
Bellos, et al. (2016)	S	PV-AAHP & STC-WAHP & PVT-WAHP & STC+PV-WAHP	Sim (TRNSYS)
Bellos, Evangelos, & Tzivandis (2017)	S	STC-WAHP	Sim (TRNSYS)
Busato, Lazzarin, & Noro (2015)	P/S	STC-WWHP	Sim (TRNSYS)
Calgar, Ahmet, & Yamali (2012)	S	STC-AAHP	Exp & Sim (Mathcad)
Cao, et al. (2016)	S	PVT-AWHP	Sim (TRNSYS)
Chargui, Ridha, & Awani (2017)	S	STC-Dual (A+W)W HP	Sim (TRNSYS)
Del Amo, et al. (2020)	S	PVT-WWHP	Sim (TRNSYS)
Emmi, et al. (2015)	S	STC-WWHP	Sim (TRNSYS)
Girard, et al. (2015)	S	STC-WWHP	Sim (Microsoft Excel)
Hailu, Dash, & Fung (2015)	S	PVT-AAHP	Sim (TRNSYS)
Li, et al. (2015)	P/S	PVT-AWHP	Exp & Sim (TRNSYS)
Li, et al. (2018)	S	STC-WWHP	Exp & Sim (TRNSYS)
Liang, et al. (2011)	P	STC-AWHP	Exp & Sim
Liu, et al. (2016)	S	STC-Dual (A+W)W HP	Exp
Plytaria, et al. (2018)	S	STC-WWHP & STC+PV-WWHP & PVT-WWHP	Sim (TRNSYS)
Plytaria, et al. (2019)	S	STC-WWHP & STC+PV-WWHP & PVT-WWHP	Sim (TRNSYS)
Qu, et al. (2015)	P/S	STC-WWHP	Exp

Table A-2 cont: Reviewed studies of SAHP systems for space heating

Reference	Integration between solar component and Heat Pump	System configuration	Approach
Shan, Yu, & Yang (2016)	P	STC-AWHP	Exp
Simonetti, Molinaroli, & Manzolini (2019)	S	PVT-Dual (A+W)W HP	Exp & Sim (Matlab)
Tzivanidis, et al. (2016)	S	STC-WAHP	Sim (TRNSYS)
Vallati, et al. (2019)	S	PVT-WWHP	Sim (Matlab)
Yang, Sun, & Chen (2015)	P/S	STC-WWHP	Exp & Sim (TRNSYS)
Zhao, et al. (2017)	P	STC- AWHP	Exp

Table A-3: Reviewed studies of SAHP systems for both DHW and space heating

Reference	Integration between solar component and Heat Pump	System configuration	Approach
Asaee, Ugursal, & Beausoleil-Morrison (2017)	P/S	STC-WWHP	Sim (ESP-r)
Bertram, Parisch, & Tepe (2012)	P/S	STC-WWHP	Sim (TRNSYS)
Bertram, Glembin, & Rockendorf (2012)	S	PVT-WWHP	Exp & Sim (TRNSYS)
Bertram (2013)	P/S	STC-WWHP	Sim (TRNSYS)
Carbonell, Haller, & Frank (2013)	P	STC-AWHP & STC-WWHP	Sim (Polysun & TRNSYS)
Carbonell, et al. (2013)	P/S	STC-AWHP & STC-WWHP	Sim (Polysun & TRNSYS)
Carbonell, et al. (2015)	P/S	STC-WWHP	Exp
Carbonell, et al. (2016)	P/S	STC-WWHP	Exp & Sim (TRNSYS)
Carbonell, et al. (2016)	P/S	STC-WWHP	Exp & Sim
Chen, Dai, & Wang (2016)	P	STC-AWHP	Exp & Sim (TRNSYS)
Chow, et al. (2012)	P/S	STC-WAHP	Sim (TRNSYS)
Deng, Dai, & Wang (2013)	P	STC-AWHP	Sim (TRNSYS)
Dott, Genkinger, & Afjei (2012)	P	STC-AWHP, STC+PV-AWHP, PV-AWHP, STC-WWHP, PVT-WWHP	Sim (Polysun)
Eicher, et al. (2013)	S & P	STC-WWHP	Sim (TRNSYS)
Emmi, Zarrella, & De Carli (2017)	S & P	PVT-WWH & PVT-Dual (A&W)WHP	Sim (TRNSYS)
Fraga, et al. (2017)	P/S	STC-WWHP	Exp & Sim (TRNSYS)
Haller, et al. (2013)	P	STC-AWHP	Sim (TRNSYS)
Haller & Frank (2011)	P/S	STC-Dual (A&W)WHP	Sim (TRNSYS)
Jonas, et al. (2017)	P	STC-AWHP & STC-WWHP	Sim (TRNSYS)

Table A-3 cont: Reviewed studies of SAHP systems for both DHW and space heating

Reference	Integration between solar component and Heat Pump	System configuration	Approach
Jonas, Frey, & Theis (2017)	P	STC-AWHP & STC-WWHP	Sim (TRNSYS)
Jonas & Frey (2018)	P/S & P & S	STC-AWHP & STC-WWHP	Sim (TRNSYS)
Lerch, Heinz, & Heimrath (2013)	P/S	STC-Dual (A&W)WHP	Sim (TRNSYS)
Lerch, Heinz, & Heimrath (2015)	P/S & P	STC-Dual (A&W)WHP & STC-AWHP	Sim (TRNSYS)
Li, Sun, & Zhang (2014)	S	STC-WWHP+AWHP	Sim (TRNSYS)
Mojic, et al. (2013)	P/S & P	STC-AWHP & STC-WWHP	Sim (TRNSYS)
Ochs, Dermentzis, & Feist (2013)	P	PV+STC-AWHP PV+STC-WWHP	Sim (Matlab)
Poppi, et al (2016)	P	STC-AWHP	Sim (TRNSYS)
Poppi, et al. (2016)	P	STC-AWHP & STC-WWHP	Sim (TRNSYS)
Rad, Fung, & Leong (2013)	S	STC-WWHP	Exp & Sim (TRNSYS)
Razavi, Ahmadi, & Zahedi (2018)	P/S	STC-WWHP	Sim (TRNSYS)
Sakellariou, et al. (2019)	S	PVT-WWHP	Sim (TRNSYS)
Simonetti, et al. (2020)	P/S & P	PV-AWHP PVT-WWHP PVT-Dual (A&W)WHP	Sim (TRNSYS)
Sommerfeldt & Madani (2019)	S	PVT-WWHP	Sim (TRNSYS)
Tamasaukas, et al. (2012)	P/S	STC-WWHP	Exp & Sim (TRNSYS + GenOpt)
Vega & Cuevas (2018)	P	STC-AWHP	Sim (TRNSYS)
Winteler, et al. (2013)	S	STC-WWHP	Sim (Matlab)

Appendix B: Normalized data files of heat pumps

Table B-1: Normalized heating data file of the WaterFurnace (model NSW040) liquid-to-liquid heat pump

Entering Load Temperature (°C)	Entering Source Temperature (°C)	Normalized Load Flow Rate	Normalized Source Flow Rate	Normalized Capacity	Normalized Power
15.55	-1.11	0.5	0.5	0.65	0.63
15.55	10	0.5	0.5	0.86	0.64
15.55	21.11	0.5	0.5	1.07	0.66
15.55	32.22	0.5	0.5	1.28	0.68
26.66	-1.11	0.5	0.5	0.63	0.83
26.66	10	0.5	0.5	0.82	0.84
26.66	21.11	0.5	0.5	1.02	0.86
26.66	32.22	0.5	0.5	1.24	0.87
37.77	-1.11	0.5	0.5	0.61	1.02
37.77	10	0.5	0.5	0.79	1.05
37.77	21.11	0.5	0.5	0.97	1.07
37.77	32.22	0.5	0.5	0.97	1.07
48.88	-1.11	0.5	0.5	0.59	1.22
48.88	10	0.5	0.5	0.76	1.25
48.88	21.11	0.5	0.5	0.92	1.27
48.88	32.22	0.5	0.5	0.92	1.27
15.55	-1.11	0.5	0.75	0.67	0.63
15.55	10	0.5	0.75	0.90	0.64
15.55	21.11	0.5	0.75	1.12	0.64
15.55	32.22	0.5	0.75	1.33	0.69
26.66	-1.11	0.5	0.75	0.65	0.83
26.66	10	0.5	0.75	0.86	0.84
26.66	21.11	0.5	0.75	1.07	0.85
26.66	32.22	0.5	0.75	1.29	0.88
37.77	-1.11	0.5	0.75	0.62	1.03
37.77	10	0.5	0.75	0.82	1.05
37.77	21.11	0.5	0.75	1.01	1.06
37.77	32.22	0.5	0.75	1.25	1.08
48.88	-1.11	0.5	0.75	0.59	1.23
48.88	10	0.5	0.75	0.78	1.25
48.88	21.11	0.5	0.75	0.96	1.27

Table B-1 cont: Normalized heating data file of the WaterFurnace (model NSW040) liquid-to-liquid heat pump

Entering Load Temperature (°C)	Entering Source Temperature (°C)	Normalized Load Flow Rate	Normalized Source Flow Rate	Normalized Capacity	Normalized Power
48.88	32.22	0.5	0.75	0.96	1.27
15.55	-1.11	0.5	1	0.70	0.63
15.55	10	0.5	1	0.94	0.63
15.55	21.11	0.5	1	1.17	0.63
15.55	32.22	0.5	1	1.37	0.69
26.66	-1.11	0.5	1	0.67	0.83
26.66	10	0.5	1	0.89	0.84
26.66	21.11	0.5	1	1.11	0.84
26.66	32.22	0.5	1	1.34	0.89
37.77	-1.11	0.5	1	0.64	1.04
37.77	10	0.5	1	0.84	1.05
37.77	21.11	0.5	1	1.05	1.06
37.77	32.22	0.5	1	1.31	1.08
48.88	-1.11	0.5	1	0.60	1.24
48.88	10	0.5	1	0.80	1.26
48.88	21.11	0.5	1	0.99	1.27
48.88	32.22	0.5	1	0.99	1.27
15.55	-1.11	0.75	0.5	0.64	0.61
15.55	10	0.75	0.5	0.85	0.62
15.55	21.11	0.75	0.5	1.06	0.63
15.55	32.22	0.75	0.5	1.23	0.64
26.66	-1.11	0.75	0.5	0.63	0.81
26.66	10	0.75	0.5	0.82	0.82
26.66	21.11	0.75	0.5	1.01	0.83
26.66	32.22	0.75	0.5	1.18	0.83
37.77	-1.11	0.75	0.5	0.61	1.00
37.77	10	0.75	0.5	0.79	1.01
37.77	21.11	0.75	0.5	0.97	1.03
37.77	32.22	0.75	0.5	0.97	1.03
48.88	-1.11	0.75	0.5	0.59	1.20
48.88	10	0.75	0.5	0.76	1.21
48.88	21.11	0.75	0.5	0.92	1.23
48.88	32.22	0.75	0.5	0.92	1.23
15.55	-1.11	0.75	0.75	0.67	0.61

Table B-1 cont: Normalized heating data file of the WaterFurnace (model NSW040) liquid-to-liquid heat pump

Entering Load Temperature (°C)	Entering Source Temperature (°C)	Normalized Load Flow Rate	Normalized Source Flow Rate	Normalized Capacity	Normalized Power
15.55	10	0.75	0.75	0.89	0.62
15.55	21.11	0.75	0.75	1.11	0.62
15.55	32.22	0.75	0.75	1.26	0.65
26.66	-1.11	0.75	0.75	0.65	0.81
26.66	10	0.75	0.75	0.85	0.81
26.66	21.11	0.75	0.75	1.06	0.82
26.66	32.22	0.75	0.75	1.22	0.84
37.77	-1.11	0.75	0.75	0.62	1.00
37.77	10	0.75	0.75	0.82	1.01
37.77	21.11	0.75	0.75	1.01	1.02
37.77	32.22	0.75	0.75	1.17	1.03
48.88	-1.11	0.75	0.75	0.60	1.20
48.88	10	0.75	0.75	0.78	1.21
48.88	21.11	0.75	0.75	0.96	1.22
48.88	32.22	0.75	0.75	0.96	1.22
15.55	-1.11	0.75	1	0.70	0.61
15.55	10	0.75	1	0.93	0.61
15.55	21.11	0.75	1	1.16	0.62
15.55	32.22	0.75	1	1.29	0.65
26.66	-1.11	0.75	1	0.67	0.81
26.66	10	0.75	1	0.89	0.81
26.66	21.11	0.75	1	1.10	0.82
26.66	32.22	0.75	1	1.25	0.84
37.77	-1.11	0.75	1	0.64	1.01
37.77	10	0.75	1	0.84	1.01
37.77	21.11	0.75	1	1.05	1.02
37.77	32.22	0.75	1	1.21	1.03
48.88	-1.11	0.75	1	0.61	1.21
48.88	10	0.75	1	0.80	1.22
48.88	21.11	0.75	1	0.99	1.22
48.88	32.22	0.75	1	0.99	1.22
15.55	-1.11	1	0.5	0.64	0.59
15.55	10	1	0.5	0.85	0.59
15.55	21.11	1	0.5	1.05	0.59

Table B-1 cont: Normalized heating data file of the WaterFurnace (model NSW040) liquid-to-liquid heat pump

Entering Load Temperature (°C)	Entering Source Temperature (°C)	Normalized Load Flow Rate	Normalized Source Flow Rate	Normalized Capacity	Normalized Power
15.55	32.22	1	0.5	1.18	0.60
26.66	-1.11	1	0.5	0.62	0.79
26.66	10	1	0.5	0.82	0.79
26.66	21.11	1	0.5	1.01	0.79
26.66	32.22	1	0.5	1.13	0.79
37.77	-1.11	1	0.5	0.61	0.98
37.77	10	1	0.5	0.78	0.98
37.77	21.11	1	0.5	0.96	0.98
37.77	32.22	1	0.5	0.96	0.98
48.88	-1.11	1	0.5	0.59	1.17
48.88	10	1	0.5	0.76	1.18
48.88	21.11	1	0.5	0.92	1.18
48.88	32.22	1	0.5	0.92	1.18
15.55	-1.11	1	0.75	0.67	0.59
15.55	10	1	0.75	0.88	0.59
15.55	21.11	1	0.75	1.10	0.60
15.55	32.22	1	0.75	1.19	0.60
26.66	-1.11	1	0.75	0.65	0.78
26.66	10	1	0.75	0.85	0.79
26.66	21.11	1	0.75	1.05	0.79
26.66	32.22	1	0.75	1.14	0.80
37.77	-1.11	1	0.75	0.63	0.98
37.77	10	1	0.75	0.81	0.98
37.77	21.11	1	0.75	1.00	0.98
37.77	32.22	1	0.75	1.09	0.98
48.88	-1.11	1	0.75	0.60	1.17
48.88	10	1	0.75	0.78	1.18
48.88	21.11	1	0.75	0.96	1.18
48.88	32.22	1	0.75	0.96	1.18
15.55	-1.11	1	1	0.70	0.59
15.55	10	1	1	0.92	0.59
15.55	21.11	1	1	1.14	0.60
15.55	32.22	1	1	1.20	0.60
26.66	-1.11	1	1	0.67	0.78

Table B-1 cont: Normalized heating data file of the WaterFurnace (model NSW040) liquid-to-liquid heat pump

Entering Load Temperature (°C)	Entering Source Temperature (°C)	Normalized Load Flow Rate	Normalized Source Flow Rate	Normalized Capacity	Normalized Power
26.66	10	1	1	0.88	0.79
26.66	21.11	1	1	1.09	0.79
26.66	32.22	1	1	1.16	0.80
37.77	-1.11	1	1	0.65	0.98
37.77	10	1	1	0.84	0.98
37.77	21.11	1	1	1.04	0.98
37.77	32.22	1	1	1.11	0.98
48.88	-1.11	1	1	0.62	1.17
48.88	10	1	1	0.81	1.18
48.88	21.11	1	1	1.00	1.18
48.88	32.22	1	1	1.00	1.18

Table B-2: Normalized cooling data file of the WaterFurnace (model NSW040) liquid-to-liquid heat pump

Entering Load Temperature (°C)	Entering Source Temperature (°C)	Normalized Load Flow Rate	Normalized Source Flow Rate	Normalized Capacity	Normalized Power
10	-1.11	0.5	0.5	1.08	0.60
10	10	0.5	0.5	0.99	0.76
10	21.11	0.5	0.5	0.91	0.92
10	32.22	0.5	0.5	0.81	1.18
10	43.33	0.5	0.5	0.71	1.44
21.11	-1.11	0.5	0.5	1.04	0.55
21.11	10	0.5	0.5	1.12	0.75
21.11	21.11	0.5	0.5	1.20	0.95
21.11	32.22	0.5	0.5	1.09	1.21
21.11	43.33	0.5	0.5	0.99	1.47
32.22	-1.11	0.5	0.5	1.01	0.51
32.22	10	0.5	0.5	1.25	0.74
32.22	21.11	0.5	0.5	1.48	0.97
32.22	32.22	0.5	0.5	1.38	1.23
32.22	43.33	0.5	0.5	0.99	1.47
43.33	-1.11	0.5	0.5	0.97	0.46
43.33	10	0.5	0.5	1.38	0.73
43.33	21.11	0.5	0.5	1.48	0.97
43.33	32.22	0.5	0.5	1.38	1.23
43.33	43.33	0.5	0.5	0.99	1.47
10	-1.11	0.5	0.75	1.05	0.57
10	10	0.5	0.75	0.98	0.73
10	21.11	0.5	0.75	0.92	0.89
10	32.22	0.5	0.75	0.81	1.14
10	43.33	0.5	0.75	0.71	1.40
21.11	-1.11	0.5	0.75	1.01	0.53
21.11	10	0.5	0.75	1.09	0.71
21.11	21.11	0.5	0.75	1.17	0.90
21.11	32.22	0.5	0.75	1.08	1.16
21.11	43.33	0.5	0.75	1.00	1.42
32.22	-1.11	0.5	0.75	0.97	0.49
32.22	10	0.5	0.75	1.20	0.70
32.22	21.11	0.5	0.75	1.43	0.91
32.22	32.22	0.5	0.75	1.35	1.17

Table B-2 cont: Normalized cooling data file of the WaterFurnace (model NSW040) liquid-to-liquid heat pump

Entering Load Temperature (°C)	Entering Source Temperature (°C)	Normalized Load Flow Rate	Normalized Source Flow Rate	Normalized Capacity	Normalized Power
32.22	43.33	0.5	0.75	1.00	1.42
43.33	-1.11	0.5	0.75	0.92	0.45
43.33	10	0.5	0.75	1.31	0.69
43.33	21.11	0.5	0.75	1.43	0.91
43.33	32.22	0.5	0.75	1.35	1.17
43.33	43.33	0.5	0.75	1.00	1.42
10	-1.11	0.5	1	1.02	0.54
10	10	0.5	1	0.97	0.70
10	21.11	0.5	1	0.92	0.85
10	32.22	0.5	1	0.82	1.10
10	43.33	0.5	1	0.72	1.36
21.11	-1.11	0.5	1	0.97	0.51
21.11	10	0.5	1	1.06	0.68
21.11	21.11	0.5	1	1.15	0.85
21.11	32.22	0.5	1	1.08	1.11
21.11	43.33	0.5	1	1.01	1.36
32.22	-1.11	0.5	1	0.92	0.47
32.22	10	0.5	1	1.15	0.66
32.22	21.11	0.5	1	1.38	0.85
32.22	32.22	0.5	1	1.33	1.11
32.22	43.33	0.5	1	1.01	1.36
43.33	-1.11	0.5	1	0.87	0.44
43.33	10	0.5	1	1.24	0.65
43.33	21.11	0.5	1	1.60	0.86
43.33	32.22	0.5	1	1.33	1.11
43.33	43.33	0.5	1	1.01	1.36
10	-1.11	0.75	0.5	1.11	0.60
10	10	0.75	0.5	1.04	0.76
10	21.11	0.75	0.5	0.97	0.92
10	32.22	0.75	0.5	0.86	1.18
10	43.33	0.75	0.5	0.75	1.45
21.11	-1.11	0.75	0.5	1.06	0.54
21.11	10	0.75	0.5	1.16	0.74
21.11	21.11	0.75	0.5	1.25	0.95

Table B-2 cont: Normalized cooling data file of the WaterFurnace (model NSW040) liquid-to-liquid heat pump

Entering Load Temperature (°C)	Entering Source Temperature (°C)	Normalized Load Flow Rate	Normalized Source Flow Rate	Normalized Capacity	Normalized Power
21.11	32.22	0.75	0.5	1.14	1.21
21.11	43.33	0.75	0.5	1.04	1.48
32.22	-1.11	0.75	0.5	1.01	0.48
32.22	10	0.75	0.5	1.27	0.73
32.22	21.11	0.75	0.5	1.53	0.98
32.22	32.22	0.75	0.5	1.43	1.24
32.22	43.33	0.75	0.5	1.04	1.48
43.33	-1.11	0.75	0.5	0.96	0.42
43.33	21.11	0.75	0.5	1.53	0.98
43.33	32.22	0.75	0.5	1.43	1.24
43.33	43.33	0.75	0.5	1.04	1.48
10	-1.11	0.75	0.75	1.08	0.57
10	10	0.75	0.75	1.03	0.73
10	21.11	0.75	0.75	0.98	0.88
10	32.22	0.75	0.75	0.87	1.14
10	43.33	0.75	0.75	0.75	1.40
21.11	-1.11	0.75	0.75	1.02	0.52
21.11	10	0.75	0.75	1.12	0.71
21.11	21.11	0.75	0.75	1.23	0.90
21.11	32.22	0.75	0.75	1.14	1.16
21.11	43.33	0.75	0.75	1.05	1.42
32.22	-1.11	0.75	0.75	0.97	0.47
32.22	10	0.75	0.75	1.22	0.69
32.22	21.11	0.75	0.75	1.47	0.92
32.22	32.22	0.75	0.75	1.41	1.17
32.22	43.33	0.75	0.75	1.05	1.42
43.33	-1.11	0.75	0.75	0.92	0.42
43.33	10	0.75	0.75	1.31	0.67
43.33	21.11	0.75	0.75	1.47	0.92
43.33	32.22	0.75	0.75	1.41	1.17
43.33	43.33	0.75	0.75	1.05	1.42
10	-1.11	0.75	1	1.04	0.55
10	10	0.75	1	1.01	0.70
10	21.11	0.75	1	0.99	0.84

Table B-2 cont: Normalized cooling data file of the WaterFurnace (model NSW040) liquid-to-liquid heat pump

Entering Load Temperature (°C)	Entering Source Temperature (°C)	Normalized Load Flow Rate	Normalized Source Flow Rate	Normalized Capacity	Normalized Power
10	32.22	0.75	1	0.87	1.10
10	43.33	0.75	1	0.76	1.36
21.11	-1.11	0.75	1	0.98	0.51
21.11	10	0.75	1	1.09	0.68
21.11	21.11	0.75	1	1.20	0.85
21.11	32.22	0.75	1	1.13	1.10
21.11	43.33	0.75	1	1.06	1.36
32.22	-1.11	0.75	1	0.93	0.46
32.22	10	0.75	1	1.17	0.66
32.22	21.11	0.75	1	1.41	0.85
32.22	32.22	0.75	1	1.38	1.11
32.22	43.33	0.75	1	1.06	1.36
43.33	-1.11	0.75	1	0.87	0.42
43.33	10	0.75	1	1.25	0.64
43.33	21.11	0.75	1	1.62	0.86
43.33	32.22	0.75	1	1.38	1.11
43.33	43.33	0.75	1	1.06	1.36
10	-1.11	1	0.5	1.14	0.60
10	10	1	0.5	1.09	0.76
10	21.11	1	0.5	1.04	0.92
10	32.22	1	0.5	0.91	1.18
10	43.33	1	0.5	0.79	1.45
21.11	-1.11	1	0.5	1.08	0.53
21.11	10	1	0.5	1.19	0.74
21.11	21.11	1	0.5	1.31	0.95
21.11	32.22	1	0.5	1.20	1.21
21.11	43.33	1	0.5	1.09	1.48
32.22	-1.11	1	0.5	1.01	0.46
32.22	10	1	0.5	1.29	0.72
32.22	21.11	1	0.5	1.58	0.98
32.22	32.22	1	0.5	1.48	1.24
32.22	43.33	1	0.5	1.09	1.48
43.33	-1.11	1	0.5	0.94	0.39
43.33	10	1	0.5	1.40	0.70

Table B-2 cont: Normalized cooling data file of the WaterFurnace (model NSW040) liquid-to-liquid heat pump

Entering Load Temperature (°C)	Entering Source Temperature (°C)	Normalized Load Flow Rate	Normalized Source Flow Rate	Normalized Capacity	Normalized Power
43.33	21.11	1	0.5	1.58	0.98
43.33	32.22	1	0.5	1.48	1.24
43.33	43.33	1	0.5	1.09	1.48
10	-1.11	1	0.75	1.10	0.57
10	10	1	0.75	1.07	0.73
10	21.11	1	0.75	1.05	0.88
10	32.22	1	0.75	0.92	1.14
10	43.33	1	0.75	0.79	1.40
21.11	-1.11	1	0.75	1.03	0.51
21.11	10	1	0.75	1.16	0.70
21.11	21.11	1	0.75	1.28	0.90
21.11	32.22	1	0.75	1.19	1.16
21.11	43.33	1	0.75	1.10	1.42
32.22	-1.11	1	0.75	0.97	0.45
32.22	10	1	0.75	1.24	0.69
32.22	21.11	1	0.75	1.51	0.92
32.22	32.22	1	0.75	1.46	1.17
32.22	43.33	1	0.75	1.10	1.42
43.33	-1.11	1	0.75	0.91	0.40
43.33	10	1	0.75	1.32	0.66
43.33	21.11	1	0.75	1.51	0.92
43.33	32.22	1	0.75	1.46	1.17
43.33	43.33	1	0.75	1.10	1.42
10	-1.11	1	1	1.06	0.55
10	10	1	1	1.06	0.70
10	21.11	1	1	1.05	0.84
10	32.22	1	1	0.93	1.10
10	43.33	1	1	0.80	1.35
21.11	-1.11	1	1	0.99	0.50
21.11	10	1	1	1.12	0.67
21.11	21.11	1	1	1.25	0.85
21.11	32.22	1	1	1.18	1.10
21.11	43.33	1	1	1.11	1.35
32.22	-1.11	1	1	0.93	0.45

Table B-2 cont: Normalized cooling data file of the WaterFurnace (model NSW040) liquid-to-liquid heat pump

Entering Load Temperature (°C)	Entering Source Temperature (°C)	Normalized Load Flow Rate	Normalized Source Flow Rate	Normalized Capacity	Normalized Power
32.22	10	1	1	1.19	0.65
32.22	21.11	1	1	1.44	0.85
32.22	32.22	1	1	1.43	1.10
32.22	43.33	1	1	1.11	1.35
43.33	-1.11	1	1	0.87	0.40
43.33	10	1	1	1.25	0.63
43.33	21.11	1	1	1.63	0.86
43.33	32.22	1	1	1.43	1.10
43.33	43.33	1	1	1.11	1.35

Table B-3: Normalized heating data file of the Carrier (Model 30AWH012-3Ph) air-to-water heat pump

Entering Water Temperature (°C)	Entering Air Temperature (°C)	Normalized Capacity	Normalized Power
30	-20	0.33	0.74
30	-15	0.56	0.95
30	-7	0.59	0.96
30	-3	0.64	0.98
30	0	0.65	0.99
30	2	0.71	0.97
30	7	1.00	1.00
30	10	1.07	0.98
30	20	1.35	0.96
40	-20	0.25	0.62
40	-15	0.53	1.25
40	-7	0.49	0.93
40	-3	0.52	0.93
40	0	0.56	0.96
40	2	0.63	1.00
40	7	0.93	1.20
40	10	1.00	1.26
40	20	1.28	1.42
50	-20	0.25	0.62
50	-15	0.24	0.60
50	-7	0.48	1.12
50	-3	0.53	1.14
50	0	0.53	1.09
50	2	0.62	1.18
50	7	0.92	1.41
50	10	0.99	1.41
50	20	1.24	1.50
55	-20	0.25	0.62
55	-15	0.24	0.60
55	-7	0.45	1.24
55	-3	0.49	1.36
55	0	0.50	1.34
55	2	0.59	1.24
55	7	0.89	1.42
55	10	0.97	1.48
55	20	1.18	1.51

Table B-4: Normalized cooling data file of the Carrier (Model 30AWH012-3Ph) air-to-water heat pump

Entering Water Temperature (°C)	Entering Air Temperature (°C)	Normalized Capacity	Normalized Power
10	5	1.35	0.68
10	15	1.11	0.64
10	25	1.02	0.82
10	35	0.94	1.01
10	45	0.87	1.10
12	5	1.26	0.47
12	15	1.19	0.63
12	25	1.09	0.81
12	35	1.00	1.00
12	45	0.91	1.07
15	5	1.11	0.30
15	15	1.30	0.61
15	25	1.20	0.80
15	35	1.09	0.99
15	45	0.98	1.04
20	5	0.67	0.12
20	15	1.48	0.58
20	25	1.38	0.78
20	35	1.24	0.97
20	45	1.09	0.99
23	5	0.73	0.11
23	15	1.59	0.57
23	25	1.49	0.77
23	35	1.32	0.96
23	45	1.16	0.97